



Universiteit  
Leiden  
The Netherlands

## **Understanding protein complex formation: the role of charge distribution in the encounter complex**

Di Savino, A.

### **Citation**

Di Savino, A. (2021, June 15). *Understanding protein complex formation: the role of charge distribution in the encounter complex*. Retrieved from <https://hdl.handle.net/1887/3185507>

Version: Publisher's Version

License: [Licence agreement concerning inclusion of doctoral thesis in the Institutional Repository of the University of Leiden](#)

Downloaded from: <https://hdl.handle.net/1887/3185507>

**Note:** To cite this publication please use the final published version (if applicable).

Cover Page



Universiteit Leiden



The handle <http://hdl.handle.net/1887/3185507> holds various files of this Leiden University dissertation.

**Author:** Di Savino, A.

**Title:** Understanding protein complex formation: the role of charge distribution in the encounter complex

**Issue date:** 2021-06-15

# Understanding protein complex formation:

## The role of charge distribution in the encounter complex

Proefschrift

ter verkrijging van

de graad van doctor aan de Universiteit Leiden,

op gezag van rector magnificus prof.dr.ir. H. Bijl,

volgens besluit van het college voor promoties

te verdedigen op dinsdag 15 juni 2021

klokke 10:00 uur

door

**Antonella Di Savino**

geboren te Turijn, Italië

in 1986

Promotores: Prof. dr. M. Ubbink

Prof. dr. J. M. F. G. Aerts

Promotiecommissie: Prof. dr. H. S. Overkleeft (voorzitter)

Prof. dr. R. T. Dame (secretaris)

Prof. dr. G. Schreiber (Weizmann Institute of Science, Rehovot)

Dr. S. Pauleta (Universidade Nova de Lisboa)

Dr. M. I. Huber

The research described in this thesis was performed in the Protein Chemistry Department of the Leiden Institute of Chemistry at the Universiteit Leiden in Leiden, the Netherlands.

This work was financially supported by the Netherlands Organisation for Scientific Research (NWO-CW grant 711.013.007).

**To my family**

*“A li pccnunn mj”*

# Table of Contents

<b>Chapter 1</b> Introduction to protein-protein interactions .....	7
<b>Chapter 2</b> Introductions to cytochrome c and cytochrome c peroxidase .....	41
<b>Chapter 3</b> Efficient encounter complex formation and electron transfer to cytochrome c peroxidase with an added distant electrostatic binding site .....	53
<b>Chapter 4</b> Charge distribution on a protein surface determines whether productive or futile encounter complexes are formed .....	80
<b>Chapter 5</b> Enhancing the population of encounter complex affects protein complex formation efficiency .....	108
<b>Chapter 6</b> General discussion and concluding remarks .....	130
English summary .....	139
Nederlandse samenvatting .....	142
Curriculum Vitae .....	145
List of publications .....	145

# Abbreviations

$\Delta\chi$	magnetic susceptibility anisotropy tensor
$\tau_c$	rotational correlation time
A $\beta$	amyloid $\beta$
AdR	adrenodoxin reductase
Adx	adrenodoxin
ATP	adenosine triphosphate
BPTI	bovine pancreatic trypsin inhibitor
ca.	circa
CcP	cytochrome <i>c</i> peroxidase
CL	crosslinked complex
CLaNP	caged lanthanide NMR probe
Cc	cytochrome <i>c</i>
Cc6	cytochrome <i>c</i> <sub>6</sub>
CpdI	Compound I
CpdII	Compound II
Cytf	cytochrome <i>f</i>
DOTAM	1,4,7,10-tetraazacyclododecane-1,4,7,10-tetraacetamide
DOTP	1,4,7,10-tetraazacyclododecane-1,4,7,10-tetrakis (methylenephosphonate)
EDTA	ethylenediaminetetraacetic acid
EIN	Enzyme I
EM	electron microscopy
Fd	ferredoxin
EPR	electron paramagnetic resonance
FRET	fluorescence resonance energy transfer
FTR	ferredoxin:thioredoxin reductase
HPr	histidine-containing phosphocarrier protein
HSQC	heteronuclear single quantum coherence
IFN- $\gamma$	interferon gamma

$k_a$	association rate constant
$K_B$	binding constant
$K_D$	dissociation constant
$k_{ex}$	exchange rate
$k_{off}$	dissociation rate constant
$k_{on}$	association rate constant
Lac	lactose
LBP	lanthanide-binding peptide
MTS	1-acetoxy-2,2,5,5-tetramethyl-d3-pyrroline-3-methyl-methanethiosulfonate
MTSL	1-oxyl-2,2,5,5-tetramethyl-2,5-dihydropyrrol-3-ylmethyl-methanethiosulfonate
NADPH	nicotinamide adenine dinucleotide phosphate (reduced state)
NOE	nuclear Overhauser enhancement
NOESY	nuclear Overhauser spectroscopy
NS2Bc	C-terminal segment of NS2B
NS2B-NS3pro	NS2B-NS3 protease
P450cam	cytochrome P450cam
Pc	plastocyanin
PCS	pseudocontact shift
PDB	protein data bank
Pdx	putidaredoxin
piRDC	paramagnetically induced residual dipolar coupling
PRE	paramagnetic relaxations enhancement
PPI	protein-protein interaction
RD	relaxation dispersion
RDC	residual dipolar coupling
RMSD	root mean square deviation
SAXS	small-angle X-ray scattering
SNAP	synaptosomal-associated protein
SNARE	soluble NSF attachment protein
sPRE	solvent paramagnetic relaxations enhancement



Syt1	synaptotagmin-1
Trx	thioredoxin
WT	wild type
XRD	X-ray diffraction

# Chapter 1

## Introduction to protein-protein interactions

Based on the chapter of the book:

Ubbink, M., and Di Savino, A. (2018) Chapter 5: Protein-protein interactions, in *New Developments in NMR - Paramagnetism in Experimental Biomolecular NMR* (Luchinat, C., Parigi, G., and Ravera, E., Eds.), pp 134–162. The Royal Society of Chemistry, Cambridge, UK. ISBN: 9781788014960

### **Abstract**

Paramagnetic NMR methods are excellently suited for the study of protein-protein complexes in solution. Intermolecular pseudocontact shifts (PCS), residual dipolar couplings (RDC) and paramagnetic relaxations enhancements (PRE) can be used, ideally in combination, for docking proteins and determining their orientation in the complex. PCS can be used for breaking the structure symmetry in dimer complexes. PCS also can be applied to detect structural differences in proteins and protein complexes in solution in comparison to crystal structures. RDC are sensitive to the degree of alignment of both partners in a protein complex and are thus very useful to detect dynamics within complexes. PRE can detect states in which nuclei approach a paramagnetic centre closely, even if it exists only for a small fraction of the time. Thus, PRE are used to detect minor states and characterize ensembles. PRE studies have been the foundation for characterizing encounter states and the process of protein complex formation. In weak complexes, such as found in electron transfer chains, proteins can be in an encounter state for a large fraction of the complex lifetime. Both electrostatic interactions and the hydrophobic effect have been shown to contribute to the formation of encounter states. Paramagnetic NMR tools thus have found many applications for studying protein complexes, and more may be on the horizon. An overview of the possibilities is provided and many examples from the literature are discussed.

## 1.1 Introduction

Proteins function by interactions with other molecules. These can be small, such as enzyme substrates and allosteric modulators or large, such as lipids, polysaccharides, nucleic acids and other proteins. Protein-protein interactions (PPI) are ubiquitous in living organisms and vital to life. The nature of the interaction is tuned to biological function, from very strong and semi-permanent to weak and highly-transient. Structural characterization of protein-protein complexes can be done with X-ray diffraction of crystals, electron microscopy (EM), mass spectrometry or NMR. For stable, long-lived complexes the approach is largely the same as for single proteins and in those cases paramagnetic NMR is complementary. It can provide additional distance and angle restraints for structure calculations, solve symmetry problems in dimers and assist in mapping of binding sites. For weak complexes, which are difficult to crystallize and too unstable for EM, NMR is the only method that can provide atom-level insight. Not only can the stereospecific, ground state structure of the complex be characterized, also the dynamic encounter state can be studied. For PPI, the relevant paramagnetic effects are pseudocontact shifts (PCS), paramagnetic relaxation enhancement (PRE)<sup>2-5</sup> and paramagnetically induced residual dipolar couplings (piRDC).

## 1.2 Protein-Protein Interactions

The affinities of PPI range from picomolar to millimolar. For a simple complex of two proteins, the dissociation constant,  $K_D$  (in M), is the ratio of the dissociation rate constant ( $k_{off}$ , in  $s^{-1}$ ) and the association rate constant ( $k_{on}$ , in  $M^{-1}s^{-1}$ ):

$$K_D = \frac{k_{off}}{k_{on}} \quad (1.1)$$

The association of two proteins into a well-defined, stereospecific complex requires that the partners find each other via diffusion. The chance that they meet in the correct orientation to form the complex is very small, which implies that many collisions are non-productive. The number of collisions is limited by diffusion and is of the order of  $10^9 M^{-1}s^{-1}$ . However, for non-optimized PPI, the  $k_{on}$  –the rate constant for *productive* complex formation– will only be around  $10^4 - 10^5 M^{-1}s^{-1}$ , assuming that no major conformational changes are required to form the complex. If rapid formation of the complex is not required for its function, such association rates will be found. Association can be accelerated by electrostatic complementarity to enhance the chance of collision and the lifetime of the encounter. Also, if the charges are distributed non-symmetrically on the protein, creating a dipole, electrostatic pre-orientation during the encounter can favour certain collisional orientations over others. Thus, with complementary charged patches near the stereospecific binding sites on both proteins, the chance of colliding in approximately the correct orientation can be enhanced. In this way, the fraction of productive encounters, which lead to the active complex, can be dramatically enhanced, to  $k_{on}$  values near to the diffusion limit in favourable cases.<sup>6, 7</sup>

The biological function of the complex often determines the  $k_{\text{off}}$ . The lifetime of the complex is defined as  $1/k_{\text{off}}$ , so complexes that require a long life-time must have a low  $k_{\text{off}}$ , for example of the order of  $10^{-3} \text{ s}^{-1}$ . With  $k_{\text{on}} = 10^5 \text{ M}^{-1}\text{s}^{-1}$ , the affinity is then already in the low nanomolar range ( $K_D = 10^{-8} \text{ M}$ , see equation 1.1). For complexes that require even higher affinity, for example toxin-inhibitor complexes, the association rate constant is raised by electrostatic interactions, bringing the  $K_D$  in the picomolar range.<sup>8</sup> On the other end of the spectrum are the weak interactions, which are meant to exist fleetingly, such as electron transfer and cell signalling complexes. Their biological function is to act quickly, so  $k_{\text{off}}$  values are of the order of  $10^3 \text{ s}^{-1}$ . To still get some affinity –and thus specificity– electrostatic interactions are often invoked, resulting in  $K_D$  values in the micromolar range. Even weaker interactions, with  $K_D > 1 \text{ mM}$ , are observed in the case of self-association, i.e. dimerisation or polymerisation of proteins at high concentrations. Such interactions can be relevant in fibril formation.<sup>7</sup>

The association and dissociation rates have a direct bearing on the NMR spectra, because they determine the exchange regime. In very tight complexes, the amount of free protein can be neglected and exchange effects between free and bound forms will be minimal. However, in weaker complexes, the fraction of free protein will be significant. In ‘classic’ NMR the effects of exchange on the observed chemical shift and linewidth are well established and described by the McConnell equations.<sup>9</sup> In general, any NMR observable will exhibit averaging effects when a nucleus exchanges between states in which that observable has different values. As is explained below, in the case of paramagnetic NMR on protein-protein complexes, the paramagnetic centre is usually on one protein and the effects are observed on the other. Thus, for the complex, the paramagnetic effect is observed, whereas the free protein does not experience such an effect. In the case that the exchange rate ( $k_{\text{ex}}$ ) is very fast, of the order of  $10^3$  times faster than the difference between the frequencies of the NMR observable in the different states (expressed in  $\text{rad s}^{-1}$  for shifts and  $\text{s}^{-1}$  for relaxation), the measured value of the observable will be the average of the values of the individual states, weighted with their populations. This assumption is often made, but it should be realized that, in particular for PRE, it may not be valid, because PRE can be very large indeed for nuclei that are close to the paramagnetic centre, resulting in underestimation of the PRE in that state.<sup>10,11</sup> Therefore, it is common to use lower bounds only for restraints derived from large PRE.

### 1.3 The New Toolbox

For weak complexes, conformational changes often do not occur upon complex formation and only the binding site and orientation of the proteins need to be determined to establish the overall structure of the complex, provided the structures of the free proteins are available. In such cases, backbone labelling of the smaller protein and paramagnetic tagging of the larger one can provide sufficient information to obtain a model of the complex in solution. Paramagnetic NMR is particularly suited for the study of such protein complexes. The paramagnetic effects can usually be measured in simple 2D HSQC-like spectra, requiring only low sample concentrations. Due to the strong spin of an unpaired

electron, long-range effects can be observed when measuring paramagnetic nucleus-electron interactions.

PCS have been reported up to 70 Å (Figure 1.1) using a rigid tag and  $\text{Tm}^{3+}$  as the paramagnetic ion. Protein complexes are usually rather large and tags should not be close to the interface, so long-range distance restraints are necessary for structural characterisation. PCS are obtained by determining resonance positions in the spectra of the paramagnetic sample and a diamagnetic control that should be as similar as possible. Usually, this is achieved by using a sample with the same components except that the paramagnetic metal is replaced by a diamagnetic one with similar properties (e.g.  $\text{Lu}^{3+}$  for lanthanoids). PCS, like chemical shifts, can be measured with high precision and are described very well by the standard point-dipole approximation<sup>14</sup> for nuclei further than 5 Å from the paramagnetic centre. Contact contributions can generally be neglected for nuclei more than four bonds away and certainly in complexes in which one protein is tagged and the other observed. Thus, with the proper diamagnetic control PCS can be measured with high accuracy, and for larger PCS, also high precision. PCS of  $^1\text{H}$  nuclei are preferred over those of heavy atoms because the latter are more affected by residual chemical shift anisotropy and pRDC. It is non-trivial to determine the orientation and size of the  $\Delta\chi$  tensor and the location of the metal in the case of protein complexes, because the nuclei are in one protein and the centre is on the other. Ideally, these parameters are determined independently using a sample in which the protein with the paramagnetic centre is isotope-labelled. Then, the tensor is determined in the regular way described for free proteins.<sup>15</sup> If this is not possible, the tensor parameters must be optimized iteratively during the structure calculations.<sup>16</sup>

Paramagnetic centres with an anisotropic magnetic susceptibility (described by the  $\Delta\chi$  tensor) not only cause PCS but also induce partial alignment of the protein or protein complex in a strong magnetic field. Similar to alignment caused by external media (bicelles, gels, bacteriophages), residual dipolar couplings are observed as a consequence. In rigid complexes, the degree of alignment in the partner with the paramagnetic centre and

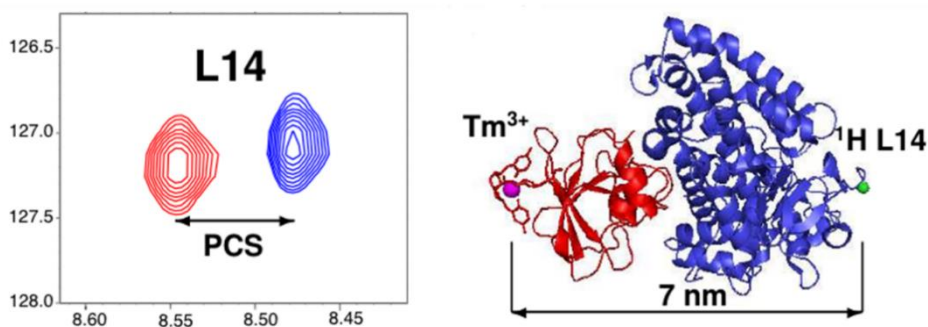


**Figure 1.1** Illustration of the long-range effect of PCS. A clearly significant intermolecular PCS was observed for the amide proton of Leu14 of cytochrome P450cam caused by a  $\text{Tm}^{3+}$  ion in the paramagnetic tag CLaNP-7<sup>12</sup> attached to putidaredoxin over a distance of 70 Å (7 nm).<sup>13</sup> Reprinted from<sup>1</sup>, Copyright (2014), with permission from Elsevier.

the one without is the same. Such intermolecular RDC can be used along with the PCS and PRE for determination of the structure of the complex. Perhaps even more interesting is the use of such piRDC to demonstrate the presence of dynamics in a protein complex, in analogy to multidomain dynamics.<sup>17</sup> RDC are not dependent on the distance between paramagnetic centre and the nuclear vector, only on the degree of alignment. If the partners in a complex show dynamics, the alignment of the protein without the paramagnetic centre will be reduced relative to that of the protein that contains the centre (see below).

PRE effects at 35-45 Å can be measured in cases where the complex is big, resulting in a long rotational correlation time ( $\tau_c$ ), and  $Gd^{3+}$  is used as the paramagnetic centre.<sup>2,7</sup> PRE are normally generated by paramagnetic centres with long electronic relaxation times (> 100 ns), such as spin labels and  $Gd^{3+}$  ions. Such systems are isotropic, implying the absence of PCS and piRDC. Relaxation is then dominated by Solomon dipole interactions.<sup>14</sup> An advantage is that only peak intensity reductions occur due to PRE but no resonance shifts, so reassignment of the spectrum is not required. PRE are particularly sensitive to minor states, such as present in ensembles of the encounter state. Apart from the stereospecific complex, other orientations of the proteins in the complex occur, collectively forming the encounter state. In particular in a weak complex with strong electrostatic interactions, the fraction of the encounter state can be prominent, as will be discussed in more detail later. The encounter state is best described as an ensemble of orientations that rapidly interconvert. The orientations in which an observed nucleus approaches a paramagnetic centre closely will result in (very) high PRE for that nucleus. Consequently, even orientations within the complex with a low population can be detected due to the PRE. Thus, this paramagnetic effect has been instrumental in the description of encounter complexes.

Similarly, paramagnetic centres that are not attached to a protein but are used as co-solutes cause PRE on the protein nuclei near to the solvent. By comparing such 'solvent PRE' (sPRE) for free protein and protein in a complex, binding sites can be identified due to a shielding effect in the complex from the sPRE effect.<sup>18</sup> The sPRE data are dependent on the kind of probe, its concentration and solubility limit. Usually sPRE are expressed as the increase in relaxation rates or decrease of signal intensities per mM of paramagnetic probe. Metal ions, organic radicals or metal chelates have been used as probes.<sup>19</sup> For example,  $[Gd-DOTAM]^{3+}$  and  $[Gd-DOTP]^{5-}$  are two charged paramagnetic probes tested in the study of the protein-protein complex formed by rubredoxin and cytochrome  $c_3$ , two proteins with opposite charges at their binding sites. sPRE experiments based on the interactions of the two probes with the surface of the proteins allowed to gain information about charged patches on the protein surface and to characterize the binding site in the protein complex.<sup>20</sup>

As each of the paramagnetic effects has its peculiarities, it is emphasized that combining restraints based on PCS, RDC and PRE is a safeguard against biased results. For example, structure calculations based only on PRE may be prone to bias toward minor states, because the PRE is so sensitive to those. Such minor states can also represent weak non-specific interactions in concentrated protein solutions. PCS and RDC are not sensitive to such interactions because the effects will be weaker and, anyway, average out for dynamic

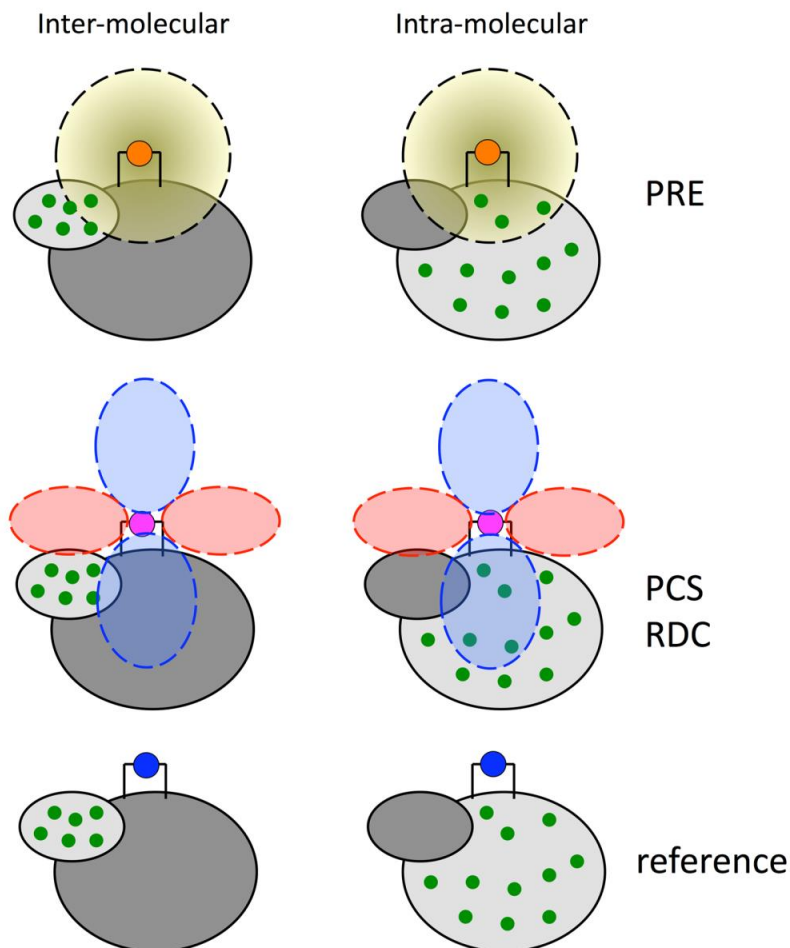


**Figure 1.2** Strategy for measuring PCS, PRE and piRDC for structure determination of protein–protein complexes. Six samples are produced. PRE are extracted from a complex tagged with an isotropic paramagnetic centre, for example,  $\text{Gd}^{3+}$ . PCS and RDC are obtained from complex tagged with an anisotropic paramagnetic centre, for example,  $\text{Tm}^{3+}$ . A diamagnetic control complex, for example tagged with  $\text{Lu}^{3+}$ , serves a reference. To decrease signal overlap the inter-molecular and intra-molecular are determined independently with different samples in which either one or the other proteins is isotope labelled (green dots). The intra-molecular restraints are used to position the paramagnetic centre and orient the magnetic susceptibility tensor. A combination of ten 2D spectra (such as TROSY and HSQC) is sufficient to obtain a complete set of intermolecular and intra-molecular PRE, RDC, and PCS. Reprinted from<sup>1</sup> Copyright (2014), with permission from Elsevier.



systems.<sup>21</sup> PCS are dominated by their distance dependence, whereas RDC are distance independent and sensitive to rotation but not translation. RDC are also less tolerant than PCS to variations in the structures of the free proteins.<sup>22</sup> All three effects are degenerate because none determine a unique position of a nucleus relative to the paramagnetic centre. For example, the PRE depends on the distance  $d$  in an isotropic way, thus a PRE only defines a sphere with radius  $d$  around the centre on which the nucleus will lie. Similarly, multiple combinations of two angles and a distance of the position of a nucleus in the frame of the  $\Delta\chi$  tensor yield the same PCS. It is advisable to use data from more than a single paramagnetic centre for the purpose of triangulation. Also the use of data from techniques other than paramagnetic NMR (NOE, SAXS, EPR, FRET) can help to reduce bias.<sup>23,24</sup> It is noted, however, that paramagnetic NMR is capable of delivering a wealth of information because paramagnetic spectra yield hundreds of data points in one experiment, one for each nucleus, whereas FRET and EPR usually produce a single distance for one sample.<sup>25</sup> Figure 1.2 shows schematically which set of experiments is required to obtain a complete set of PCS, RDC and PRE for structure determination of a protein complex.

Various tags can be used to introduce paramagnetic centres.<sup>26</sup> Clearly, for long-range effects, the stronger paramagnetic metals ( $\text{Tm}^{3+}$ ,  $\text{Tb}^{3+}$ ,  $\text{Dy}^{3+}$ ,  $\text{Er}^{3+}$ ) should be used. Also, the more rigid the centre is relative to the protein, the less averaging effects will occur, resulting in larger and more accurate paramagnetic effects.

## 1.4 Tight Complexes: Breaking Symmetry

Structure determination of tight obligate or non-obligate complexes<sup>27</sup> can be performed via the classic approaches (XRD, EM, NMR). Paramagnetic NMR can provide distance and angle restraints additional to NOE and chemical shift information. A particular application of paramagnetic NMR is in breaking the symmetry in dimers. Solving the structure of a dimer composed of symmetric units can be very difficult using conventional NMR because of the necessity to distinguish between NOE generated by nuclei within one subunit (intra-subunit NOE) and those generated by nuclei in different subunits (inter-subunit NOE). Several solutions have been proposed, such as asymmetric isotope labelling in combination with filtered NOESY experiments,<sup>28</sup> or by computationally extracting the correct orientation of one of the two units in the complex using a function describing the contributions generated by intra- and intermolecular NOE.<sup>29</sup> Another solution is offered by paramagnetic NMR, which can give an unambiguous answer to the symmetry problem and at the same time provide long-range intermolecular restraints for the determination of the structure of the dimer. The solution consists of tagging of just one of the two subunits with a paramagnetic centre. By tagging only one of the subunits, asymmetry is introduced that is reflected in the generation of non-equivalent paramagnetic effects, e.g. PCS for nuclei in the tagged subunit (intra-subunit PCS) and in the untagged subunit (inter-subunit PCS).<sup>30</sup> CylR2, a protein involved in the cytolysin production in *Enterococcus faecalis*, forms a symmetric homodimer of 15.4 kDa. The structure in solution was determined using

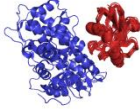
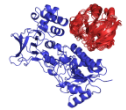
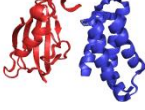
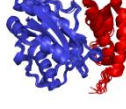
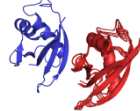
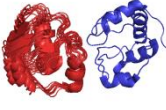
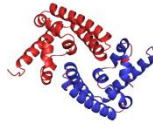
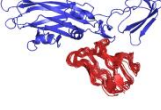
different sources for experimental intersubunit information, followed by rigid-body docking. The following sets of restraints were compared: PRE, PRE and RDC, PRE, NOE and RDC, and NOE and RDC. PRE were collected using two samples of single mutants of CylR2 tagged with MTSL at different locations. The structure obtained with only PRE deviated from the X-ray structure used as reference with a backbone root means square deviation (RMSD) of 3.0 Å, and the addition of RDC reduced the deviation to 1.5 Å. The combination of PRE, RDC and NOE increased the accuracy of the model slightly, whereas restraints from only NOE and RDC showed a deviation of 2 Å from the crystal structure. Docking without experimental restraints yielded an accuracy comparable to the one obtained with only the set of experimental PRE. The inclusion of RDC restraints gave a high-resolution structure.<sup>31</sup>

## 1.5 Ground States Structures of Protein Complexes

In cases where determination of the structure of a protein complex is difficult using XRD and classic NMR approaches, paramagnetic NMR can offer a valid alternative, at least for cases in which the individual structures are available and no backbone conformational changes occur upon complex formation. Paramagnetism can provide long-range restraints for rigid-body docking to determine the location and orientation of the partners in the complex. In principle, also conformational changes upon complex formation can be modelled, provided sufficient restraints are obtained. However, inherent in measuring long-range distance restraints is that they are less sensitive for small structural variations, so contrary to NOE, paramagnetic restraints obtained with strong paramagnetic centres are not suitable for modelling details of structures. Weak paramagnetic centres provide information over shorter distances, as do contact contributions but they require the centre to be close to the nuclei of interest. Thus, the structures of protein complexes reported so far have usually been obtained via rigid body docking on the basis of the paramagnetic restraints. Table 1.1 gives examples of such structures based on anisotropic paramagnetic centres (PCS/RDC data).<sup>1</sup> The idea to determine a protein-protein complex structure through PCS was applied for the first time to the transient complex of two photosynthetic electron transfer proteins from plants, plastocyanin and cytochrome *f*.<sup>32</sup> The low-spin paramagnetic haem Fe<sup>3+</sup> ion in cytochrome *f* was used to generate intermolecular PCS in <sup>15</sup>N labelled plastocyanin. The structure showed how a short electron transfer pathway can be formed between the haem in the cytochrome and the copper in plastocyanin, in line with the rapid electron transfer that occurs between these proteins, solving a long-standing debate about the main site of interaction of plastocyanin. The use of naturally occurring paramagnetic ions is, unfortunately, only possible in few cases. In the structure determination of the 30 kDa complex of the  $\theta$  subunit and the N-terminal domain of the  $\epsilon$  proof-reading exonuclease subunit,  $\epsilon$ 186, from *Escherichia coli* polymerase III, tagging of the proteins was also not necessary.<sup>22</sup> In this case, metal-substitution was used to create a paramagnetic centre within the  $\epsilon$  subunit. The pair of divalent cations (Mn<sup>2+</sup>/Mg<sup>2+</sup>) in its active site were substituted by lanthanoid ions. Dy<sup>3+</sup> or Er<sup>3+</sup> were used generate inter-subunit PCS, whereas the diamagnetic control was the apo-complex. The rigid-body structure of the complex

## Chapter 1

**Table 1.1** Structure of protein complexes solved using restraints from anisotropic paramagnetic centres. Reprinted from<sup>1</sup>, Copyright (2014), with permission from Elsevier.

Molecule 1 (mass)	Molecule 2 (mass)	Paramagnet	Tag/Me- ligand	Structure	Reference (PDB ID)	Comment
Cyt P450cam (45 kDa)	putidaredoxin (11 kDa)	Tm <sup>3+</sup> , Gd <sup>3+</sup>	ClaNP-7		[24] (2M56)	
ADR (51 kDa)	Adrenodoxin (14 kDa)	Tm <sup>3+</sup> , Eu <sup>3+</sup> , Gd <sup>3+</sup>	ClaNP-5		[34] (not in PDB)	
FKBP12 (12 kDa)	mTOR FRB (11 kDa)	Dy <sup>3+</sup> , Tb <sup>3+</sup>	LBT- peptide		[28] (2RSE)	
ε186 (21 kDa)	Θ (9 kDa)	Dy <sup>3+</sup> , Er <sup>3+</sup> , Ho <sup>3+</sup>	Native Mg <sup>2+</sup> /Mn <sup>2+</sup> site		[29,39] (2XY8)	
PB1 (10 kDa)	PB1 (10 kDa)	Tb <sup>3+</sup> , Dy <sup>3+</sup> , Er <sup>3+</sup> , Tm <sup>3+</sup>	LBT- peptide		[35] (2KTR)	Asymmetric homodimer
Cyt c (12 kDa)	Adrenodoxin (12 kDa)	Fe <sup>3+</sup>	Native heme		[43](2JQR)	Covalently cross-linked
STAT-4-NT (14 kDa)	STAT-4-NT (14 kDa)	Co <sup>2+</sup>	EDTA tag		[38] [58] <sup>a</sup> (1BGF) <sup>a</sup>	Symmetric dimer
Cyt f (27 kDa)	plastocyanin (11 kDa)	Fe <sup>3+</sup>	Native heme		[36] (2PCF, 1TU2,1TKW,2J XM)	Solved for different species

<sup>a</sup> Crystal structure, no solution structure deposited

obtained using PCS based restraints was verified with NOE measured in complexes composed of  $^{15}\text{N}/^1\text{H}$  labelled  $\epsilon 186$  and unlabelled  $\Theta$  as well as with  $^{15}\text{N}$  labelled  $\Theta$  and unlabelled  $\epsilon 186$ .

An early example of structure determination of a non-metalloprotein complex using paramagnetic tagging with a double-arm LBP<sup>26</sup> is provided by the p62 PB1 domain.<sup>33</sup> p62 is a multidomain protein involved in autophagy.<sup>34</sup> It forms multimers through PB1 domain interactions in a front-to-back fashion but it was possible to obtain a 20 kDa dimer of the PB1 domain through mutagenesis. PCS generated by four different lanthanoid ions were used to solve the structure of the dimer.<sup>35</sup>

The power of PCS in the determination of protein-protein complexes was also illustrated by the large complex (65 kDa) of adrenoxin reductase (AdR) and adrenodoxin (Adx) using the CLaNP-5 tag.<sup>36,37</sup> This complex is part of the electron transfer pathway from NADH to mitochondrial cytochromes P450 in the adrenals. In this study, AdR (51 kDa) was tagged at two positions and Adx (14 kDa) was isotope-labelled with  $^{15}\text{N}$  and  $^2\text{H}$  for observation. Inter-subunit PCS, generated by  $\text{Tm}^{3+}$ -CLaNP-5, and PRE, ( $\text{Gd}^{3+}$ ) were used to dock Adx on AdR on the basis of the structure of the free proteins.<sup>16</sup> The  $\Delta\chi$ -tensor parameters for  $\text{Tm}^{3+}$ -CLaNP-5 were optimized during the docking in an iterative approach. No NMR information on AdR was used in this study. A complicating factor was the naturally occurring paramagnetic FeS cluster in Adx. In this case, this cluster could not be used to generate restraints, as no assignments were available for AdR nuclei. Rather, it complicated the study because its relaxation properties broaden out the signals from many hydrogens in its environment. The cluster is close to the interface in the complex, so most of the resonances of Adx that could be expected to exhibit chemical shift perturbations upon complex formation were not observed. However, the inter-subunit PCS are long-range (up to 56 Å in this case) and could be observed for Adx nuclei far from the cluster and the binding site and the derived restraints could be used for rigid-body docking. The calculated location and orientation of Adx on AdR were in good agreement with a crystal structure of the complex obtained via cross-linking.<sup>38</sup>

## 1.6 Dynamics and Encounter States

Figure 1.3 gives a schematic model of the process of protein complex formation. When two freely diffusing protein molecules approach each other, they will, generally, not collide in the correct orientation to form the stereospecific complex. First, an encounter complex is formed in which the partners sample multiple orientations by rotational diffusion and weak interactions. Encounters can be futile, i.e. not lead to the stereospecific complex. The proteins part again without having formed a productive complex.<sup>39</sup> In other cases, the encounter complex will proceed to the stereospecific complex, a productive encounter. In that case the association is successful. The association rate constant  $k_{\text{on}}$  reports successful encounters. As explained above, the fraction of productive encounters can be increased by prolonging the encounter state and directing the partner toward the stereospecific binding site. Prolongation of the encounter state enables the proteins to sample a larger area of the

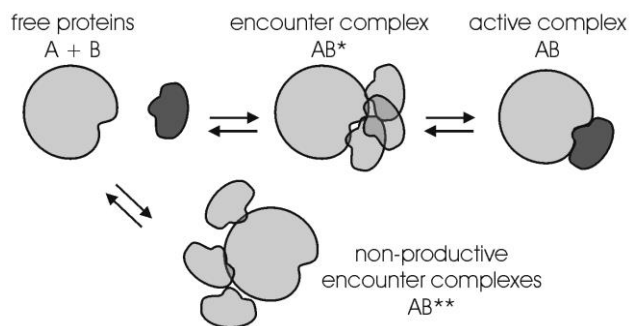


**Figure 1.3** Model for protein complex formation. The free proteins A and B can associate in productive or non-productive encounter complexes. The former can evolve into the active, stereospecific complex.

partner, in what has been considered as a reduced dimensionality search for the binding site.<sup>40,41</sup> Directing the partner to the binding site reduces the sampling of irrelevant areas. Both effects can be achieved by complementary charge interactions and also hydrophobic contacts in the encounter state can lead to enhanced association rates.

Paramagnetic NMR techniques have played an essential role in providing evidence for the model of protein complex formation and the characterisation of the encounter states. These states usually (though not always, see below) represent a small fraction of the complex, with the proteins being the stereospecific complex the majority of the time. Furthermore, it appears from many studies that chemical shift perturbations in the encounter state are minimal. They are mostly caused by the interactions in the stereospecific state. The chemical shift perturbations observed in  $^{15}\text{N}$ - $^1\text{H}$  HSQC-like spectra are due to changes in the polarization and hydrogen bond formation propensity of the amide groups, requiring changes in solvation. It is likely that in the encounter state the proteins are still fully solvated, so no large chemical shift changes are expected. The encounter state consists of an ensemble of many orientations in fast exchange, making it hard to detect NOE or indeed PCS and impossible to crystallize. PRE, with its sensitivity for minor states, is excellently suited for the characterization of encounter states. Orientations in which nuclei are brought close to a spin label will result in a PRE, even if the population of that orientation is very low ( $< 1\%$ ). However, the observed PRE is an average of all orientations, provided they are in fast exchange relative to the largest PRE (which can several  $1000\text{ s}^{-1}$ ). As an infinite number of combinations of orientations can yield the same average PRE, it is not possible to determine the orientations present in the encounter ensemble directly from the PRE. Additional assumptions and models must be invoked to visualize the encounter state.<sup>17</sup> By using PRE tags on multiple sites on the protein surface and observing the effects on the partner protein it is possible to map the areas that are *not* visited. In this way, an exclusion map can be made, limiting the extent of the encounter state.<sup>42-46</sup> The absence of inter-molecular PRE is the most solid evidence obtained in such experiments. Observing PRE indicates that the region where the tag is localized is being visited but not to what extent. It is possible that nuclei that experience the PRE get very close to the tag very briefly or

spend more time at a somewhat larger distance. The effect on the average PRE will be the same. It should also be realized that tags can influence the complex. For structure determination of ground states, its effects are easily spotted, because chemical shift perturbations or the  $K_D$  of the complex with the tagged protein may differ from the WT complex. Such tag positions should then be discarded. However, tags may also affect the encounter state and such effects may go unnoticed. It is thus advisable to use small tags, such as MTSL, and use data from many locations on the protein surface. Several examples of encounter state complex studies will be discussed later.

Some processes, like the formation of crystals, viral capsids, amyloid fibrils or amorphous aggregates, are driven by the spontaneous association of macromolecules, identical subunits that form a complex of a high level of order. During the formation of these structures, the molecules shift from the free state in solution to a macromolecular cluster by employing ultra-weak intermolecular interactions ( $K_D > 1$  mM). Visualization of the complexes formed by ultra-weak interactions is particularly difficult with most common biophysical techniques because their population is extremely low. In principle PRE can be used to explore such complexes and elucidate the nature of the ultra-weak association because of its high sensitivity to lowly populated states. This approach was employed to investigate the properties of the formation of non-fibrillar oligomers formed by the amyloid  $\beta$  (A $\beta$ ) peptide,<sup>47</sup> which could be the primarily responsible agent for neurotoxicity in the Alzheimer's disease. While A $\beta$  fibrils are extremely stable, it was found that the A $\beta$ (1-40) peptide forms large, dynamic oligomers, in which the peptide state changes continuously from the free to the bound state. No transverse PRE rate enhancements were measured above the reliable detection limit of about 5 s<sup>-1</sup>. Since the PRE experiment is able to visualize lowly populated states in fast exchange, it was concluded that the population of transient oligomers amounts to less than 1-2%, or that the exchange between bound and free state is slow on the PRE time scale (<ca. 1 ms).

## 1.7 Examples of Applications

### 1.7.1 Breaking the Symmetry of the STAT4 Complex

Paramagnetic NMR was used to break the symmetry and determine the structure of the 28 kDa symmetric complex formed by two copies of the N-terminal domain of STAT4 (STAT4<sub>NT</sub>).<sup>30</sup> STAT4 is involved in signal transduction and activation of transcription in hematopoietic cells, required for the differentiation of Th1 cells and optimal IFN- $\gamma$  production.<sup>48</sup> The complex was tagged sub-stoichiometrically with a thiol-reactive EDTA bound to Co<sup>2+</sup> as paramagnetic probe, labelling just one subunit. It was then possible to obtain PCS and RDC, providing long-range restraints, both for distance and orientation, to understand how the two subunits bind. The PCS observed for the nuclei in one subunit were mostly of the opposite sign compared to those for nuclei in the second subunit, which facilitated the analysis. Moreover, the comparison between the observed PCS and those calculated on the basis of the crystal structure and the NOE-derived structure of the subunit showed a good correlation. The PCS were then used as unambiguous intermolecular

orientational and distance restraints to study the molecular dynamics and establish the orientation of the two subunits in the dimer in solution, obtaining a structure that agreed well with the PCS restraints. The RDC were used to determine the relative orientation of the two subunits independently from the PCS, obtaining the same result. This approach is a good solution for symmetry problems in dimers, in particular for large complexes for which perdeuteration is necessary.

### ***1.7.2 Synaptotagmin-1-SNARE Complex***

A recent example of application of PCS to study dynamics in a protein-protein complex is the work on the synaptotagmin-1 C<sub>2</sub>B domain bound to the SNARE complex, with a total size of the complex of 51 kDa.<sup>49</sup> One of the processes which allow a neurotransmitter to be released is Ca<sup>2+</sup> dependent and the mechanism is controlled by proteins like synaptotagmin-1 (Syt1) and the SNARE complex, comprising synaptobrevin, syntaxin-1 and SNAP-25. The interactions between Syt1 bound to Ca<sup>2+</sup>, the SNARE complex and complexins allow Syt1 to rapidly release the neurotransmitter, but a molecular model of the mechanism was still lacking, because no high-resolution structure of Syt1-SNARE complex was available. PCS induced by tagging the SNARE complex at two sites with the Dy<sup>3+</sup>-C2 probe<sup>50</sup> were used to investigate the nature of the Syt1:SNARE complex. The paramagnetic effects on Syt1 show that the basic region on the C<sub>2</sub>B domain of Syt1 binds to an acidic region of the SNARE complex, constituted by residues of syntaxin-1 and SNAP-25. On the basis of these and other results a model for the role of Syt1 in membrane fusion was proposed. Moreover, the complex was found to be dynamic, as it was not possible to explain the PCS data by a single location and orientation of Syt1 with respect to the SNARE complex. It is possible that the dynamic nature of the Syt1-SNARE complex is necessary for the complex function, to allow a fast release of the neurotransmitter.

### ***1.7.3 Cytochrome *f* and Plastocyanin***

In photosynthesis, inter-protein electron transfer needs to be fast to avoid limiting the overall rate of the light reactions that are responsible for the production of NADPH and ATP, required for carbon fixation. A key electron transfer step is the one from cytochrome *f* (Cytf) in the cytochrome *b<sub>6</sub>f* complex to the copper protein plastocyanin (Pc). Pc shuttles the electrons, one at a time, to photosystem I. In different branches of the tree of life, it appears that different solutions have been found to ensure rapid formation and dissociation of the Cytf-Pc complex. To obtain fast electron transfer from one redox centre (the haem in Cytf) to the next (the copper ion in Pc), Marcus theory<sup>51</sup> states that the distance between the

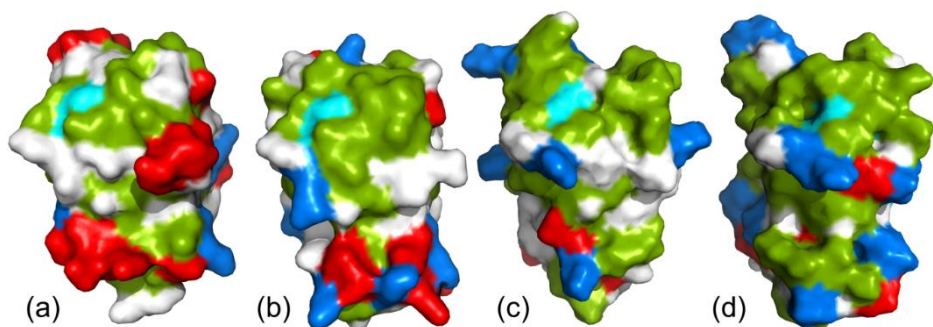


**Figure 1.4** Surfaces of Pc for which the complex with Cytf was determined. (a) Spinach<sup>57</sup> (PDB entry 1AG6); (b) *Phormidium laminosum* (PDB entry 2Q5B); (c) *Prochlorothrix hollandica*<sup>58</sup> (PDB entry 1B3I); (d) *Nostoc* sp. (*Anabaena variabilis*)<sup>59</sup> (PDB entry 1NIN). Pc is shown in surface representation coloured according to surface charge, with red for Asp and Glu and blue for Lys and Arg residue. His residues are in cyan. Aliphatic and aromatic groups are in green. The figure was produced using PyMol (The PyMOL Molecular Graphics System, Version 1.3 Schrödinger, LLC)

centres should be short ( $< 16 \text{ \AA}$ ,<sup>52</sup>). As long as the distance is short and the proteins make contact to reduce the penalty of through-space exchange coupling, the exact orientation of the proteins does not matter for electron transfer, contrary to reactions in which atoms are transferred. Thus, the aim in electron transfer complexes is not necessarily to reach a single stereospecific complex. Rapid formation and dissociation are more important. Consequently, it is observed that in such complexes often the encounter state represents a large fraction of the complex.

The first Cytf-Pc complex studied was that of plants. The plant Pc has a hydrophobic patch close to one of the ligands of the copper ion and a negative patch on the side of the protein (e.g. PDB entry 4PCY<sup>53</sup>), illustrated in Figure 1.4. Plant Cytf is mostly negative but has positive residues in a patch close to the haem group.<sup>54</sup> Thus, it is no surprise that complex formation depends much on the ionic strength, indicating a favourable electrostatic interaction.<sup>55</sup> Intermolecular PCS from the Cytf haem iron on isotope labelled Pc could be observed and used to dock Pc in a well-defined orientation on Cytf.<sup>32</sup> The results suggested the presence of an orientation that was populated for a considerable fraction of the time, but the data also provided evidence that the complex visited an encounter state. The well-defined state (PDB entry 2PCF) clearly showed that fast electron transfer was possible from the iron to the copper via the His ligand located in the hydrophobic patch of Pc. See Figure 1.4, in which the cyan surface represents His and the hydrophobic areas are coloured green. Subsequent work on the same complex from the cyanobacterium *Phormidium laminosum* showed a different picture.<sup>56</sup> This complex was much less sensitive to the presence of salt, suggesting a reduced role of electrostatic interactions. This finding was in line with the surface of *P. laminosum* Pc, which lacks the negative patch (Figure 1.4). Cytf from *P. laminosum*, on the contrary, is overall very negatively charged, indicating that the lack of electrostatic interactions is due to the properties of Pc. Again, intermolecular PCS could be



detected, however, a single structure could not describe the data. An ensemble of orientations was necessary to obtain a reasonable fit and in this ensemble Pc only binds via its hydrophobic patch, contrary to plant Pc. Results intermediary between plant and *Phormidium* were obtained for the complexes from *Nostoc*<sup>60</sup> and *Prochlorothrix hollandica*.<sup>61</sup> The Pc surfaces are not highly charged, similar to *Phormidium* Pc (Figure 1.4). As the studies indicated the presence of a substantial fraction of encounter complex, *Nostoc* Cytf was tagged with MTSL radicals to generate intermolecular PRE on Pc and sample the Cytf surface area that is visited.<sup>62-64</sup> It was observed that Pc samples a large area of Cytf in approximately the same orientation, involving a prominent positive residue (Arg) and the Pc hydrophobic patch. Electrostatic calculations clearly demonstrate that charge interactions alone cannot explain the encounter orientations observed. Hydrophobic interactions also contribute to the stability of the encounter complex in the *Nostoc* Cytf-Pc complex, in line with theoretical studies.<sup>65,66</sup> This work led to a model in which the rate of the formation of an electron transfer active complex is enhanced by gradual increase of the hydrophobic overlap between the surface of Cytf and Pc to smooth out the transition barrier of desolvation (Figure 1.5).<sup>63</sup>

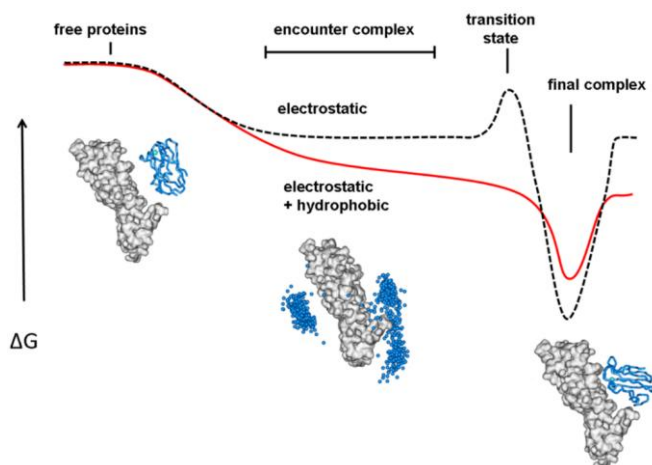


**Figure 1.5** Free energy diagrams of association pathways with high (dashed black line) and no (solid red line) energy barrier for the transition state from the encounter to the final complex. Complexes based on electrostatic interactions are proposed to follow the dashed line because formation of the stereospecific complex requires the interaction interface to go from solvated to desolvated abruptly. If hydrophobic interactions gradually increase in the encounter state, the desolvation occurs more smoothly resulting in a smaller energetic barrier (red line), increasing the association rate. Reprinted with permission from <sup>63</sup>. Copyright 2010 American Chemical Society.

### 1.7.4 Cytochrome *f* and Cytochrome *c*<sub>6</sub>

Interestingly, in some organisms, in the photosynthetic redox chain Pc (see previous section) can be substituted by a cytochrome, cytochrome *c*<sub>6</sub> (Cc6) to accept electrons from Cytf. Cc6 is a *c*-type cytochrome (with a covalent haem group) with a molecular mass of 10 kDa. The complex of Cc6 and Cytf was reported to be dynamic and hydrophobic interactions are involved in the interaction.<sup>67,68</sup> Intermolecular PRE were generated by tagging Cytf from *Nostoc* with MTSL on five positions surrounding the haem, and measured on isotope-labelled Cc6. The resulting distance restraints were used for rigid-body docking calculations.<sup>69</sup> Large PRE were measured for each of the tagged Cytf molecules and the PRE effects were mostly found in the region on Cc6 that also displays most of the chemical shift perturbations upon complex formation. This observation was explained by assuming that Cc6 pre-orientates upon its approach of the Cytf, due to long-range electrostatic interactions between the positive patch on Cc6 and the wide-spread negative charges on Cytf. Moreover, it was not possible to explain the PRE data with a single orientation of Cc6 with respect to Cytf. Instead, the PRE were well described by an ensemble of orientations in which Cc6 samples mostly the hydrophobic patch close to the haem on Cytf, describing a form of “hydrophobic sliding” in which the desolvation of the hydrophobic patches increases gradually leading to the most stable orientations, very similar to what was described for Pc (Figure 1.5).<sup>69</sup>

### 1.7.5 Cytochrome *c* and Adrenodoxin

Cc is a small (12.5 kDa) haem protein found in mitochondria. Adx (11 kDa) was already mentioned in the section “Ground states structures of protein complexes”. Both proteins are electron transfer proteins, involved in shuttling electrons from one enzyme to the next. As they occur in different compartments of the cell, it is not expected that they form a physiologically relevant complex. Interestingly, however, electrons can be rapidly transferred from Adx to Cc and this reaction has been used as a substitute for the natural reaction of Adx with cytochromes P450. In line with what was discussed on electron transfer complexes above (section “Cytochrome *f* and plastocyanin”) it can be expected that between two small proteins, with the redox centres relatively close to the surface, electron transfer should occur in many orientations and a single stereospecific complex does not need to be formed for activity. This hypothesis was tested by establishing the degree of dynamics in the Cc-Adx complex with the use of paramagnetic NMR. One study used the paramagnetic centres in Cc (low-spin haem Fe<sup>3+</sup>) and Adx (FeS cluster) to generate intermolecular PCS and PRE, respectively on both the native complex and a cross-linked form that served as a model for a well-defined stereospecific complex.<sup>70</sup> In the crosslinked form, both intermolecular PCS and PRE could be detected and also the chemical shift perturbations due to complex formation were significant. In the native complex, all these effects were eliminated due to averaging, indicative of high mobility. MTSL tagging of Cc caused PRE over a large area of the Adx surface, again indicating extensive mobility in the complex. Ultimate proof was given by attaching a CLaNP-5-Yb<sup>3+</sup> tag on Cc and measuring

the RDC on both Cc and Adx in the native complex. The RDC for Adx were insignificant, whereas for Cc they were readily measured.<sup>71</sup> Thus, extensive mobility must be present in the complex, which was described as a pure encounter complex. This work demonstrates that indeed in the small redox proteins electron transfer can occur rapidly in the absence of a stereospecific complex, in line with Marcus theory.

### 1.7.6 Cytochrome P450cam and Putidaredoxin

A combination of PCS, RDC and PRE was used in the recent determination of the solution structure of the complex of cytochrome P450cam (P450cam) and putidaredoxin (Pdx), which was subsequently confirmed by crystallography. It showed the power of paramagnetic NMR, as not only did it establish the orientations of the proteins in the complex in solution, the work also identified the presence of a lowly populated encounter complex.<sup>13</sup> P450cam is a soluble haem enzyme that catalyses the oxidation of camphor using molecular oxygen. It receives electrons from the small iron-sulphur protein Pdx. At the time, the structures of the free proteins were available but that of the complex was lacking. P450cam was tagged with CLaNP-7<sup>12</sup> at two sites and Pdx at one. Amide assignments for both proteins were available and extended.<sup>72,73</sup> Intramolecular PCS from CLaNP-7(Yb<sup>3+</sup>) were used to establish the  $\Delta\chi$ -tensor orientations and intermolecular PCS, RDC (using Tm<sup>3+</sup>) and PRE (Gd<sup>3+</sup>) were obtained with CLaNP-7(Lu<sup>3+</sup>) as the diamagnetic control. In this way, 446 restraints were obtained to dock Pdx as a rigid body on P450cam, resulting in an ensemble of structures with an average root mean square deviation of 1.3 Å for the heavy atoms from the mean. Independently, the crystal structure was determined by the same authors and by another group,<sup>13,74</sup> showing Pdx in the same position as in the solution structure (Figure 1.6). All PCS and RDC restraints as well most of the PRE distances were satisfied very well by the calculated structure. However, the distances derived from the PRE of Pdx amide hydrogens from one of the tags on P450cam were much shorter than those calculated from the final structure (Figure 1.6). This observation suggested that Pdx assumes another state(s) in which it approaches that tag more closely than in the major, stereospecific complex. The PCS and RDC data were fitted well, suggesting that the additional state had a low population and was picked up by the PRE effects only because of their exquisite sensitivity for minor states. Further tagging with CLaNP-7 and MTSL on both Pdx and P450cam confirmed the presence of an encounter state with a population of only a few percent, in which Pdx samples the surface of P450cam widely and in various orientations. Detailed calculations using the MaxOR approach<sup>17</sup> were applied to an encounter complex for the first time, leading the identification of sites that were thought to represent productive encounters and others suggested to be futile encounters.<sup>75</sup>

The crystal structures of the complex had suggested that P450cam opens its substrate entry channel upon binding of Pdx. EPR and modelling studies also provided evidence for this.<sup>76-78</sup> To test this model in solution at ambient temperature, a CLaNP-7 tag loaded with Yb<sup>3+</sup> was attached to one of the  $\alpha$ -helices that constitute the cover of the entry channel. PCS were

obtained for amide nuclei in P450cam, selectively labelled with  $^{15}\text{N}$ -Leu in the absence and presence of Pdx, clearly showing that no changes occurred upon Pdx binding. The observed PCS fitted the closed structure much better than the open structure. These results suggested that in solution P450cam does not open its substrate entry channel, or at most very slightly.<sup>79</sup>

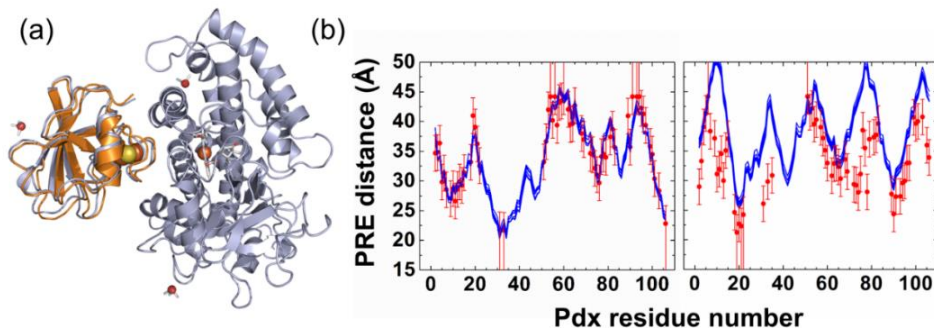


**Figure 1.6** The complex of P450cam and Pdx. (a) The crystal structure (orange) and the solution structure closest to the mean (gray) of the oxidized Pdx–P450cam complex are shown in a ribbon representation with the P450cam structures aligned. The positions of  $\text{Ln}^{3+}$  ions,  $\Delta\chi$  tensors and redox centers of Pdx and P450cam are depicted in sticks and spheres. (b) Violation analysis of PRE-derived distances plotted against Pdx residue numbers. Red circles and blue lines represent experimental and back-calculated effects for the 10 lowest-energy solutions, respectively. The left panel shows that the calculated structures fit the PRE obtained from probe A for Pdx nuclei. The right panel shows that Pdx nuclei experience larger PRE (shorted distances) from probe B than predicted by the 10 lowest-energy structures, presenting evidence for an encounter state. Reprinted from <sup>13</sup>, Copyright (2013), with permission from Elsevier.

### 1.7.7 Ferredoxin, Ferredoxin:Thioredoxin Reductase and Thioredoxin

The study of the complex formed by ferredoxin (Fd), ferredoxin:thioredoxin reductase (FTR) and thioredoxin (Trx) is a good example of how X-ray crystallography and paramagnetic NMR can complement each other to obtain a more complete picture of how a protein complex is formed and functions. These three proteins form a ternary electron transfer complex, as part of the signalling pathway that links the light reactions of oxygenic photosynthesis with the carbon fixation reactions in the Calvin cycle. The structure of the ternary complex was visualized by X-ray crystallography showing that Fd and Trx bind on either side of the flat, elongated FTR surface, allowing them to bind simultaneously and form a redox chain (PDB 2PVO).<sup>80</sup> In the structure, FRT is cross-linked to a cysteine of Trx through a transient intermolecular disulphide bond. The formation of this intermediate complex was further investigated using paramagnetic NMR, exploiting the presence of a  $[\text{4Fe-4S}]$  cluster in FTR. Intermolecular PRE data for Trx were used as distance restraints for docking of Trx on FTR, obtaining a model of the intermediate that precedes the

formation of the transient crosslink. The NMR-based model shows Trx in an orientation in the noncovalent complex that differs from that in the cross-linked crystal structure, suggesting it needs to rotate about 50° to proceed to the cross-linked complex.<sup>81</sup>

### 1.7.8 Cytochrome *c* Peroxidase and Cytochrome *c*

Cytochrome *c* peroxidase (CcP) is a mitochondrial haem enzyme from yeast that can reduce hydrogen peroxide. Cytochrome *c* (Cc) acts as the electron donor. The CcP-Cc complex is probably the best studied electron transfer complex. Paramagnetic NMR was important for our understanding of this complex, providing precious information about transient protein-protein complexes and encounter states. The crystal structure of the complex was already published in 1992.<sup>82</sup> The structure of the complex in solution was determined using solely PRE restraints, by tagging CcP at five different sites with MTSL and measuring the intermolecular relaxation changes of amide hydrogens in uniformly labelled Cc.<sup>43</sup> The major form of the complex was similar to the one observed in the crystal structure. The work also demonstrated that a substantial fraction of the complex must be in an encounter state, because part of the PRE could not be explained by the major state of the complex. To visualize the encounter complex the number of tags was extended to 10 sites on CcP. In this way, it was shown that the encounter site is limited to the immediate environment of the stereospecific binding site. Structural ensembles from docking calculations based solely on the electrostatic interactions between CcP and Cc were in good agreement with the experimental PRE, assuming that the encounter state represented no less than 30% of the complex, with 70% being in the stereospecific complex observed in the crystal structure.<sup>44</sup> Using the ensemble obtained from these calculations, the encounter state could be visualized (Figure 1.7) and it was shown that Cc samples just 15% of the CcP surface.<sup>44</sup> This can be explained by the charge distribution present on CcP and Cc, which are highly dipolar, with strong negative and positive patches close to the respective binding sites. The fraction of encounter state could readily be changed by mutations in the binding site, in the range between 10% to 90% encounter state.<sup>83</sup> In the sections above, it was explained that for electron transfer complexes a stereospecific binding site is not a requirement, as long as the distance between the redox centres is short enough, e.g. in the complex of Cc and Adx. In the CcP-Cc complex, the stereospecific complex appears to be necessary to reduce the distance between the Cc haem and the CcP Trp residue that acts as the first electron acceptor. The Trp and haem in CcP are deeply buried. The delicate balance between stereospecific complex and encounter state may be a consequence of competing interests. The encounter complex results from the strong electrostatic interactions that raise the association rate, the stereospecific complex is necessary for fast electron transfer. The complex cannot be too tight ( $K_D$  for Cc is 5  $\mu\text{M}$ <sup>84</sup>) because that would limit dissociation. However, it is also possible that electron transfer occurs partly from at another site that seems to bind Cc, at least weakly under low ionic strength conditions. Recently, this binding site was localized using paramagnetic NMR methods. The high-affinity binding site on CcP first was blocked by crosslinking isotope-labelled CcP and unlabelled Cc through an

intermolecular disulphide bond.<sup>85</sup> In this way, it was possible to study the low-affinity interaction between the crosslinked complex (CL) and Cc. PRE were obtained using Cc tagged at three sites with an EDTA-based tag containing  $\text{Mn}^{2+}$ . The experiments revealed that the weak complex is composed of a dominant species, which is thought to be inactive in electron transfer since the haems are too far apart (22 Å), and an ensemble of minor species, in which the haems are close enough for electron transfer (< 16 Å). Therefore, it is possible that, under certain conditions, Cc binding at the low affinity site contributes much to the electron transfer activity.<sup>85</sup>

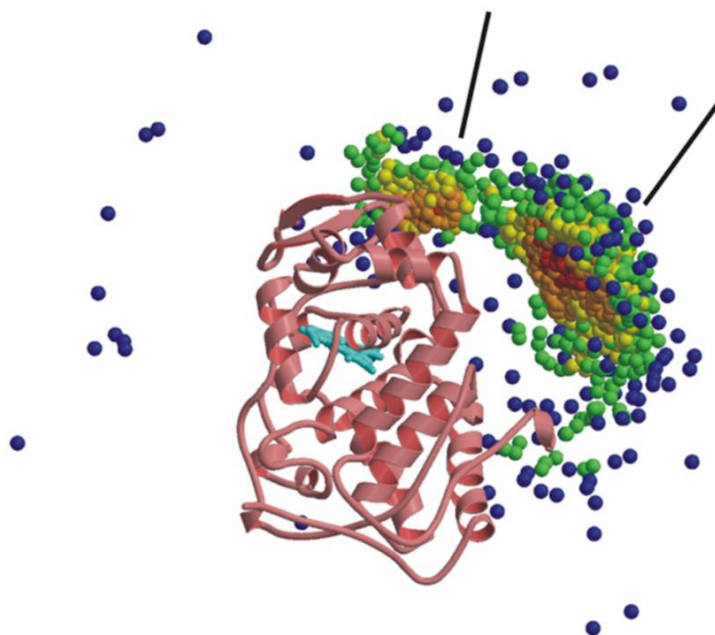


**Figure 1.7** Simulated encounter complex of the CcP-Cc complex based on Monte Carlo calculations of the electrostatic interactions. CcP is shown in pink ribbons and the haem in cyan sticks. The centres of mass of Cc are shown as spheres, coloured to indicate the density of the distributions, decreasing from red to blue. The highest densities denote the most favorable electrostatic orientations. The lines indicate the two centers of high density. The model was shown to be in good agreement with extensive PRE data assuming that the encounter complex is populated for 30%. Reprinted with permission from <sup>44</sup>. Copyright 2010 American Chemical Society.

### 1.7.9 Enzyme I and the Histidine-Containing Phosphocarrier Protein

HPr and Enzyme I are the two general components of the phosphotransferase system involved in transport of a variety of carbohydrates into the prokaryotic cell. PRE was applied to gain insight into the mechanistic details of the interactions present in the transient encounter complex formed by the N-terminal domain of Enzyme I (EIN) and the

histidine-containing phosphocarrier protein (HPr).<sup>46,86</sup> The measurement of the sedimentation velocity of HPr, which is monomeric in solution, revealed that any higher-order species is populated less than 1-2% of the total soluble HPr.<sup>86</sup> Intermolecular PRE were collected on 1:1 solutions of <sup>15</sup>N-labelled HPr and HPr tagged with an EDTA-Mn<sup>2+</sup> tag (or Ca<sup>2+</sup> as diamagnetic ion) at three sites. PRE were observed for two of the labelled HPr, revealing ultra-weak self-association of HPr molecules in solution. The intermolecular PRE were abolished by adding the N-terminal domain of enzyme I (EIN) to form the EIN:HPr complex, which suggests that the EIN-HPr interface is the same as the one used for HPr self-association. A similar effect was seen by increasing the salt concentration, evidence for an electrostatic component in the interaction, even though hydrophobic interactions are also present, as shown by the differences in the degree of reduction of the intermolecular PRE by the addition of salt for different regions. The quantitative analysis of the PRE data through the rigid body/torsion angle simulated annealing calculations suggested that an ensemble of self-association interactions can explain the observed PRE and that the K<sub>D</sub> for the HPr-HPr self-association is  $\geq 15$  mM.<sup>86</sup>

HPr was investigated also for its interaction with EIN. PRE experiments were applied to study the encounter complexes formed by the two proteins in relation to the ionic strength.<sup>87</sup> EIN was <sup>2</sup>H and <sup>15</sup>N-labelled, while HPr was tagged with EDTA-Mn<sup>2+</sup> in two positions. Observed PRE were divided in PRE caused by the stereospecific complex, which showed just a weak salt dependency, and PRE generated by the ensemble of nonspecific encounter complexes, which was much more affected by the salt concentration. In particular, the latter PRE decreased with an increasing salt concentration, indicating a shift in the equilibrium from encounter state to stereospecific complex. Other PRE experiments allowed further characterization of the encounter complex formed by HPr and EIN. Again, HPr was tagged with EDTA-Mn<sup>2+</sup> at three different sites and PRE were measured on <sup>15</sup>N-labeled EIN.<sup>46</sup> The analysis of the energy landscape of the protein-protein interactions leading to the formation of the specific complex showed the presence of two classes of encounter complexes. It was suggested that the main function of one class is to guide HPr to the stereospecific site, in the first part of the productive complex formation, when the binding site is empty. The second class, instead, can form an ensemble of ternary complexes with the stereospecific complex and it is more populated when the binding site is occupied. For this reason, it was proposed that the function of this class is to “reload” the EIN with HPr to have a more efficient sugar transport.<sup>46</sup> It is estimated that ternary complex ensemble engages about the 1% of the Enzyme I molecules *in vivo*, a percentage that could be higher due to intracellular crowding and compartmentalization.

#### 1.7.10 NS2B-NS3 Protease

Protein structure determination is often done for drug discovery. This is the case for the complex formed by NS2B and NS3, two non-structural proteins of the dengue virus serotype 2. Many studies were conducted on segments of these two proteins linked together forming the NS2B-NS3 protease (NS2B-NS3pro). The development of an inhibitor for this protein was problematic, and even though it is an established drug target, its exact structure

was difficult to solve. It was not possible to solve the structure in solution with conventional NMR techniques because of low spectral dispersion, poor protein stability and line broadening caused by protein dynamics. The first crystal structure showed that the C-terminal segment of NS2B (NS2Bc) was far from the active site, in an open and inactive conformation,<sup>88</sup> but other structures obtained with NMR in solution showed that the complex is in a closed conformation, with NS2Bc near the substrate binding site both in presence and absence of inhibitors.<sup>21,89,90</sup> For example, one of these studies analysed the NS2B-NS3pro complex with bovine pancreatic trypsin inhibitor (BPTI), a complex of 35 kDa. In this study, NS3pro was tagged with the lanthanoid tag<sup>50</sup> C2-Tb<sup>3+</sup> (C2-Y<sup>3+</sup> as diamagnetic control) and PCS were measured of backbone amides in the complex with either partner being <sup>15</sup>N-labelled, demonstrating that the complex in solution and in presence of BPTI adopts a closed conformation. The quality of the model was confirmed by the good correlation between the experimental and back-calculated PCS.<sup>91</sup> However, differences in peak intensities in the spectra indicated that NS2B-NS3 protease experiences conformational exchange, which made it possible that an open conformation of NS2Bc of up to 10% would go undetected. On the other hand, it is also possible that the open conformation of the protease-BPTI complex could be a crystallization artefact.<sup>91</sup> Some studies have also been done on the unlinked NS2B-NS3pro construct. For example, the complex was tagged on three different positions with paramagnetic C1- and C2-lanthanoid tags<sup>50,92</sup> loaded with Tm<sup>3+</sup> and Tb<sup>3+</sup> and PCS were measured.<sup>21</sup> The obtained model was consistent with the structure in the closed state detected in presence of inhibitors,<sup>50</sup> even though the C-terminal segment of NS2B (NS2Bc) showed an increasing conformational exchange at the increasing of the pH and ionic strength. This did not result in the dissociation from NS3pro even at high concentration of salt.

## 1.8 Conclusions and Perspective

Paramagnetic NMR offers a new toolbox for the study of protein-protein complexes in solution. Due to the strong spins of unpaired electrons, long-range interactions with nuclei are observed and the theory of PCS, RDC and PRE is well described, making it possible to extract accurate structural restraints from these observables. The advantage is that the effects are ‘clean’. Usually, only a single paramagnetic centre is present in the sample, so, provided a suitable diamagnetic control sample is present, the paramagnetic effect can be isolated and readily attributed to the observed nucleus – electron(s) interaction. As compared to NOE, no ambiguities of assignments and spin diffusion need to be considered and the absence of a paramagnetic effect is also very informative. On the other hand, a dense network as observed for NOE will not be obtained for paramagnetic restraints, because only a single paramagnetic centre is used at a time. The longer distance range also precludes very detailed structural analysis. An exception is the immediate environment of the paramagnetic centre, however, in the case of protein-protein complex studies, the paramagnetic centre itself is not of interest.

The long-range nature makes it possible to study large systems, for example the PRE-based study of the complex of nitrite reductase and pseudoazurin of 152 kDa,<sup>93</sup> and the PCS



observed for the 90 kDa Lac repressor complex<sup>94</sup> and the 300 kDa transcarbamylase.<sup>95</sup> Provided that the structures of the free proteins are available and for at least one partner nuclei can be observed and assigned, paramagnetic restraints can be obtained relatively easily, using simple experiments and low protein concentrations. With ranges up to 70 Å, or perhaps even more, measurable with PCS, very large systems can be investigated in principle.

So far, paramagnetic NMR has been used to determine protein-protein complexes of ground states based on rigid body docking. This is a relatively simple six-dimensional problem that can be solved with a limited number of restraints. Such an approach does not take into account conformational changes in the proteins upon complex formation and generally also does not consider side-chain orientations. Thus, such structures are no match yet for crystallography. To obtain high resolution structures, a very large set of restraints, for side-chain as well as backbone nuclei, is required. It can be questioned whether this is a goal worth striving for. Paramagnetic NMR seems to play its most important role in the study of ensembles and dynamics. PRE analysis has opened the avenue to experimental studies of the encounter complexes and with that to the process of protein complex formation. It has made us realize that the stereospecific complex is not the only representation of the complex. In many protein complexes, especially the weaker ones that are so important in processes such as signalling and electron transfer, the encounter state is an essential part of the complex. Paramagnetic NMR, in particular PCS, can also be very useful to detect structural changes, i.e. to validate crystal structure models in solution. PCS can readily distinguish between open and closed forms of proteins and protein complexes that may appear in crystals, but for which it is unknown whether they exist in solution. Finally, there may be a future for paramagnetic relaxation dispersion (RD) studies. RD-NMR is well-established for measurement of  $\mu\text{s}$  –  $\text{ms}$  dynamics in proteins, based on exchange effects that cause line-broadening. The underlying chemical shift differences between the exchanging states are, however, difficult to interpret in structural terms. It has been shown that combining RD with PCS can potentially be very powerful but paramagnetic tag mobility is still a large problem, because it causes additional, undesired RD effects.<sup>96,97</sup>

In conclusion, paramagnetic NMR has shown to have many applications for protein NMR and it is expected that its star will brighten in the future. PRE has been used widely, but the power of PCS and piRDC is still to be appreciated more by many in the NMR field.

## References

- (1) Hass, M. A. S., and Ubbink, M. (2014) Structure determination of protein-protein complexes with long-range anisotropic paramagnetic NMR restraints, *Curr. Opin. Struct. Biol.* 24, 45-53.

- (2) Otting, G. (2010) Protein NMR using paramagnetic ions, In *Annu. Rev. Biophys.* (Rees, D. C., Dill, K. A., and Williamson, J. R., Eds.), p 387, *Annu. Rev. Biophys.*, Palo Alto.
- (3) Keizers, P. H. J., and Ubbink, M. (2011) Paramagnetic tools in protein NMR, In *Protein NMR Spectroscopy: Practical Techniques and Applications* (Roberts, L.-Y. L. a. G., Ed.), p 193, John Wiley & Sons, Ltd, Chichester,UK.
- (4) Keizers, P. M., and Ubbink, M. (2011) Paramagnetic tagging for protein structure and dynamics analysis, *Prog. Nucl. Magn. Reson. Spectrosc.* 58, 88-96.
- (5) Koehler, J., and Meiler, J. (2011) Expanding the utility of NMR restraints with paramagnetic compounds: Background and practical aspects, *Prog. Nucl. Magn. Reson. Spectrosc.* 59, 360-389.
- (6) Ubbink, M. (2009) The courtship of proteins: Understanding the encounter complex, *FEBS Lett.* 583, 1060-1066.
- (7) Clore, G. M., and Iwahara, J. (2009) Theory, practice, and applications of paramagnetic relaxation enhancement for the characterization of transient low-population states of biological macromolecules and their complexes, *Chem. Rev.* 109, 4108-4139.
- (8) Schreiber, G., Haran, G., and Zhou, H. X. (2009) Fundamental Aspects of Protein-Protein Association Kinetics, *Chem. Rev.* 109, 839-860.
- (9) McConnell, H. M. (1958) Reaction rates by nuclear magnetic resonance, *J. Chem. Phys.* 28, 430-431.
- (10) Yu, D. M., Volkov, A. N., and Tang, C. (2009) Characterizing dynamic protein-protein interactions using differentially scaled paramagnetic relaxation enhancement, *J. Am. Chem. Soc.* 131, 17291-17297.
- (11) Iwahara, J., and Clore, G. M. (2006) Detecting transient intermediates in macromolecular binding by paramagnetic NMR, *Nature* 440, 1227-1230.
- (12) Liu, W. M., Keizers, P. H. J., Hass, M. A. S., Blok, A., Tirnmer, M., Sarris, A. J. C., Overhand, M., and Ubbink, M. (2012) A pH-sensitive, colorful, lanthanide-chelating paramagnetic NMR probe, *J. Am. Chem. Soc.* 134, 17306-17313.
- (13) Hiruma, Y., Hass, M. A. S., Kikui, Y., Liu, W. M., Olmez, B., Skinner, S. P., Blok, A., Kloosterman, A., Koteishi, H., Lohr, F., Schwalbe, H., Nojiri, M., and Ubbink, M. (2013) The structure of the cytochrome P450cam-putidaredoxin complex

- determined by paramagnetic NMR spectroscopy and crystallography, *J. Mol. Biol.* **425**, 4353-4365.
- (14) Parigi, G., and Luchinat, C. (2018) Chapter 1 NMR Consequences of the Nucleus–Electron Spin Interactions, In *Paramagnetism in Experimental Biomolecular NMR*, pp 1-41, The Royal Society of Chemistry.
- (15) Prestegard, J. H., and Rogals, M. J. (2018) Chapter 3 Structural and Dynamic Characterization of Protein Domains using Paramagnetic Data, In *Paramagnetism in Experimental Biomolecular NMR*, pp 85-106, The Royal Society of Chemistry.
- (16) Keizers, P. H. J., Mersinli, B., Reinle, W., Donauer, J., Hiruma, Y., Hannemann, F., Overhand, M., Bernhardt, R., and Ubbink, M. (2010) A solution model of the complex formed by adrenodoxin and adrenodoxin reductase determined by paramagnetic NMR spectroscopy, *Biochemistry* **49**, 6846-6855.
- (17) Andrałojć, W., and Ravera, E. (2018) Chapter 4 Treating Biomacromolecular Conformational Variability, In *Paramagnetism in Experimental Biomolecular NMR*, pp 107-133, The Royal Society of Chemistry.
- (18) Arumugam, S., Hemme, C. L., Yoshida, N., Suzuki, K., Nagase, H., Bejanskii, M., Wu, B., and Van Doren, S. R. (1998) TIMP-1 contact sites and perturbations of stromelysin 1 mapped by NMR and a paramagnetic surface probe, *Biochemistry* **37**, 9650-9657.
- (19) Hocking, H. G., Zangger, K., and Madl, T. (2013) Studying the structure and dynamics of biomolecules by using soluble paramagnetic probes, *ChemPhysChem* **14**, 3082-3094.
- (20) Almeida, R. M., Geraldes, C., Pauleta, S. R., and Moura, J. J. G. (2011) Gd(III) chelates as NMR probes of protein-protein interactions. Case study: Rubredoxin and cytochrome c(3), *Inorg. Chem.* **50**, 10600-10607.
- (21) de la Cruz, L., Chen, W. N., Graham, B., and Otting, G. (2014) Binding mode of the activity-modulating C-terminal segment of NS2B to NS3 in the dengue virus NS2B-NS3 protease, *Febs J.* **281**, 1517-1533.
- (22) Pintacuda, G., Park, A. Y., Keniry, M. A., Dixon, N. E., and Otting, G. (2006) Lanthanide labeling offers fast NMR approach to 3D structure determinations of protein-protein complexes, *J. Am. Chem. Soc.* **128**, 3696-3702.

- (23) van Ingen, H., and Bonvin, A. (2014) Information-driven modeling of large macromolecular assemblies using NMR data, *J. Magn. Reson.* **241**, 103-114.
- (24) Cowieson, N. P., Kobe, B., and Martin, J. L. (2008) United we stand: combining structural methods, *Curr. Opin. Struct. Biol.* **18**, 617-622.
- (25) Anthis, N. J., and Clore, G. M. (2015) Visualizing transient dark states by NMR spectroscopy, *Quart. Rev. Biophys.* **48**, 35-116.
- (26) Nitsche, C., and Otting, G. (2018) Chapter 2 Intrinsic and Extrinsic Paramagnetic Probes, In *Paramagnetism in Experimental Biomolecular NMR*, pp 42-84, The Royal Society of Chemistry.
- (27) Nooren, I. M. A., and Thornton, J. M. (2003) Diversity of protein-protein interactions, *Embo J.* **22**, 3486-3492.
- (28) Leupin, W., Otting, G., Amacker, H., and Wuthrich, K. (1990) Application of C-13 (omega-1)-half-filtered H-1,H-1-NOESY for studies of a complex formed between DNA and a C-13-labeled minor-groove-binding drug *FEBS Lett.* **263**, 313-316.
- (29) Nilges, M. (1993) A calculation strategy for the structure determination of symmetrical dimers by H-1-NMR, *Proteins* **17**, 297-309.
- (30) Gaponenko, V., Altieri, A. S., Li, J., and Byrd, R. A. (2002) Breaking symmetry in the structure determination of (large) symmetric protein dimers, *J. Biomol. NMR* **24**, 143-148.
- (31) Rumpel, S., Becker, S., and Zweckstetter, M. (2008) High-resolution structure determination of the CylR2 homodimer using paramagnetic relaxation enhancement and structure-based prediction of molecular alignment, *J. Biomol. NMR* **40**, 1-13.
- (32) Ubbink, M., Ejdeback, M., Karlsson, B. G., and Bendall, D. S. (1998) The structure of the complex of plastocyanin and cytochrome f, determined by paramagnetic NMR and restrained rigid-body molecular dynamics, *Structure* **6**, 323-335.
- (33) Saio, T., Ogura, K., Yokochi, M., Kobashigawa, Y., and Inagaki, F. (2009) Two-point anchoring of a lanthanide-binding peptide to a target protein enhances the paramagnetic anisotropic effect, *J. Biomol. NMR* **44**, 157-166.
- (34) Bjorkoy, G., Lamark, T., Brech, A., Outzen, H., Perander, M., Overvatn, A., Stenmark, H., and Johansen, T. (2005) p62/SQSTM1 forms protein aggregates degraded by

- autophagy and has a protective effect on huntingtin-induced cell death, *J. Cell Biol.* **171**, 603-614.
- (35) Saio, T., Yokochi, M., Kumeta, H., and Inagaki, F. (2010) PCS-based structure determination of protein-protein complexes, *J. Biomol. NMR* **46**, 271-280.
- (36) Keizers, P. H. J., Desreux, J. F., Overhand, M., and Ubbink, M. (2007) Increased paramagnetic effect of a lanthanide protein probe by two-point attachment, *J. Am. Chem. Soc.* **129**, 9292-9293.
- (37) Keizers, P. H. J., Saragliadis, A., Hiruma, Y., Overhand, M., and Ubbink, M. (2008) Design, synthesis, and evaluation of a lanthanide chelating protein probe: CLaNP-5 yields predictable paramagnetic effects independent of environment, *J. Am. Chem. Soc.* **130**, 14802-14812.
- (38) Muller, J. J., Lapko, A., Bourenkov, G., Ruckpaul, K., and Heinemann, U. (2001) Adrenodoxin reductase-adrenodoxin complex structure suggests electron transfer path in steroid biosynthesis, *J. Biol. Chem.* **276**, 2786-2789.
- (39) Spaar, A., Dammer, C., Gabdoulline, R. R., Wade, R. C., and Helms, V. (2006) Diffusional encounter of barnase and barstar, *Biophys. J.* **90**, 1913-1924.
- (40) Adam, G., and Delbrück, M. (1968) Reduction of dimensionality in biological diffusion processes, In *Structural Chemistry and Molecular Biology* (A. Rich, N. D., Ed.), p 198, W. H. Freeman and Co., San Francisco.
- (41) McLendon, G. (1991) Control of biological electron transport via molecular recognition and binding: The “velcro” model, In *Long-Range Electron Transfer in Biology*, p 159, Springer Berlin Heidelberg, Berlin, Heidelberg.
- (42) Kim, Y. C., Tang, C., Clore, G. M., and Hummer, G. (2008) Replica exchange simulations of transient encounter complexes in protein-protein association, *P. Natl. Acad. Sci. USA* **105**, 12855-12860.
- (43) Volkov, A. N., Worrall, J. A. R., Holtzmann, E., and Ubbink, M. (2006) Solution structure and dynamics of the complex between cytochrome c and cytochrome c peroxidase determined by paramagnetic NMR, *P. Natl. Acad. Sci. USA* **103**, 18945-18950.
- (44) Bashir, Q., Volkov, A. N., Ullmann, G. M., and Ubbink, M. (2010) Visualization of the encounter ensemble of the transient electron transfer complex of cytochrome c and cytochrome c peroxidase, *J. Am. Chem. Soc.* **132**, 241-247.

- (45) Tang, C., Iwahara, J., and Clore, G. M. (2006) Visualization of transient encounter complexes in protein-protein association, *Nature* *444*, 383-386.
- (46) Fawzi, N. L., Doucleff, M., Suh, J. Y., and Clore, G. M. (2010) Mechanistic details of a protein-protein association pathway revealed by paramagnetic relaxation enhancement titration measurements, *P. Natl. Acad. Sci. USA* *107*, 1379-1384.
- (47) Fawzi, N. L., Ying, J. F., Torchia, D. A., and Clore, G. M. (2010) Kinetics of amyloid beta monomer-to-oligomer exchange by NMR relaxation, *J. Am. Chem. Soc.* *132*, 9948-9951.
- (48) Zhao, L., Ji, G., Le, X., Luo, Z., Wang, C., Feng, M., Xu, L., Zhang, Y., Lau, W. B., Lau, B., Yang, Y., Lei, L., Yang, H., Xuan, Y., Chen, Y., Deng, X., Yi, T., Yao, S., Zhao, X., Wei, Y., and Zhou, S. (2017) An integrated analysis identifies STAT4 as a key regulator of ovarian cancer metastasis, *Oncogene* *36*, 3384-3396.
- (49) Brewer, K. D., Bacaj, T., Cavalli, A., Camilloni, C., Swarbrick, J. D., Liu, J., Zhou, A., Zhou, P., Barlow, N., Xu, J. J., Seven, A. B., Prinslow, E. A., Voleti, R., Haussinger, D., Bonvin, A., Tomchick, D. R., Vendruscolo, M., Graham, B., Sudhof, T. C., and Rizo, J. (2015) Dynamic binding mode of a synaptotagmin-1-SNARE complex in solution, *Nat. Struct. Mol. Biol.* *22*, 555-564.
- (50) de la Cruz, L., Thi, H. D. N., Ozawa, K., Shin, J., Graham, B., Huber, T., and Otting, G. (2011) Binding of low molecular weight inhibitors promotes large conformational changes in the dengue virus NS2B-NS3 protease: Fold analysis by pseudocontact shifts, *J. Am. Chem. Soc.* *133*, 19205-19215.
- (51) Marcus, R. A., and Sutin, N. (1985) Electron transfers in chemistry and biology *Biochim. Biophys. Acta* *811*, 265-322.
- (52) Moser, C. C., Keske, J. M., Warncke, K., Farid, R. S., and Dutton, P. L. (1992) Nature of biological electron-transfer *Nature* *355*, 796-802.
- (53) Guss, J. M., Harrowell, P. R., Murata, M., Norris, V. A., and Freeman, H. C. (1986) Crystal structure analyses of reduced (CuI) poplar plastocyanin at six pH values, *J. Mol. Biol.* *192*, 361-387.
- (54) Martinez, S. E., Huang, D., Szczepaniak, A., Cramer, W. A., and Smith, J. L. (1994) Crystal structure of chloroplast cytochrome freveals a novel cytochrome fold and unexpected heme ligation, *Structure* *2*, 95-105.

## Chapter 1

- (55) Kannt, A., Young, S., and Bendall, D. S. (1996) The role of acidic residues of plastocyanin in its interaction with cytochrome *f*, *Biochim. Biophys. Acta, Bioenergetics* 1277, 115-126.
- (56) Crowley, P. B., Otting, G., Schlarb-Ridley, B. G., Canters, G. W., and Ubbink, M. (2001) Hydrophobic interactions in a cyanobacterial plastocyanin-cytochrome *f* complex, *J. Am. Chem. Soc.* 123, 10444-10453.
- (57) Xue, Y., Okvist, M., Hansson, O., and Young, S. (1998) Crystal structure of spinach plastocyanin at 1.7 Å resolution, *Protein Sci* 7, 2099-2105.
- (58) Babu, C. R., Volkman, B. F., and Bullerjahn, G. S. (1999) NMR solution structure of plastocyanin from the photosynthetic prokaryote, *Prochlorothrix hollandica*, *Biochemistry* 38, 4988-4995.
- (59) Badsberg, U., Jorgensen, A. M., Gesmar, H., Led, J. J., Hammerstad, J. M., Jespersen, L. L., and Ulstrup, J. (1996) Solution structure of reduced plastocyanin from the blue-green alga *Anabaena variabilis*, *Biochemistry* 35, 7021-7031.
- (60) Diaz-Moreno, I., Diaz-Quintana, A., De la Rosa, M. A., and Ubbink, M. (2005) Structure of the complex between plastocyanin and cytochrome *f* from the cyanobacterium *Nostoc* sp PCC 7119 as determined by paramagnetic NMR - The balance between electrostatic and hydrophobic interactions within the transient complex determines the relative orientation of the two proteins, *J. Biol. Chem* 280, 18908-18915.
- (61) Hulsker, R., Baranova, M. V., Bullerjahn, G. S., and Ubbink, M. (2008) Dynamics in the transient complex of plastocyanin-cytochrome *f* from *Prochlorothrix hollandica*, *J. Am. Chem. Soc.* 130, 1985-1991.
- (62) Scanu, S., Forster, J., Finiguerra, M. G., Shabestari, M. H., Huber, M., and Ubbink, M. (2012) The complex of cytochrome *f* and plastocyanin from *Nostoc* sp PCC 7119 is highly dynamic, *ChemBioChem* 13, 1312-1318.
- (63) Scanu, S., Foerster, J. M., Ullmann, G. M., and Ubbink, M. (2013) Role of hydrophobic interactions in the encounter complex formation of the plastocyanin and cytochrome *f* complex revealed by paramagnetic NMR spectroscopy, *J. Am. Chem. Soc.* 135, 7681-7692.

- (64) Scanu, S., Foerster, J. M., Timmer, M., Ullmann, G. M., and Ubbink, M. (2013) Loss of electrostatic interactions causes increase of dynamics within the plastocyanin-cytochrome f complex, *Biochemistry* 52, 6615-6626.
- (65) Camacho, C. J., Weng, Z., Vajda, S., and DeLisi, C. (1999) Free energy landscapes of encounter complexes in protein-protein association, *Biophys. J.* 76, 1166-1178.
- (66) Camacho, C. J., Kimura, S. R., DeLisi, C., and Vajda, S. (2000) Kinetics of desolvation-mediated protein-protein binding, *Biophys. J.* 78, 1094-1105.
- (67) Grove, T. Z., Ullmann, G. M., and Kostic, N. M. (2012) Simultaneous true, gated, and coupled electron-transfer reactions and energetics of protein rearrangement, *J. Inorg. Biochem.* 106, 143-150.
- (68) Grove, T. Z., and Kostic, N. M. (2003) Metalloprotein association, self-association, and dynamics governed by hydrophobic interactions: Simultaneous occurrence of gated and true electron-transfer reactions between cytochrome f and cytochrome c(6) from *Chlamydomonas reinhardtii*, *J. Am. Chem. Soc.* 125, 10598-10607.
- (69) Diaz-Moreno, I., Hulsker, R., Skubak, P., Foerster, J. M., Cavazzini, D., Finiguerra, M. G., Diaz-Quintana, A., Moreno-Beltran, B., Rossi, G. L., Ullmann, G. M., Pannu, N. S., De la Rosa, M. A., and Ubbink, M. (2014) The dynamic complex of cytochrome c(6) and cytochrome f studied with paramagnetic NMR spectroscopy, *Biochim. Biophys. Acta, Bioenergetics* 1837, 1305-1315.
- (70) Xu, X. F., Reinle, W. G., Hannemann, F., Konarev, P. V., Svergun, D. I., Bernhardt, R., and Ubbink, M. (2008) Dynamics in a pure encounter complex of two proteins studied by solution scattering and paramagnetic NMR spectroscopy, *J. Am. Chem. Soc.* 130, 6395-6403.
- (71) Xu, X. F., Keizers, P. H. J., Reinle, W., Hannemann, F., Bernhardt, R., and Ubbink, M. (2009) Intermolecular dynamics studied by paramagnetic tagging, *J. Biomol. NMR* 43, 247-254.
- (72) Lyons, T. A., Ratnaswamy, G., and Pochapsky, T. C. (1996) Redox-dependent dynamics of putidaredoxin characterized by amide proton exchange, *Protein Sci.* 5, 627-639.
- (73) OuYang, B., Pochapsky, S. S., Dang, M., and Pochapsky, T. C. (2008) A functional proline switch in cytochrome P450(cam), *Structure* 16, 916-923.



- (74) Tripathi, S., Li, H. Y., and Poulos, T. L. (2013) Structural basis for effector control and redox partner recognition in cytochrome P450, *Science* **340**, 1227-1230.
- (75) Andralojc, W., Hiruma, Y., Liu, W. M., Ravera, E., Nojiri, M., Parigi, G., Luchinat, C., and Ubbink, M. (2017) Identification of productive and futile encounters in an electron transfer protein complex, *P. Natl. Acad. Sci. USA* **114**, E1840-E1847.
- (76) Myers, W. K., Lee, Y. T., Britt, R. D., and Goodin, D. B. (2013) The conformation of P450cam in complex with putidaredoxin is dependent on oxidation state, *J. Am. Chem. Soc.* **135**, 11732-11735.
- (77) Liou, S. H., Mahomed, M., Lee, Y. T., and Goodin, D. B. (2016) Effector roles of putidaredoxin on cytochrome P450cam conformational states, *J. Am. Chem. Soc.* **138**, 10163-10172.
- (78) Liou, S.-H., Myers, W. K., Oswald, J. D., Britt, R. D., and Goodin, D. B. (2017) Putidaredoxin binds to the same site on cytochrome P450cam in the open and closed conformation, *Biochemistry* **56**, 4371-4378.
- (79) Skinner, S. P., Liu, W. M., Hiruma, Y., Timmer, M., Blok, A., Hass, M. A. S., and Ubbink, M. (2015) Delicate conformational balance of the redox enzyme cytochrome P450cam, *P. Natl. Acad. Sci. USA* **112**, 9022-9027.
- (80) Dai, S. D., Friemann, R., Glauser, D. A., Bourquin, F., Manieri, W., Schurmann, P., and Eklund, H. (2007) Structural snapshots along the reaction pathway of ferredoxin-thioredoxin reductase, *Nature* **448**, 92-102.
- (81) Xu, X. F., Schurmann, P., Chung, J. S., Hass, M. A. S., Kim, S. K., Hirasawa, M., Tripathy, J. N., Knaff, D. B., and Ubbink, M. (2009) Ternary Protein Complex of Ferredoxin, Ferredoxin:Thioredoxin Reductase, and Thioredoxin Studied by Paramagnetic NMR Spectroscopy, *J. Am. Chem. Soc.* **131**, 17576-17582.
- (82) Pelletier, H., and Kraut, J. (1992) Crystal-structure of a complex between electron-transfer partners, cytochrome-c peroxidase and cytochrome-c *Science* **258**, 1748-1755.
- (83) Volkov, A. N., Bashir, Q., Worrall, J. A. R., Ullmann, G. M., and Ubbink, M. (2010) Shifting the equilibrium between the encounter state and the specific form of a protein complex by interfacial point mutations, *J. Am. Chem. Soc.* **132**, 11487-11495.

- (84) Worrall, J. A. R., Kolczak, U., Canters, G. W., and Ubbink, M. (2001) Interaction of yeast iso-1-cytochrome c with cytochrome c peroxidase investigated by N-15,H-1 heteronuclear NMR spectroscopy, *Biochemistry* 40, 7069-7076.
- (85) Van de Water, K., Sterckx, Y. G. J., and Volkov, A. N. (2015) The low-affinity complex of cytochrome c and its peroxidase, *Nat. Commun.* 6, 7073.
- (86) Tang, C., Ghirlando, R., and Clore, G. M. (2008) Visualization of transient ultra-weak protein self-association in solution using paramagnetic relaxation enhancement, *J. Am. Chem. Soc.* 130, 4048-4056.
- (87) Suh, J. Y., Tang, C., and Clore, G. M. (2007) Role of electrostatic interactions in transient encounter complexes in protein-protein association investigated by paramagnetic relaxation enhancement, *J. Am. Chem. Soc.* 129, 12954-12955.
- (88) Erbel, P., Schiering, N., D'Arcy, A., Renatus, M., Kroemer, M., Lim, S. P., Yin, Z., Keller, T. H., Vasudevan, S. G., and Hommel, U. (2006) Structural basis for the activation of flaviviral NS3 proteases from dengue and West Nile virus, *Nat. Struct. Mol. Biol.* 13, 372-373.
- (89) Kim, Y. M., Gayen, S., Kang, C. B., Joy, J., Huang, Q. W., Chen, A. S., Wee, J. L. K., Ang, M. J. Y., Lim, H. A., Hung, A. W., Li, R., Noble, C. G., Lee, L. T., Yip, A., Wang, Q. Y., Chia, C. S. B., Hill, J., Shi, P. Y., and Keller, T. H. (2013) NMR analysis of a novel enzymatically active unlinked dengue NS2B-NS3 protease complex, *J. Biol. Chem* 288, 12891-12900.
- (90) Noble, C. G., Seh, C. C., Chao, A. T., and Shi, P. Y. (2012) Ligand-bound structures of the Dengue virus protease reveal the active conformation, *J. Virol.* 86, 438-446.
- (91) Chen, W. N., Loscha, K. V., Nitsche, C., Graham, B., and Otting, G. (2014) The dengue virus NS2B-NS3 protease retains the closed conformation in the complex with BPTI, *FEBS Lett.* 588, 2206-2211.
- (92) Graham, B., Loh, C. T., Swarbrick, J. D., Ung, P., Shin, J., Yagi, H., Jia, X., Chhabra, S., Barlow, N., Pintacuda, G., Huber, T., and Otting, G. (2011) DOTA-amide lanthanide tag for reliable generation of pseudocontact shifts in protein NMR spectra, *Bioconjugate Chem.* 22, 2118-2125.
- (93) Vlasie, M. D., Fernandez-Busnadiego, R., Prudencio, M., and Ubbink, M. (2008) Conformation of pseudoazurin in the 152 kDa electron transfer complex with nitrite reductase determined by paramagnetic NMR, *J. Mol. Biol.* 375, 1405-1415.

## Chapter 1

- (94) Peters, F., Maestre-Martinez, M., Leonov, A., Kovacic, L., Becker, S., Boelens, R., and Griesinger, C. (2011) Cys-Ph-TAHA: a lanthanide binding tag for RDC and PCS enhanced protein NMR, *J. Biomol. NMR* 51, 329-337.
- (95) Velyvis, A., Schachman, H. K., and Kay, L. E. (2009) Assignment of Ile, Leu, and Val methyl correlations in supra-molecular systems: An application to aspartate transcarbamoylase, *J. Am. Chem. Soc.* 131, 16534-16543.
- (96) Hass, M. A. S., Liu, W. M., Agafonov, R. V., Otten, R., Phung, L. A., Schilder, J. T., Kern, D., and Ubbink, M. (2015) A minor conformation of a lanthanide tag on adenylate kinase characterized by paramagnetic relaxation dispersion NMR spectroscopy, *J. Biomol. NMR* 61, 123-136.
- (97) Hass, M. A. S., Keizers, P. H. J., Blok, A., Hiruma, Y., and Ubbink, M. (2010) Validation of a lanthanide tag for the analysis of protein dynamics by paramagnetic NMR spectroscopy, *J. Am. Chem. Soc.* 132, 9952-9953.

# Chapter 2

**Introduction to cytochrome *c* and cytochrome *c* peroxidase**

## An electron transfer complex

The aim of the research reported in this thesis is to test how critical the charge distribution on protein surfaces is for the protein complex formation. Redox proteins are evolutionary optimized to perform efficient electron transfer, forming transient complexes with a high population of encounter complex. The subject of this thesis is the well characterized complex formed by cytochrome *c* (Cc) and cytochrome *c* peroxidase (CcP) from baker's yeast (*Saccharomyces cerevisiae*). Electrostatic interactions drive the formation to the Cc:CcP complex.<sup>1-5</sup> In this work we modified the charge distribution of CcP and studied how the disturbance of the electrostatic surface impacted on the encounter complex with Cc and on the formation of the active complex. The complex was mentioned in Chapter 1 and the proteins are further introduced here.

### Cytochrome *c*

Cytochrome *c* (Cc) was discovered in 1925 by David Keilin.<sup>8</sup> More than one hundred variants are known today and they show a highly conserved sequence among eukaryotes.<sup>9</sup> Cc is one of the main electron transfer (ET) proteins in the eukaryotic respiratory chain, where it functions in the energy production. In this role, it accepts a single electron at a time from cytochrome *c* reductase (cytochrome *bc*<sub>1</sub>, Complex III) to reduce cytochrome *c* oxidase (Complex IV).<sup>10</sup> Cc has additional roles in the regulation of apoptosis as defense mechanism against DNA damage<sup>11</sup> and in baker's yeast (*Saccharomyces cerevisiae*) in the neutralization of oxidative stress caused by hydrogen peroxide, with the aid of cytochrome *c* peroxidase (CcP).<sup>9</sup> The interaction with this enzyme will be discussed further in this thesis.

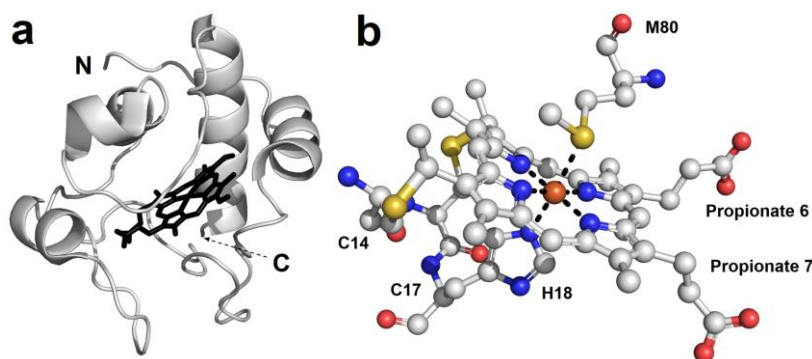


**Figure 2.1** Three dimensional structure of Cc. a) Structure of Cc with the haem in sticks. “N” and “C” indicate the two termini of the polypeptide chain. b) Representation of the haem (iron ion in orange) covalently bound to the residues C14 and C17, and axially coordinated to M80 and H18. The molecular coordinates were taken from the crystal structure of the oxidized Cc (PDB entry 2YCC)<sup>6</sup>.

In this work the native iso-1 isoform of *S. cerevisiae* Cc was used, the most studied so far.<sup>12</sup> The yeast iso-1 form of Cc is a small, positively charged protein (+6 at pH 6)<sup>13</sup> with 108 amino acids and a haem prosthetic group resulting in a total molecular weight of 12.1 kDa.<sup>4</sup> The native yeast iso-1 Cc harbours a post-translational modification of the residue Lys 72, the N- $\epsilon$ -trimethylation, which blocks the apoptotic activity of the protein.<sup>14</sup> The protein can easily be purified from *S. cerevisiae*<sup>15–17</sup> or from *Escherichia coli*<sup>18,19</sup>. Protein produced in bacteria generally do not have post-translational modifications, thus Cc is not trimethylated in *E. coli*. To obtain a high yield in *E. coli*, Cc is produced in the cytoplasm of the cell along with the haem lyase for the insertion of the haem group into the protein.<sup>20</sup> Cc consists of five  $\alpha$ -helices and a small  $\beta$ -strand, folded nearly into a sphere (Figure 2.1a). Its *c*-type haem group is connected to two cysteine residues (14 and 17) by thioether bonds, as part of the conserved with the C-X-Y-C-H sequence.<sup>4</sup> The low-spin iron ion of the haem group is hexacoordinated, equatorially to the four pyrrole nitrogens of the haem and axially to the residue H18 and M80 (Figure 2.1b). The iron ion, which can be reduced Fe(II) or oxidized Fe(III), has magnetic properties that depend on the oxidation state. In the reduced state it is diamagnetic and when oxidized it is paramagnetic.<sup>9</sup> Various high resolution X-ray crystallography and solution NMR structures were published for both the ferrous<sup>21,22</sup> and ferric form.<sup>4,23,24</sup>

### Cytochrome *c* peroxidase

Cytochrome *c* peroxidase (CcP) was discovered in the mitochondrial intermembrane space of *S. cerevisiae* by Altschul, Abrams and Hogness in 1940.<sup>25</sup> As previously mentioned, CcP inactivates hydrogen peroxide, reducing it to water, by transferring the electrons accepted from two molecules of Cc. Yeast CcP is a negatively charged protein (-4 at pH 6)<sup>26</sup> with 294 amino acids and a molecular weight of 34.2 kDa. The crystal structure of CcP<sup>27</sup> shows a secondary structure predominantly composed of  $\alpha$ -helices and a *b*-type haem at the center, enclosed in a hydrophobic pocket (Figure 2.2a). Contrary to the *c*-type, the *b*-type haems are not covalently bound to the polypeptide chain. The iron of the haem is axially coordinated to the N<sub>e2</sub> atom of H175 and equatorially to the four pyrrole nitrogens of the haem group. The last coordination position is occupied by a water molecule in the resting state of CcP and available to bind the substrate (Figure 2.2b).<sup>27</sup> During the reaction, CcP goes through several states. In the resting state (RS), the high-spin iron ion Fe<sup>3+</sup> is pentacoordinated and paramagnetic. When binding hydrogen peroxide, CcP forms the oxyferryl intermediate, called compound I (CpdI),<sup>28,29</sup> in which the iron ion is oxidized to Fe<sup>4+</sup> and the side chain of Trp191 is oxidized to a cation indole radical.<sup>30–32</sup> One water molecule is released. Each of two molecules of Cc transfer an electron to CcP. The first electron reduces CpdI to form compound II (CpdII) while the second electron restores the RS CcP and releases the second water molecule.<sup>33</sup> For more details on the mechanism of the reaction see chapter III. Similar to Cc, CcP can be purified from *S. cerevisiae*<sup>34–36</sup> or recombinantly overproduced in *E. coli*,<sup>37–42</sup> which yields *apo*-protein. The haem group can be incorporated during the purification process.

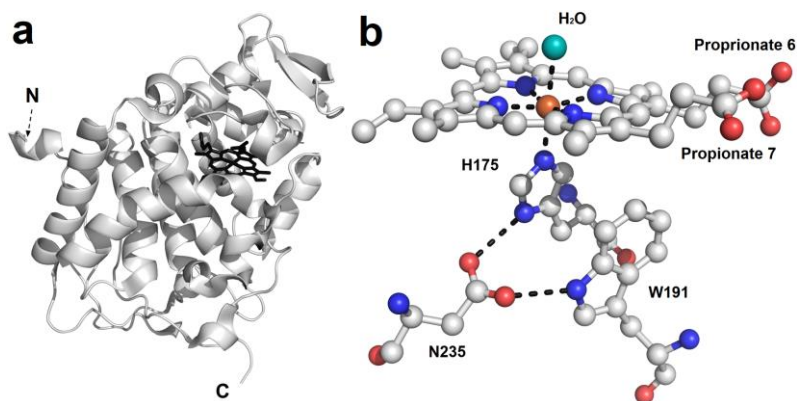


**Figure 2.2** Three dimensional structure of CcP. a) Structure of CcP with the haem in sticks. “N” and “C” indicate the two termini of the polypeptide chain. b) Representation of the haem (iron ion in orange) axially coordinated H175 and to water. The catalytically important W191 and the D235 are also indicated. The molecular coordinates were provided by the crystal structure of resting state CcP (PDB entry 1ZBY)<sup>20</sup>.

### Cc-CcP complex

The complex formed by Cc and CcP is one of the best characterized ET complexes and extensive literature is available on the subject.<sup>12,43–45</sup> To perform an efficient reaction, the Cc:CcP complex is highly dynamic (see Chapter 1) and the interactions between the two proteins are based on electrostatic interactions between the negatively binding site on CcP and the positively one on Cc (Figure 2.3b).<sup>2,5–7</sup> Despite being a transient complex, a co-crystal structure was reported by Pelletier and Kraut in 1992<sup>1</sup> (Figure 2.3). Although the structure appeared initially stabilized by a single hydrogen bond between N70 of Cc and E290 of CcP<sup>1</sup>, other studies suggest the presence of two additional hydrogen bonds: One between Q16 of Cc and A193 on CcP, and a second between K87 of Cc and E32 of CcP.<sup>46</sup> Site-directed mutagenesis and biophysical techniques were used to investigate the importance of several residues for the activity of the complex.<sup>43,47–49</sup> Although the crystal structure shows one stereospecific binding site, the stoichiometry of the Cc:CcP complex has been discussed for decades. The 1:1 stoichiometry model was observed under many experimental conditions.<sup>12</sup> On the other hand, several kinetic studies suggested the presence of a second low-affinity binding site<sup>50–52</sup> at which Cc also binds at low salt concentrations (less than 100 mM salt).<sup>53–56</sup> The possible location of the second binding site was investigated by mutagenesis and simulations, suggesting the regions close to the residues D148<sup>5,57</sup> and between D217 and Y39<sup>58,59</sup> as possible interaction sites. A PRE experiment confirmed the presence of a second binding site in 2015.<sup>56</sup> Isotopically labelled CcP and Cc were cross-linked at the crystallographic binding site while free Cc was tagged with a paramagnetic tag. Thus, paramagnetic relaxation was observed on the spectrum of CcP showing that the low-affinity complex consists of an ensemble of minor states sampling two non-overlapping regions of the CcP surface: One between the residues D148, D217,

D33 and E35 and a second region in proximity of the residues E167, D261 and E267. The residues D148 and D217 play an important role for binding at the low-affinity binding site (Figure 2.3).<sup>56</sup>

Different models have been used to describe the Cc and CcP interactions. Numerous kinetic studies<sup>50,52–55,57,60–63</sup> and computer simulations<sup>5,58,59</sup> suggest the presence of a high-affinity but low-reactivity binding site (the crystallographic one), and a low-affinity but high reactivity binding site that only functions at low ionic strengths. In this model the two Cc molecules do not interact with each other<sup>12</sup> and the low affinity binding site promotes the dissociation of Cc from the high affinity binding site (the only ET active site).<sup>63–66</sup> Various solution NMR studies (at an ionic strength of 120 mM, pH 6) describing the Cc:CcP complex as an highly dynamic one,<sup>6,67–70</sup> suggest a 1:1 model in which a single Cc molecule transiently binds CcP in different areas and orientations (see Chapter 1), one of which is the crystallographic structure.<sup>5,59</sup> It is assumed that under physiological conditions, the crystallographic complex is the active complex.<sup>56</sup> More details on the binding mode, ET and encounter complex between Cc and CcP are provided in the reviews<sup>12</sup> and <sup>43</sup> and in the following chapters.

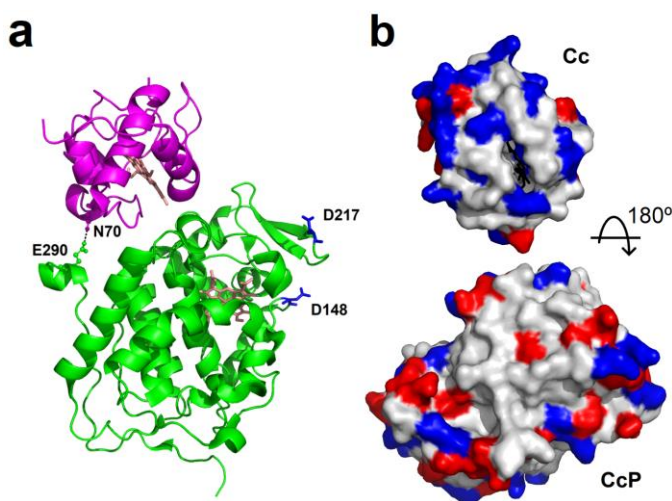


**Figure 2.3** Cc:CcP interactions. a) Three-dimensional structure of the Cc:CcP complex: Cc in magenta ribbons and CcP in green ribbons. The haem groups in salmon sticks. The residues N70 and E290 (in spheres and sticks) stabilize the complex forming a single hydrogen bond (dotted line). The residues D217 and D148 (blue sticks) identify the secondary low-affinity binding site according to Van de Water *et.al.* 2015.<sup>55</sup> b) Distribution of charged residues in the crystallographic binding sites of Cc and CcP. The negatively charged residues are indicated in red and the positively charged ones in blue. (PDB entry 2PCC)<sup>44</sup>. The view shows the interfaces of the stereospecific binding site as present in the crystal structure.



### Thesis outline

The aim of the research presented in this thesis is to test the importance of the charge distribution on protein surfaces for the formation protein complexes. The main question to be answered is whether optimization of the charge distribution is critical for rapid formation of an active complex. This question is addressed by introduction of new charged patches on the surface of CcP and studying the effects on complex formation with its partner Cc. It is predicted that disturbing the optimized charge distribution that guides Cc to the binding site for ET<sup>2,5-7</sup> by strong charged patches elsewhere will result in more futile encounters and thus a lower rate of active complex formation. The methods to test this hypothesis comprise Monte Carlo simulations of the electrostatic interactions during encounter complex formation, paramagnetic relaxation enhancement (PRE) experiments to probe the surface of CcP sampled by Cc and stopped flow experiments to measure association rates. **Chapter I** gives an introduction to the applications of paramagnetic NMR for the study of protein-protein interactions supported by several examples. **Chapter II** provides a brief introduction on the proteins used in this work, Cc and CcP. **Chapter III** describes the effect of the addition of a negatively charged patch, located on one side of CcP, on the encounter complex with Cc and the association rate of the protein complex. This approach is extended in **Chapter IV** to the kinetic characterization of five variants with different charge distributions on the CcP surface. **Chapter V** describes the effect of an additional negative patch on one side of CcP for complex formation with a variant of Cc that is known to spend more time in the encounter state with CcP.<sup>71</sup> **Chapter VI** provides a general discussion and concluding remarks. In combination, these studies show that additional charged patches can, in fact, enhance the formation of the active complex, resulting in additional productive encounters. On the other hand, upon disruption of the charged patch around the binding site, the additional charged patches lose their role in complex formation.

### References

- (1) Pelletier, H., and Kraut, J. (1992) Crystal structure of a complex between electron transfer partners, cytochrome *c* peroxidase and cytochrome *c*. *Science* (80-. ). 258, 1748–1755.
- (2) Gabdoulline, R. R., and Wade, R. C. (2001) Protein-protein association: investigation of factors influencing association rates by Brownian dynamics simulations. *J. Mol. Biol.* 306, 1139–1155.
- (3) Poulos, T. L., Freer, S. T., Alden, R. A., Edwards, S. L., Skogland, U., Takio, K., Eriksson, B., Xuong, N. H., Yonetani, T., and Kraut, J. (1980) Crystal-structure of cytochrome-c peroxidase. *J. Biol. Chem.* 255, 575–580.
- (4) Louie, G. V., Hutcheon, W. L. B., and Brayer, G. D. (1988) Yeast iso-1-cytochrome *c*: A 2.8 Å resolution three-dimensional structure determination. *J. Mol. Biol.* 199, 295–314.
- (5) Northrup, S. H., Boles, J. O., and Reynolds, J. C. (1988) Brownian dynamics of

cytochrome *c* and cytochrome *c* peroxidase association. *Science* (80-. ). 241, 67–70.

(6) Bashir, Q., Volkov, A. N., Ullmann, G. M., and Ubbink, M. (2010) Visualization of the encounter ensemble of the transient electron transfer complex of cytochrome *c* and cytochrome *c* peroxidase. *J. Am. Chem. Soc.* 132, 241–247.

(7) Castro, G., Boswell, C. A., and Northrup, S. H. (1998) Dynamics of protein-protein docking: Cytochrome *c* and cytochrome *c* peroxidase revisited. *J. Biomol. Struct. Dyn.* 16, 413–424.

(8) Keilin, D., and Hardy, W. B. (1925) On cytochrome, a respiratory pigment, common to animals, yeast, and higher plants. *Proc. R. Soc. London. Ser. B, Contain. Pap. a Biol. Character* 98, 312–339.

(9) Banci, L., and Assfalg, M. (2006) Mitochondrial cytochrome *c*, in *Handbook of Metalloproteins*. John Wiley & Sons, Ltd.

(10) Berg, J. M., Tymoczko, J. L., and Stryer, L. Oxidative phosphorylation. *Biochemistry* (Berg, J. M., Tymoczko, J. L., and Stryer, L., Eds.). Freeman, New York, 2002.

(11) Liu, X., Kim, C. N., Yang, J., Jemmerson, R., and Wang, X. (1996) Induction of apoptotic program in cell-free extracts: Requirement for dATP and cytochrome *c*. *Cell* 86, 147–157.

(12) Volkov, A. N., Nicholls, P., and Worrall, J. A. R. (2011) The complex of cytochrome *c* and cytochrome *c* peroxidase: The end of the road? *Biochim. Biophys. Acta-Bioenergetics* 1807, 1482–1503.

(13) Barker, P. D., Mauk, M. R., and Mauk, A. G. (1991) Proton titration curve of yeast iso-1-ferricytochrome *c*. Electrostatic and conformational effects of point mutations. *Biochemistry* 30, 2377–2383.

(14) Kluck, R. M., Ellerby, L. M., Ellerby, H. M., Naiem, S., Yaffe, M. P., Margoliash, E., Bredesen, D., Mauk, A. G., Sherman, F., and Newmeyer, D. D. (2000) Determinants of cytochrome *c* pro-apoptotic activity: The role of lysine 72 trimethylation. *J. Biol. Chem.* 275, 16127–16133.

(15) Sherman, F., Taber, H., and Campbell, W. (1965) Genetic determination of iso-cytochromes *c* in yeast. *J. Mol. Biol.* 13, 21–39.

(16) Sherman, F., Stewart, J. W., Parker, J. H., Inhaber, E., Shipman, N. A., Putterman, G. J., Gardisky, R. L., and Margoliash, E. (1968) The mutational alteration of the primary structure of yeast iso-1-cytochrome *c*. *J. Biol. Chem.*

(17) Willie, A., Liu, R. Q., Durham, B., Millett, F., McLean, M., Sligar, S. G., Hilgen-Willis, S., Saunders, A. J., and Pielak, G. J. (1993) Intracomplex electron transfer between ruthenium-65-cytochrome *b5* and position-82 variants of yeast iso-1-cytochrome *c*. *Biochemistry* 32, 7519–7525.

(18) Pollock, W. B., Rosell, F. I., Twitchett, M. B., Dumont, M. E., and Mauk, A. G. (1998)

## Chapter 2

Bacterial expression of a mitochondrial cytochrome *c*. Trimethylation of lys72 in yeast iso-1-cytochrome *c* and the alkaline conformational transition. *Biochemistry* 37, 6124–6131.

(19) Morar, A. S., Kakouras, D., Young, G. B., Boyd, J., and Pielak, G. J. (1999) Expression of 15N-labeled eukaryotic cytochrome *c* in *Escherichia coli*. *J. Biol. Inorg. Chem.* 4, 220–222.

(20) Dumont, M. E., Ernst, J. F., Hampsey, D. M., and Sherman, F. (1987) Identification and sequence of the gene encoding cytochrome *c* heme lyase in the yeast *Saccharomyces cerevisiae*. *EMBO J.* 6, 235–241.

(21) Louie, G. V., and Brayer, G. D. (1990) High-resolution refinement of yeast iso-1-cytochrome *c* and comparisons with other eukaryotic cytochromes *c*. *J. Mol. Biol.* 214, 527–555.

(22) Baistrocchi, P., Banci, L., Bertini, I., Turano, P., Bren, K. L., and Gray, H. B. (1996) Three-dimensional solution structure of *Saccharomyces cerevisiae* reduced iso-1-cytochrome *c*. *Biochemistry* 35, 13788–13796.

(23) Berghuis, A. M., and Brayer, G. D. (1992) Oxidation state-dependent conformational changes in cytochrome *c*. *J. Mol. Biol.* 223, 959–976.

(24) Banci, L., Bertini, I., Bren, K. L., Gray, H. B., Sompornpisut, P., and Turano, P. (1997) Solution structure of oxidized *Saccharomyces cerevisiae* Iso-1-cytochrome *c*. *Biochemistry* 36, 8992–9001.

(25) Altschul, A. M., Abrams, R., and Hogness, T. R. (1940) Cytochrome *c* peroxidase. *J. Biol. Chem.* 136, 777–794.

(26) Conroy, C. W., and Erman, J. E. (1978) pH titration study of cytochrome *c* peroxidase and apocytochrome *c* peroxidase. *BBA - Protein Struct.* 537, 396–405.

(27) Bonagura, C. A., Bhaskar, B., Shimizu, H., Li, H. Y., Sundaramoorthy, M., McRee, D. E., Goodin, D. B., and Poulos, T. L. (2003) High-resolution crystal structures and spectroscopy of native and compound I cytochrome *c* peroxidase. *Biochemistry* 42, 5600–5608.

(28) Yonetani, T. (1966) Studies on cytochrome *c* peroxidase .IV. A comparison of peroxide-induced complexes of horseradish and cytochrome *c* peroxidases. *J. Biol. Chem.* 241, 2562-.

(29) Jordi, H. C., and Erman, J. E. (1974) Cytochrome *c* peroxidase catalyzed oxidation of ferrocyanide by hydrogen peroxide. Transient state kinetics. *Biochemistry* 13, 3734–3741.

(30) Yonetani, T., and Schleyer, H. (1966) Studies on cytochrome *c* peroxidase. VII. Electron paramagnetic resonance absorptions of the enzyme and complex ES in dissolved and crystalline forms. *J. Biol. Chem.* 241, 3240–3243.

(31) Sivaraja, M., Goodin, D. B., Smith, M., and Hoffman, B. M. (1989) Identification by ENDOR of Trp191 as the free-radical site in cytochrome *c* peroxidase compound ES.

*Science* (80-. ). 245, 738–740.

(32) Erman, J. E., Vitello, L. B., Mauro, J. M., and Kraut, J. (1989) Detection of an oxyferryl porphyrin  $\pi$ -cation-radical intermediate in the reaction between hydrogen peroxide and a mutant yeast cytochrome *c* peroxidase. Evidence for tryptophan-191 involvement in the radical site of compound. *Biochemistry* 28, 7992–7995.

(33) Kim, K. L., Kang, D. S., Vitello, L. B., and Erman, J. E. (1990) Cytochrome *c* peroxidase catalyzed oxidation of ferrocycytochrome *c* by hydrogen-peroxide - Ionic-strength dependence of the steady-state rate parameters. *Biochemistry* 29, 9150–9159.

(34) Yonetani, T. (1965) Studies on cytochrome *c* peroxidase: II. Stoichiometry between enzyme, H<sub>2</sub>O<sub>2</sub> and ferrocycytochrome *c* and enzymic determination of extinction coefficients of cytochrome *c*. *J. Biol. Chem.* 240, 4509–4514.

(35) Goodin, D. B., Mauk, A. G., and Smith, M. (1986) Studies of the radical species in compound ES of cytochrome *c* peroxidase altered by site-directed mutagenesis. *Proc. Natl. Acad. Sci. U. S. A.* 83, 1295–1299.

(36) Goodin, D. B., Mauk, A. G., and Smith, M. (1987) The peroxide complex of yeast cytochrome *c* peroxidase contains two distinct radical species, neither of which resides at methionine-172 or tryptophan-51. *J. Biol. Chem.* 262, 7719–7724.

(37) Goltz, S., Kaput, J., and Blobel, G. (1982) Isolation of the yeast nuclear gene encoding the mitochondrial protein, cytochrome *c* peroxidase. *J. Biol. Chem.* 257, 1186–1190.

(38) Goodin, D. B., Davidson, M. G., Roe, J. A., Mauk, A. G., and Smith, M. (1991) Amino-acid substitutions at tryptophan-51 of cytochrome *c* peroxidase - Effects on coordination, species preference for cytochrome *c*, and electron-transfer. *Biochemistry* 30, 4953–4962.

(39) Schilder, J., Lohr, F., Schwalbe, H., and Ubbink, M. (2014) The cytochrome *c* peroxidase and cytochrome *c* encounter complex: The other side of the story. *Febs Lett.* 588, 1873–1878.

(40) Volkov, A. N., Wohlkonig, A., Soror, S. H., and Van Nuland, N. A. J. (2013) Expression, purification, characterization, and solution nuclear magnetic resonance study of highly deuterated yeast cytochrome *c* peroxidase with enhanced solubility. *Biochemistry* 52, 2165–2175.

(41) Teske, J. G., Savenkova, M. I., Mauro, J. M., Erman, J. E., and Satterlee, J. D. (2000) Yeast cytochrome *c* peroxidase expression in *Escherichia coli* and rapid isolation of various highly pure holoenzymes. *Protein Expr. Purif.* 19, 139–147.

(42) Savenkova, M. I., Satterlee, J. D., Erman, J. E., Siems, W. F., and Helms, G. L. (2001) Expression, purification, characterization, and NMR studies of highly deuterated recombinant cytochrome *c* peroxidase. *Biochemistry* 40, 12123–12131.

(43) Erman, J. E., and Vitello, L. B. (2002, June 3) Yeast cytochrome *c* peroxidase: Mechanistic studies via protein engineering. *Biochim. Biophys. Acta - Protein Struct. Mol.*

## Chapter 2

### *Enzymol.*

- (44) McLendon, G., and Hake, R. (1992) Interprotein electron transfer. *Chem. Rev.* 92, 481–490.
- (45) Millett, F., Miller, M. A., Geren, L., and Durham, B. (1995) Electron transfer between cytochrome *c* and cytochrome *c* peroxidase. *J. Bioenerg. Biomembr.* 27, 341–351.
- (46) Bashir, Q., Meulenbroek, E. M., Pannu, N. S., and Ubbink, M. (2014) Engineering specificity in a dynamic protein complex with a single conserved mutation. *Febs J.* 281, 4892–4905.
- (47) Erman, J. E., Vitello, L. B., Pearl, N. M., Jacobson, T., Francis, M., Alberts, E., Kou, A., and Bujarska, K. (2015) Binding of yeast cytochrome *c* to forty-four charge-reversal mutants of yeast cytochrome *c* peroxidase: isothermal titration calorimetry. *Biochemistry* 54, 4845–4854.
- (48) Pearl, N. M., Jacobson, T., Arisa, M., Vitello, L. B., and Erman, J. E. (2007) Effect of single-site charge-reversal mutations on the catalytic properties of yeast cytochrome *c* peroxidase: Mutations near the high-affinity cytochrome *c* binding site. *Biochemistry* 46, 8263–8272.
- (49) Pearl, N. M., Jacobson, T., Meyen, C., Clementz, A. G., Ok, E. Y., Choi, E., Wilson, K., Vitello, L. B., and Erman, J. E. (2008) Effect of single-site charge-reversal mutations on the catalytic properties of yeast cytochrome *c* peroxidase: Evidence for a single, catalytically active, cytochrome *c* binding domain. *Biochemistry* 47, 2766–2775.
- (50) Kang, C. H., Fergusonmiller, S., and Margoliash, E. (1977) Steady-state kinetics and binding of eukaryotic cytochromes *c* with yeast cytochrome *c* peroxidase. *J. Biol. Chem.* 252, 919–926.
- (51) Kang, D. S., and Erman, J. E. (1982) The cytochrome *c* peroxidase-catalyzed oxidation of ferrocycytochrome *c* by hydrogen peroxide. Steady state kinetic mechanism. *J. Biol. Chem.* 257, 2775–2779.
- (52) Kornblatt, J. A., and English, A. M. (1986) The binding of porphyrin cytochrome *c* to yeast cytochrome *c* peroxidase: A fluorescence study of the number of sites and their sensitivity to salt. *Eur. J. Biochem.* 155, 505–511.
- (53) Stemp, E. D. A., and Hoffman, B. M. (1993) Cytochrome *c* peroxidase binds two molecules of cytochrome *c*: evidence for a low-affinity, electron-transfer-active site on cytochrome *c* peroxidase. *Biochemistry* 32, 10848–10865.
- (54) Zhou, J. S., and Hoffman, B. M. (1994) Stern-Volmer in reverse - 2/1 stoichiometry of the cytochrome *c* cytochrome *c* peroxidase electron-transfer complex. *Science* (80-. ). 265, 1693–1696.
- (55) Mauk, M. R., Ferrer, J. C., and Mauk, A. G. (1994) Proton linkage in formation of the cytochrome *c*-cytochrome *c* peroxidase complex: Electrostatic properties of the high- and low-affinity cytochrome binding sites on the peroxidase. *Biochemistry* 33, 12609–12614.

- (56) Van de Water, K., Sterckx, Y. G. J., and Volkov, A. N. (2015) The low-affinity complex of cytochrome *c* and its peroxidase. *Nat. Commun.* 6, 7073.
- (57) Leesch, V. W., Bujons, J., Mauk, A. G., and Hoffman, B. M. (2000) Cytochrome *c* peroxidase- cytochrome *c* complex: Locating the second binding domain on cytochrome *c* peroxidase with site-directed mutagenesis. *Biochemistry* 39, 10132–10139.
- (58) Morar, A. S., and Pielak, G. J. (2002) Crowding by trisaccharides and the 2:1 cytochrome *c*-cytochrome *c* peroxidase complex. *Biochemistry* 41, 547–551.
- (59) Nocek, J. M., Zhou, J. S., DeForest, S., Priyadarshy, S., Beratan, D. N., Onuchic, J. N., and Hoffman, B. M. (1996) Theory and practice of electron transfer within protein-protein complexes: Application to the multidomain binding of cytochrome *c* by cytochrome *c* peroxidase. *Chem. Rev.* 96, 2459–2489.
- (60) Miller, M. A., Geren, L., Han, G. W., Saunders, A., Beasley, J., Pielak, G. J., Durham, B., Millett, F., and Kraut, J. (1996) Identifying the physiological electron transfer site of cytochrome *c* peroxidase by structure-based engineering. *Biochemistry* 35, 667–673.
- (61) Matthis, A. L., Vitello, L. B., and Erman, J. E. (1995) Oxidation of yeast iso-1 ferrocycytochrome *c* by yeast cytochrome *c* peroxidase compounds I and II. Dependence upon ionic strength. *Biochemistry* 34, 9991–9999.
- (62) Zhou, J. S., and Hoffman, B. M. (1993) Cytochrome *c* peroxidase simultaneously binds cytochrome *c* at two different sites with strikingly different reactivities: Titrating a “substrate” with an enzyme. *J. Am. Chem. Soc.* 115, 11008–11009.
- (63) Page, T. R., and Hoffman, B. M. (2015) Control of cyclic photoinitiated electron transfer between cytochrome *c* peroxidase (W191F) and cytochrome *c* by formation of dynamic binary and ternary complexes. *Biochemistry* 54, 1188–1197.
- (64) Corin, A. F., Hake, R. A., McLendon, G., Hazzard, J. T., and Tollin, G. (1993) Effects of surface amino acid replacements in cytochrome *c* peroxidase on intracomplex electron transfer from cytochrome *c*. *Biochemistry* 32, 2756–2762.
- (65) McLendon, G., Zhang, Q., Billstone, V., Wallin, S. A., Miller, R. M., Spears, K. G., and Hoffman, B. M. (1993) Thermodynamic and kinetic aspects of binding and recognition in the cytochrome *c*/cytochrome *c* peroxidase complex. *J. Am. Chem. Soc.* 115, 3665–3669.
- (66) Yi, Q., Erman, J. E., and Satterlee, J. D. (1994) 1H NMR evaluation of yeast isoenzyme-I ferricytochrome *c* equilibrium exchange dynamics in noncovalent complexes with two forms of yeast cytochrome *c* peroxidase. *J. Am. Chem. Soc.* 116, 1981–1987.
- (67) Volkov, A. N., Worrall, J. A. R., Holtzmann, E., and Ubbink, M. (2006) Solution structure and dynamics of the complex between cytochrome *c* and cytochrome *c* peroxidase determined by paramagnetic NMR. *Proc. Natl. Acad. Sci. U. S. A.* 103, 18945–18950.
- (68) Chroni, S., Lou, B. S., Erman, J. E., Satterlee, J. D., and Moench, S. J. (1992) Proton NMR comparison of noncovalent and covalently cross-linked complexes of cytochrome *c* peroxidase with horse, tuna, and yeast ferricytochromes *c*. *Biochemistry* 31, 3661–3670.

## Chapter 2

(69) Jeng, M. F., Walter Englander, S., Pardue, K., Rogalskyj, J. S., and McLendon, G. (1994) Structural dynamics in an electron-transfer complex. *Nat. Struct. Biol.* 1, 234–238.

(70) Qian, Y., Erman, J. E., and Satterlee, J. D. (1994) Studies of protein-protein association between yeast cytochrome *c* peroxidase and yeast iso-1 ferricytochrome *c* by hydrogen-deuterium exchange labeling and proton NMR spectroscopy. *Biochemistry* 33, 12032–12041.

(71) Volkov, A. N., Bashir, Q., Worrall, J. A. R., Ullmann, G. M., and Ubbink, M. (2010) Shifting the equilibrium between the encounter state and the specific form of a protein complex by interfacial point mutations. *J. Am. Chem. Soc.* 132, 11487–11495.

# Chapter 3

**Efficient encounter complex formation and electron transfer to cytochrome *c* peroxidase with an additional, distant electrostatic binding site.**

Based on the research article:

Di Savino, A., Foerster, J., La Haye, T., Blok, A., Timmer, M., Ullmann, M., and Ubbink, M. (2020) Efficient encounter complex formation and electron transfer to cytochrome *c* peroxidase with an additional, distant electrostatic binding site. *Angew. Chemie Int. Ed.* 132, 23239–23243.



### **Abstract**

Electrostatic interactions can strongly increase the efficiency of protein complex formation. The charge distribution in redox proteins is often optimized to steer a redox partner to the electron transfer active binding site. To test whether the optimized distribution is more important than the strength of the electrostatic interactions, an additional negative patch was introduced on the surface of cytochrome *c* peroxidase, away from the stereospecific binding site, and its effect on the encounter complex as well as the rate of complex formation was determined. Monte Carlo simulations and paramagnetic relaxation enhancement NMR experiments indicate that the partner, cytochrome *c*, interacts with the new patch. Unexpectedly, the rate of the active complex formation was not reduced, but rather slightly increased. The findings support the idea that for efficient protein complex formation the strength of the electrostatic interaction is more critical than an optimized charge distribution.

## Introduction

Electrostatic interactions are fundamental in protein-protein interactions and formation of protein complexes. Charge-charge interactions guide the recognition and binding between proteins and between a protein and a ligand.<sup>1-5</sup> Before forming the stereospecific, active complex, proteins associate into an intermediate state, the encounter complex, consisting of an ensemble of transient conformations, in which the proteins sample the surface of the partner.<sup>6</sup> The encounter complex is thought to reduce the dimensionality of the search for the binding site.<sup>7</sup> During this process electrostatic interactions contribute to pre-organization of the protein orientations in the encounter complex, reducing the surface area to be sampled and promoting the formation of the stereospecific complex. The encounter complex formation is initially mostly driven by long-range electrostatic interactions. Upon closer approach of the two proteins, hydrophobic interactions also come into play, ultimately leading to the formation of the stereospecific complex.<sup>8-15</sup> The association rate constant, the measure for productive complex formation, can be four orders of magnitude lower than the diffusional collision rate constant in cases in which complex formation is not optimized, indicating that most encounters are non-productive and partners dissociate before reaching the stereospecific complex. Such encounters are called futile.<sup>16, 17</sup> On the other hand, association rate constants approach the collision rate constant for some complexes, which is thought to be caused by strong electrostatic pre-organization of the encounter complexes, with the charge interactions guiding the partners to the correct orientation for binding.<sup>1</sup> For such complexes, charge distribution over the surfaces of the proteins is expected to be optimized by evolution. The complex formed by cytochrome P450cam and putidaredoxin was previously studied to understand the function of the different encounter complexes formed by the two proteins. The data suggest that the encounter complexes located in a region with an electrostatically favorable pathway to the stereospecific binding site represent productive encounter states. On the contrary, encounter complexes located far from the binding site and in absence of a favorable charged path that extends to the binding site consist of futile interactions.<sup>18</sup> The encounter complex is therefore a key stage in the formation of a protein complex and mutations that affect the encounter complex have consequences for the stereospecific protein complex. Previous studies by Harel *et al.*<sup>16</sup> on the interactions between TEM1- $\beta$ -lactamase (TEM1) and its inhibitor,  $\beta$ -lactamase-inhibitor protein (BLIP), showed that it is difficult to define a correlation between the energy of the interaction, the surface area searched by the encounter complex and the association rate between two proteins. Recently, it was shown that futile encounter complexes could have a role in regulation of enzyme activity forming competitive encounter complexes.<sup>19, 20</sup> Interestingly, charge mutations on the protein surface far from the active site can either enhance complex formation by creating new productive encounter complexes, or decrease it by breaking diffusional pathways over the surface that would lead to the formation of the stereospecific complex.<sup>21</sup> We wondered how critical such a charge distribution is for fast complex formation in an optimized complex, as compared to the total strength of the electrostatic interactions. Good complexes to study this question are those formed by electron transfer (ET) proteins, as these are highly

transient, i.e. have a high association and dissociation rate constants, and the fraction of the encounter complex is high. The reason for these features is related to the biological function. Transfer of electrons in redox chains, such as found in photosynthesis and respiration, can be rate-limiting for the entire process and, thus, complex formation must be efficient. One of the best characterized ET complexes is the one formed by cytochrome *c* peroxidase (CcP) and cytochrome *c* (Cc) from baker's yeast (*Saccharomyces cerevisiae*). The formation of the encounter complex is driven by electrostatic interactions between positive charges on Cc and negative charges on CcP.<sup>22-26</sup> The encounter state and the stereospecific complex represent 30% and 70% of the complex, respectively.<sup>27, 28</sup> Due to the electrostatic pre-organization, the area sampled by Cc was estimated to be merely 15% of the CcP surface.<sup>28</sup> The fraction of encounter complex was found to be affected by mutations in the binding site, with the fraction of the encounter complex ranging from 10% to 90% for different mutations.<sup>29</sup> CcP catalyzes the reduction of H<sub>2</sub>O<sub>2</sub> to water using electrons donated by reduced Cc. The reaction proceeds through a complicated cycle, during which two molecules of Cc interact with CcP sequentially, each contributing one electron (Text S3.2). In line with other ET complexes, the ET rate is high ( $>50,000\text{ s}^{-1}$ )<sup>30</sup>, the lifetime of the complex is short (0.1 - 1 ms)<sup>31</sup>, the association rate constant very high ( $10^8 - 10^9\text{ M}^{-1}\text{s}^{-1}$  at 200 mM ionic strength)<sup>32</sup> and the affinity in the micromolar range ( $K_D = 5\text{ }\mu\text{M}$ ).<sup>31</sup> In a previous study by Erman and co-workers<sup>33-35</sup> several charge-reversal mutants of CcP were created to determine the impact of the charges on the surface of the protein on the association with Cc. The majority of these mutations, mainly the ones located in or around the binding site of Cc, significantly decreased the affinity between the two proteins. Interestingly, three of these mutations (D37K, E28K, and E209K) are slightly more distant from the binding site and two of them on the opposite side of the protein (D165K and D241K). Although it is possible that the mutation D241K could affect the stability of the protein, this study shows that the charged residues on the surface, also located far from the binding site, have a role in the association process of Cc and CcP.

To establish how important the optimization of the charge distribution on CcP is for achieving these ET specifications, we decided to change the charge distribution on the CcP surface by adding a new negative patch in addition to the existing one surrounding the binding site for Cc. The new patch interferes with the distribution of negative charge in native CcP that appears to be optimized for Cc honing into the stereospecific binding site. Thus, we expected that productive complex formation would be affected negatively, leading to more futile encounters. The interaction with this mutant CcP (CcP\_B) was studied using Monte Carlo electrostatic calculations, paramagnetic relaxation enhancement (PRE) NMR spectroscopy and stopped-flow kinetic measurements to determine the association rate constant as a function of ionic strength. Both modelling and PRE-NMR demonstrate that the new negative patch is visited by Cc in the encounter state. Yet, to our surprise, the association rate is not reduced relative to the interaction with wild type CcP (CcP\_A), and even appears to be enhanced slightly at moderate ionic strength. These observations indicate that the precise charge distribution around the binding site is less

critical for complex formation than expected and the increased strength of the electrostatic interactions may compensate for a less optimal encounter complex.

## Results and Discussion

### *Monte Carlo simulations show Cc to interact with the added patch on CcP*

To test how important the charge distribution of CcP is for binding and reduction by Cc, an additional negative patch was created on one side of the regular binding site for Cc, by changing four positive sidechains to negative ones (mutations K21E, K29E, K90E, and K97E), thus introducing a net charge change of -8 (Figure 3.1a, 3.1b). This construct, CcP\_B, was characterized by Monte Carlo simulations, NMR spectroscopy and stopped-flow spectroscopy. Rigid-body Monte Carlo simulations, based only on electrostatic and steric interactions, were used to simulate the encounter complexes of Cc with wild type CcP (CcP\_A) or CcP\_B. Figure 3.1c shows CcP in ribbon representation and the ensemble of Cc centers-of-mass based on electrostatic interaction energies. The densest regions represent the most favorable Cc orientations. The interactions of Cc with CcP\_A (cyan spheres) are predominantly found at the location of the stereospecific binding site, in accord with earlier calculations<sup>23, 26, 28, 37</sup> According to the simulations, the mutations introduced on the CcP\_B surface considerably affect the encounter complex, with Cc sampling the area with the added negative charges of CcP\_B (magenta spheres) more frequently than the crystallographic binding site. Note that these calculations only consider electrostatic interactions. In the stereospecific complex additional favorable interactions are present, so the total interaction is not expected to shift as dramatically as follows from these calculations. Still, it is clear that these extra negative charges should have a significant effect on the distribution of Cc in the encounter state.

### *Affinity and binding of Cc is similar for CcP\_A and CcP\_B*

NMR titration experiments of Cc and CcP\_A and CcP\_B (S. I. Text S3.1 and Figure S3.1) show that the introduction of the additional charges has surprisingly little effect on the affinity and binding effects in the HSQC spectrum. It is noted that CSP are predominantly caused by the stereospecific complex and not by the encounter complex. In the latter, solvation is likely to be similar to that for free Cc and binding occurs in many orientations. Both factors contribute to minimal perturbations of the chemical environment of the amide groups observed in the HSQC experiment. Desolvation and a well-defined orientation in the stereospecific complex are expected to cause most of the CSP.<sup>38-40</sup> So it appears that the additional charges do not cause a major shift in the equilibrium between encounter state and stereospecific complex, reported to be 30%:70%,<sup>27, 28</sup> because that would have changed the overall size of the CSP. The extremely dynamic nature of the encounter complex and the fact that it is usually present in a small fraction of the protein-complex lifetime, makes it invisible to the conventional biophysical techniques used to study protein-protein

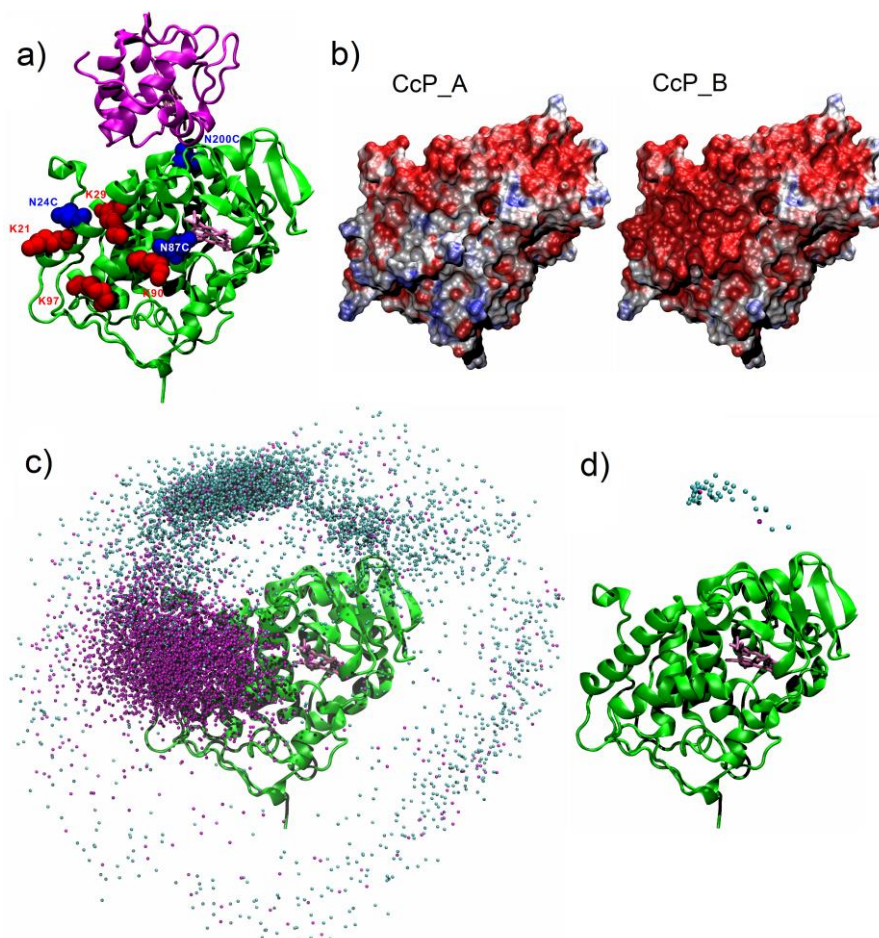


**Figure 3.1.** A new negative patch on CcP. a) Crystal structure of the stereospecific complex formed by Cc (magenta ribbons) and CcP (green ribbons) is shown (PDB 2PCC<sup>22</sup>). The heme groups are shown in pink sticks, the residues that were mutated to introduce additional negative charges in CcP\_B are in red spacefilling representation and the residues mutated to cysteines for PRE experiments in blue spacefill. Electrostatic potential on the surface of CcP\_A and CcP\_B ranging from -5 (red) to 5 kcal/e<sup>o</sup> (blue) at an ionic strength of 120 mM. c) The structure of CcP (green ribbon) is surrounded by the centers of the mass of Cc in the ensemble of encounters of the complexes Cc:CcP\_A (cyan) and Cc:CcP\_B (magenta) as obtained from rigid body Monte Carlo simulations. d) The structure of CcP (green ribbon) is surrounded by the centers of the mass of Cc in the ensemble of encounters of the complexes Cc:CcP\_A (cyan) and Cc:CcP\_B (magenta) in which the edge-to-edge distance between Cc heme and the indole of the CcP compound I radical forming Trp (Trp-191) is less than 1.6 nm, as obtained from rigid body Monte Carlo simulations. CcP is in the same orientation in all panels. The pictures were produced with VMD.<sup>36</sup>

structures.

***PRE experiments demonstrate that Cc interacts with the new negative patch***

To establish whether Cc visits the new negative patch in the encounter state, we employed paramagnetic relaxation enhancement (PRE) NMR spectroscopy. PRE are very sensitive to minor states in which a nucleus is closer to the paramagnetic center than in the major state, because of the large relaxation effect of unpaired electrons and the steep distance dependence of the effect ( $r^{-6}$ ).<sup>41, 42</sup> To probe for such Cc interactions, two amino acids surrounding the new negative patch on CcP\_B were individually mutated to cysteines (N87C and N24C, see Figure 3.1). These positions surround the new negative patch but are far from the regular Cc binding site. The mutations were also made in CcP\_A. A third cysteine was introduced near the binding site of Cc (N200C) as a control. PRE data for this site have been reported before for the complex of CcP with WT Cc as well as several mutants.<sup>29, 43</sup> The cysteine residues were used for the attachment of the small, stable spin label MTSL that causes PRE in a sphere of up to 2.5 nm. The spin labelled CcP\_B was mixed with  $^{15}\text{N}$  labelled Cc to record intermolecular PRE, from the CcP spin label on the Cc nuclei. The spin labels on the mutants N87C, N24C, and N200C of CcP\_B induced large PRE in Cc (Figure 3.2). Analogous experiments on CcP\_A mutant spin labelled at N87C and N24C showed much smaller PRE (Figure 3.2),

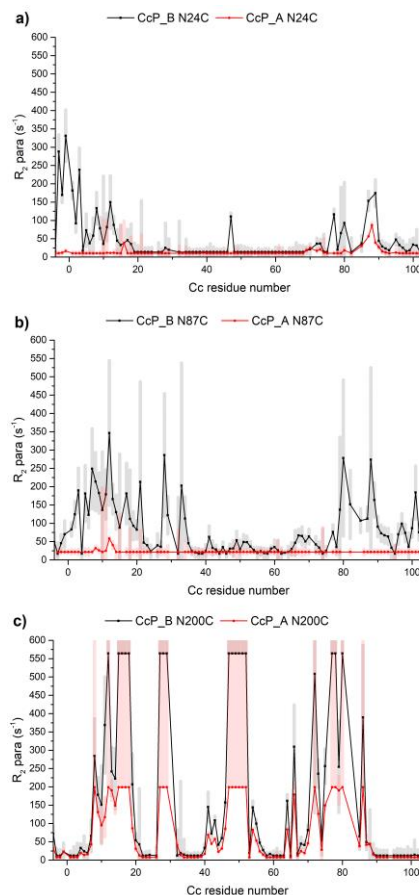


**Figure 3.2.** Probing new interactions with PRE NMR. The PRE on Cc in presence of CcP\_A (in red) or CcP\_B (in black), tagged with MTSL on N24C (a) and N87C (b), both located around the negative patch introduced in CcP\_B, and N200C (c) close to the stereospecific binding site. The errors bars are indicated as shaded regions in red for Cc:CcP\_A and in grey for Cc:CcP\_B and represent the propagated 2 SD errors of the raw data. The upper and lower limit cut-offs for PRE differ between samples, depending on the fraction of CcP that was paramagnetic, as based on EPR measurements (see the Materials and Methods in the Supplementary Information section for details).

whereas the effects for N200C were similar to those for CcP\_B and those reported before.<sup>27</sup> Thus, the large differences in PRE between CcP\_A and CcP\_B provide strong evidence that the new negative patch has become part of the encounter complex and is visited by Cc.

### ***Binding at the new negative patch yields productive encounters***

The aim of this project was to determine whether the charges involved in formation of the encounter complex need to surround the binding site for the stereospecific complex to achieve optimal electron transfer. The NMR results show that the encounter complex has changed in CcP\_B, extending the encounter complex away from the stereospecific binding site. To monitor whether the formation of productive, i.e. electron transfer active, complexes is affected by the charges added to the surface of CcP\_B, the association rate constant was determined by stopped-flow spectrometry, following early work of Miller *et al.*<sup>32</sup> In these experiments, CcP is first reacted with hydrogen peroxide to form the oxyferryl/Trp-radical species (compound I)<sup>44-46</sup> and then mixed rapidly with reduced Cc. The ensuing electron transfer from Cc(II) to compound I, forming Cc(III) and compound II,<sup>47,48</sup> is followed in time as a change in Cc absorption at 416 nm (see Text S3.2). It can be shown that the observed second order rate constant is a lower limit of the association rate constant for productive complex formation, see equation 3 in the Experimental Procedures

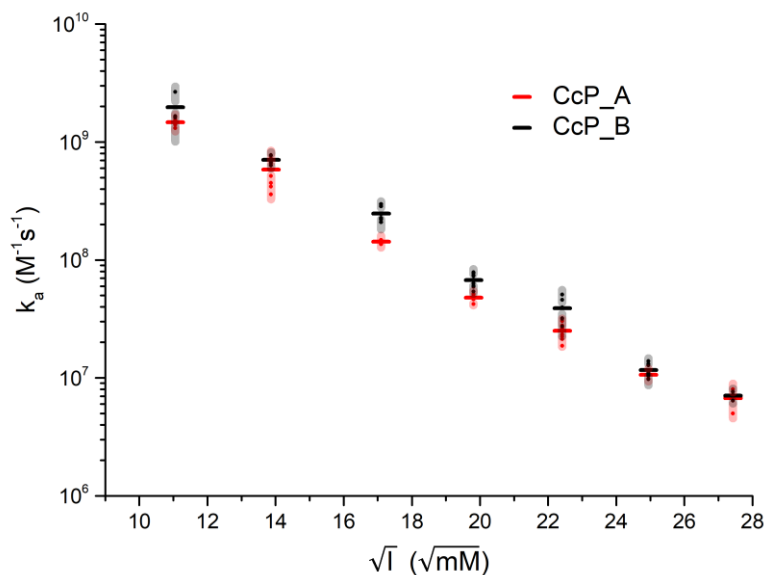


**Figure 3.3.** Association rate constants of Cc and CcP. The association rate constants ( $k_a$ ) of the complexes Cc:CcP\_A (red symbols) and Cc:CcP\_B (black symbols) plotted as a function of the root of the ionic strength. The colored dots represent the  $k_a$  values obtained from fitting averages of 14 single measurements, while the bars represent the average of the dots. The errors in the rate constants are shown as shades and represent the standard deviation between the dots (see the Materials and Methods section in the Supplementary Information for details).

in the Supplementary Information.<sup>1</sup> In the present case, the observed rate constant ( $k_2$ ) approaches the association rate constant ( $k_a$ ) because the electron transfer rate ( $k_{et}$ ) is much larger than the dissociation rate constant ( $k_{-a}$ ). Association is strongly ionic strength dependent,<sup>49-53</sup> because of the favorable electrostatic interactions between CcP and Cc. The results are shown in Figure 3.3 and Table S3.1. Interestingly, they show that Cc forms a productive, reactive complex at least as effectively with CcP\_B as with CcP\_A. At moderate ionic strength the rate constants are even slightly higher, indicating a more favorable interaction. Given the fact that the rates for the Cc-CcP\_A interaction at low ionic strength are over  $10^9 \text{ M}^{-1}\text{s}^{-1}$ , and thus close to the diffusion limit, it is remarkable that with CcP\_B Cc achieves even faster association. To check whether this could be explained by possible ET from Cc bound to the new encounter site in addition of ET in the stereospecific complex the edge-to-edge distance between Cc heme and the indole of the CcP compound I radical forming Trp (Trp-191) was measured for all Cc orientations observed in the Monte Carlo simulation of CcP\_B (Figure 3.1d). All orientations of Cc in the new negative patch yield distances  $> 1.6 \text{ nm}$ , suggesting that the rate of ET would be negligibly slow from this site. Shorter distances are only found for Cc binding near the stereospecific complex. Thus, to achieve ET Cc that binds at the new patch needs to diffuse to the binding site of the stereospecific complex to form a productive complex. It is concluded, therefore, that the additional charges enhance the chance of the formation of the productive complex, even though the new charges are on the side of CcP, relative to the stereospecific binding site (Figure 3.1). This is consistent with the idea that encounter complexes close to the binding site consist of productive encounters because they promote the formation of the stereospecific complex.<sup>18</sup>

## Conclusions

In summary, an additional negative patch was introduced on the surface of CcP, lateral to its stereospecific binding site for Cc (Figure 3.1). Both the Monte Carlo calculations and the PRE data indicate that Cc interacts with the new patch, yet this does not perturb the formation of the stereospecific complex. Earlier work demonstrated that the natural electrostatic patch of CcP optimally directs Cc to the site of stereospecific complex.<sup>22, 23, 26, 28, 37</sup> However, an optimized distribution of the charges around the stereospecific binding site is apparently not critical. Cc molecules that bind at the new negative patch can find their way to the stereospecific binding site before dissociation of the encounter complex. The new site thus produces productive rather than futile encounters.<sup>1, 41</sup> CcP\_B has a much larger negative charge compared to CcP\_A. We conclude that the positive effect of the increased strength of the electrostatic interaction on the association rate outweighs the negative effect of a less optimized charge distribution.

## References

- (1) Schreiber, G., Haran, G., and Zhou, H. X. (2009) Fundamental aspects of protein-protein association kinetics, *Chem. Rev.* **109**, 839-860.



- (2) Ubbink, M. (2012) Dynamics in transient complexes of redox proteins, *Biochem. Soc. Trans.* 40, 415-418.
- (3) Yang, J., Zeng, Y. F., Liu, Y. F., Gao, M., Liu, S., Su, Z. D., and Huang, Y. Q. Electrostatic interactions in molecular recognition of intrinsically disordered proteins, *J. Biomol. Struct. Dyn.*, 12.
- (4) Zhou, H. X., and Pang, X. D. (2018) Electrostatic interactions in protein structure, folding, binding, and condensation, *Chem. Rev.* 118, 1691-1741.
- (5) Clore, G. M. (2014) Interplay between conformational selection and induced fit in multidomain protein-ligand binding probed by paramagnetic relaxation enhancement, *Biophys. Chem.* 186, 3-12.
- (6) Schilder, J., and Ubbink, M. (2013) Formation of transient protein complexes, *Curr. Opin. Struct. Biol.* 23, 911-918.
- (7) Adam, G., and Delbrück, M. (1968) Reduction of dimensionality in biological diffusion processes, In *Structural Chemistry and Molecular Biology* (A. Rich, N. D., Ed.), p 198, W. H. Freeman and Co., San Francisco.
- (8) Kim, Y. C., Tang, C., Clore, G. M., and Hummer, G. (2008) Replica exchange simulations of transient encounter complexes in protein-protein association, *Proc. Natl. Acad. Sci. U. S. A.* 105, 12855-12860.
- (9) Van de Water, K., van Nuland, N. A. J., and Volkov, A. N. (2014) Transient protein encounters characterized by paramagnetic NMR, *Chem. Sci.* 5, 4227-4236.
- (10) Scanu, S., Foerster, J. M., Ullmann, G. M., and Ubbink, M. (2013) Role of hydrophobic interactions in the encounter complex formation of the plastocyanin and cytochrome *f* complex revealed by paramagnetic NMR spectroscopy, *J. Am. Chem. Soc.* 135, 7681-7692.
- (11) Sugase, K., Dyson, H. J., and Wright, P. E. (2007) Mechanism of coupled folding and binding of an intrinsically disordered protein, *Nature* 447, 1021-U1011.
- (12) Camacho, C. J., Weng, Z., Vajda, S., and DeLisi, C. (1999) Free energy landscapes of encounter complexes in protein-protein association, *Biophys. J.* 76, 1166-1178.
- (13) Camacho, C. J., Kimura, S. R., DeLisi, C., and Vajda, S. (2000) Kinetics of desolvation-mediated protein-protein binding, *Biophys. J.* 78, 1094-1105.
- (14) Camacho, C. J., and Vajda, S. (2002) Protein-protein association kinetics and protein docking, *Curr. Opin. Struct. Biol.* 12, 36-40.

- (15) Rajamani, D., Thiel, S., Vajda, S., and Camacho, C. J. (2004) Anchor residues in protein-protein interactions, *Proc. Natl. Acad. Sci. U. S. A.* *101*, 11287-11292.
- (16) Harel, M., Spaar, A., and Schreiber, G. (2009) Fruitful and Futile Encounters along the Association Reaction between Proteins, *Biophys. J.* *96*, 4237-4248.
- (17) Fawzi, N. L., Doucleff, M., Suh, J. Y., and Clore, G. M. (2010) Mechanistic details of a protein-protein association pathway revealed by paramagnetic relaxation enhancement titration measurements, *Proc. Natl. Acad. Sci. U. S. A.* *107*, 1379-1384.
- (18) Andralojc, W., Hiruma, Y., Liu, W. M., Ravera, E., Nojiri, M., Parigi, G., Luchinat, C., and Ubbink, M. (2017) Identification of productive and futile encounters in an electron transfer protein complex, *Proc. Natl. Acad. Sci. U. S. A.* *114*, E1840-E1847.
- (19) Strickland, M., Kale, S., Strub, M. P., Schwieters, C. D., Liu, J., Peterkofsky, A., and Tjandra, N. (2019) Potential regulatory role of competitive encounter complexes in paralogous phosphotransferase systems, *J. Mol. Biol.* *431*, 2331-2342.
- (20) Kale, S., Strickland, M., Peterkofsky, A., Liu, J., and Tjandra, N. (2019) Model of a kinetically driven crosstalk between paralogous protein encounter complexes, *Biophys. J.* *117*, 1655-1665.
- (21) An, S. Y., Kim, E.-H., and Suh, J.-Y. (2018) Facilitated protein association via engineered target search pathways visualized by paramagnetic NMR spectroscopy, *Structure* *26*, 887-893.e882.
- (22) Pelletier, H., and Kraut, J. (1992) Crystal structure of a complex between electron transfer partners, cytochrome *c* peroxidase and cytochrome *c*, *Science* *258*, 1748-1755.
- (23) Gabdoulline, R. R., and Wade, R. C. (2001) Protein-protein association: investigation of factors influencing association rates by Brownian dynamics simulations, *J. Mol. Biol.* *306*, 1139-1155.
- (24) Poulos, T. L., Freer, S. T., Alden, R. A., Edwards, S. L., Skogland, U., Takio, K., Eriksson, B., Xuong, N. H., Yonetani, T., and Kraut, J. (1980) Crystal-structure of cytochrome-*c* peroxidase, *J. Biol. Chem.* *255*, 575-580.

- (25) Louie, G. V., Hutcheon, W. L. B., and Brayer, G. D. (1988) Yeast iso-1-cytochrome *c*: A 2.8 Å resolution three-dimensional structure determination, *J. Mol. Biol.* *199*, 295-314.
- (26) Northrup, S., Boles, J., and Reynolds, J. (1988) Brownian dynamics of cytochrome *c* and cytochrome *c* peroxidase association, *Science* *241*, 67-70.
- (27) Volkov, A. N., Worrall, J. A. R., Holtzmann, E., and Ubbink, M. (2006) Solution structure and dynamics of the complex between cytochrome *c* and cytochrome *c* peroxidase determined by paramagnetic NMR, *Proc. Natl. Acad. Sci. U. S. A.* *103*, 18945-18950.
- (28) Bashir, Q., Volkov, A. N., Ullmann, G. M., and Ubbink, M. (2010) Visualization of the encounter ensemble of the transient electron transfer complex of cytochrome *c* and cytochrome *c* peroxidase, *J. Am. Chem. Soc.* *132*, 241-247.
- (29) Volkov, A. N., Bashir, Q., Worrall, J. A. R., Ullmann, G. M., and Ubbink, M. (2010) Shifting the equilibrium between the encounter state and the specific form of a protein complex by interfacial point mutations, *J. Am. Chem. Soc.* *132*, 11487-11495.
- (30) Geren, L., Hahm, S., Durham, B., and Millett, F. (1991) Photoinduced electron-transfer between cytochrome-*c* peroxidase and yeast cytochrome-*c* labeled at cys-102 with(4-bromomethyl-4'-methylbipyridine) bis(bypyridine) ruthenium<sup>2+</sup>, *Biochemistry* *30*, 9450-9457.
- (31) Worrall, J. A. R., Kolczak, U., Canters, G. W., and Ubbink, M. (2001) Interaction of yeast iso-1-cytochrome *c* with cytochrome *c* peroxidase investigated by N-15,H-1 heteronuclear NMR spectroscopy, *Biochemistry* *40*, 7069-7076.
- (32) Miller, M. A., Liu, R. Q., Hahm, S., Geren, L., Hibdon, S., Kraut, J., Durham, B., and Millett, F. (1994) Interaction domain for the reaction of cytochrome-*c* with the radical and the oxyferryl heme in cytochrome-*c* peroxidase compound-I, *Biochemistry* *33*, 8686-8693.
- (33) Erman, J. E., Vitello, L. B., Pearl, N. M., Jacobson, T., Francis, M., Alberts, E., Kou, A., and Bujarska, K. (2015) Binding of yeast cytochrome *c* to forty-four charge-reversal mutants of yeast cytochrome *c* peroxidase: isothermal titration calorimetry, *Biochemistry* *54*, 4845-4854.

- (34) Pearl, N. M., Jacobson, T., Arisa, M., Vitello, L. B., and Erman, J. E. (2007) Effect of single-site charge-reversal mutations on the catalytic properties of yeast cytochrome *c* peroxidase: Mutations near the high-affinity cytochrome *c* binding site, *Biochemistry* **46**, 8263-8272.
- (35) Pearl, N. M., Jacobson, T., Meyen, C., Clementz, A. G., Ok, E. Y., Choi, E., Wilson, K., Vitello, L. B., and Erman, J. E. (2008) Effect of single-site charge-reversal mutations on the catalytic properties of yeast cytochrome *c* peroxidase: Evidence for a single, catalytically active, cytochrome *c* binding domain, *Biochemistry* **47**, 2766-2775.
- (36) Humphrey, W., Dalke, A., and Schulten, K. (1996) VMD: Visual molecular dynamics, *J. Mol. Graph.* **14**, 33-38.
- (37) Castro, G., Boswell, C. A., and Northrup, S. H. (1998) Dynamics of protein-protein docking: Cytochrome *c* and cytochrome *c* peroxidase revisited, *J. Biomol. Struct. Dyn.* **16**, 413-424.
- (38) Worrall, J. A. R., Liu, Y. J., Crowley, P. B., Nocek, J. M., Hoffman, B. M., and Ubbink, M. (2002) Myoglobin and cytochrome *b(5)*: A nuclear magnetic resonance study of a highly dynamic protein complex, *Biochemistry* **41**, 11721-11730.
- (39) Worrall, J. A. R., Reinle, W., Bernhardt, R., and Ubbink, M. (2003) Transient protein interactions studied by NMR spectroscopy: The case of cytochrome *c* and adrenodoxin, *Biochemistry* **42**, 7068-7076.
- (40) Xu, X. F., Reinle, W. G., Hannemann, F., Konarev, P. V., Svergun, D. I., Bernhardt, R., and Ubbink, M. (2008) Dynamics in a pure encounter complex of two proteins studied by solution scattering and paramagnetic NMR spectroscopy, *J. Am. Chem. Soc.* **130**, 6395-6403.
- (41) Clore, G. M., and Iwahara, J. (2009) Theory, practice, and applications of paramagnetic relaxation enhancement for the characterization of transient low-population states of biological macromolecules and their complexes, *Chem. Rev.* **109**, 4108-4139.
- (42) Otting, G. (2010) Protein NMR using paramagnetic ions, In *Annual Review of Biophysics* (Rees, D. C., Dill, K. A., and Williamson, J. R., Eds.), p 387, Annu. Rev. Biophys., Palo Alto.

- (43) Volkov, A. N., Ubbink, M., and van Nuland, N. A. J. (2010) Mapping the encounter state of a transient protein complex by PRE NMR spectroscopy, *J. Biomol. NMR* 48, 225-236.
- (44) Erman, J. E., Vitello, L. B., Mauro, J. M., and Kraut, J. (1989) Detection of an oxyferryl porphyrin  $\pi$ -cation-radical intermediate in the reaction between hydrogen peroxide and a mutant yeast cytochrome *c* peroxidase - Evidence for tryptophan-191 involvement in the radical site of compound I, *Biochemistry* 28, 7992-7995.
- (45) Scholes, C. P., Liu, Y. J., Fishel, L. A., Farnum, M. F., Mauro, J. M., and Kraut, J. (1989) Recent ENDOR and pulsed electron paramagnetic resonance studies of cytochrome *c* peroxidase - Compound I and its site-directed mutants, *Isr. J. Chem.* 29, 85-92.
- (46) Sivaraja, M., Goodin, D. B., Smith, M., and Hoffman, B. M. (1989) Identification by ENDOR of Trp191 as the free-radical site in cytochrome *c* peroxidase compound ES, *Science* 245, 738-740.
- (47) Coulson, A. F. W., Erman, J. E., and Yonetani, T. (1971) Studies on cytochrome *c* peroxidase XVII. Stoichiometry and mechanism of the reaction of compound ES with donors, *J. Biol. Chem.* 246, 917.
- (48) Summers, F. E., and Erman, J. E. (1988) Reduction of cytochrome *c* peroxidase compounds I and II by ferrocycytochrome *c*. A stopped-flow kinetic investigation., *J. Biol. Chem.* 263, 14267-14275.
- (49) Matthis, A. L., and Erman, J. E. (1995) Cytochrome *c* peroxidase-catalyzed oxidation of yeast iso-1 ferrocycytochrome *c* by hydrogen peroxide. Ionic strength dependence of the steady-state parameters., *Biochemistry* 34, 9985-9990.
- (50) Matthis, A. L., Vitello, L. B., and Erman, J. E. (1995) Oxidation of yeast iso-1 ferrocycytochrome *c* by yeast cytochrome *c* peroxidase compounds I and II. Dependence upon ionic strength, *Biochemistry* 34, 9991-9999.
- (51) Zhou, J. S., and Hoffman, B. M. (1994) Stern-Volmer in reverse: 2:1 stoichiometry of the cytochrome *c*-cytochrome *c* peroxidase electron-transfer complex, *Science* 265, 1693-1696.
- (52) Van de Water, K., Sterckx, Y. G. J., and Volkov, A. N. (2015) The low-affinity complex of cytochrome *c* and its peroxidase, *Nat. Commun.* 6, 7073.

- (53) McLendon, G., Zhang, Q., Wallin, S. A., Miller, R. M., Billstone, V., Spears, K. G., and Hoffman, B. M. (1993) Thermodynamic and kinetic aspects of binding and recognition in the cytochrome *c*/cytochrome *c* peroxidase complex, *J. Am. Chem. Soc.* *115*, 3665-3669.

## Supplementary Information

### Materials and Methods

#### Mutagenesis

The *Saccharomyces cerevisiae* CcP gene with mutation C128A to avoid dimerization and the sequence MKT at the N-terminus was considered as the wild-type gene (CcP\_A)<sup>1,2</sup> and sub-cloned in a pET28a(+) vector.<sup>3</sup> CcP\_B additionally contained the mutations K21E, K29E, K90E, and K97E. The DNA construct was ordered from a commercial vendor. For PRE experiments, the mutations N24C, N87C and N200C were introduced one at a time in the CcP genes through site specific mutagenesis using the QuikChange method (Life technologies, Invitrogen, ThermoFisher). The sequence of constructs were verified by DNA sequencing.

#### Protein Production

CcP was produced in *E. coli* BL21 Star (DE3)pLysS (Life Technologies Europe BV, Bleiswijk, the Netherlands). The production and purification followed previously described protocols,<sup>2,4</sup> with some adaptations. The gradient for the elution during the anion-exchange chromatography for CcP\_A was performed by mixing 50 mM potassium phosphate pH 5 and 500 mM potassium phosphate pH 5, while 500 mM KCl was added to the second buffer to elute CcP\_B. *S. cerevisiae* Cc, either with or without <sup>15</sup>N labelling was produced using the iso-1-cytochrome *c* gene in a pUC19 based plasmid and purified as described.<sup>3,5,6</sup>

#### Tagging with MTS/MTSL

CcP was tagged with either MTS (1-acetoxy-2,2,5,5-tetramethyl-d3-pyrroline-3-methyl)-methanethiosulfonate) as diamagnetic tag (TRC, Canada) or MTSL (1-oxyl-2,2,5,5-tetramethyl-d3-pyrroline-3-methyl)-methanethiosulfonate) (ChemCruz, Santa Cruz Biotechnology, Texas) as paramagnetic tag, according to the published procedure.<sup>1</sup> It was found that the tagging efficiency was close to 100% according to mass spectrometry. However, after tagging not all labels remained paramagnetic according to electron paramagnetic resonance (EPR) spectroscopy, ranging between about 30% and 80% (Table S3.2). For the EPR measurement two samples were prepared in 20 mM sodium phosphate, 0.1 M NaCl, pH 6 buffer. One contained 140  $\mu$ M MTSL tagged CcP and one 100  $\mu$ M free MTSL, freshly dissolved for each experiment. The measurements were performed at 9.8 GHz, at room temperature, using 0.63 mW microwave power, 2 G modulation amplitude, 100 kHz modulation frequency and a time constant of 10.24 msec (Figure S3.4). The percentage of paramagnetic protein was calculated comparing the double integral of free MTSL and tagged CcP spectra. The error in the EPR measurement is estimated to be  $\pm$  5 percent points.

## NMR Experiments

For titration experiments, NMR samples contained 200  $\mu\text{M}$  of resting state CcP in 20 mM sodium phosphate, 0.1 M NaCl, pH 6 and 6%  $\text{D}_2\text{O}$  for lock. Oxidized  $^{15}\text{N}$  Cc was titrated in ten aliquots into the CcP solution, increasing the ratio (Cc)/(CcP) progressively from 0.3 to 3. For PRE measurements, NMR samples contained  $^{15}\text{N}$  Cc and MTS(L) labelled CcP in a 1:1 ratio and concentration of 200  $\mu\text{M}$  in the same buffer. BEST-TROSY-HSQC<sup>7</sup> spectra were recorded on a Bruker AVIII HD 850 MHz spectrometer at 293 K with 0.333 sec relaxation delay, 64 scans and 1048 and 200 complex points in the  $^1\text{H}$  and  $^{15}\text{N}$  dimensions, respectively. It is noted that the paramagnetic relaxation also affects  $R_1$  relaxation, which can lead to a larger recovery of magnetization for amide protons that experience paramagnetic relaxation. This effect can result in an underestimation of the PRE, and thus the PRE values should be considered lower limits. PREs are only interpreted qualitatively in this work and the effects are compared for CcP\_A and CcP\_B. Thus, a possible underestimation of the PRE does not affect the conclusions. Data processing was done in Topspin 4.0.6 (Bruker, Karlsruhe, Germany) and the data were analyzed with CCPN analysis version 2.4.0. Assignment of the  $^{15}\text{N}$ ,  $^1\text{H}$  resonances of free Cc was based on literature data<sup>8-10</sup> (BMRB 17845). The chemical shift perturbations (CSP) were analyzed by overlaying the spectrum of free Cc with the spectra of Cc bound with CcP at different concentrations. The  $K_D$  was calculated by fitting the data to equation (1),<sup>11</sup> describing a 1:1 binding model:

$$\Delta\nu^i = \frac{1}{2} \Delta\nu^0 \left( A - \sqrt{A^2 - \frac{4}{R}} \right) \quad A = 1 + \frac{1}{R} + \frac{P_0 R + C_0}{R P_0 C_0 K_A} \quad (1)$$

where  $P_0$  is the starting concentration CcP,  $C_0$  is the stock concentration of Cc,  $R$  is the ratio ( $\text{Cc}_i/\text{CcP}_i$ ) at step  $i$  in the titration,  $\Delta\nu^i$  is the chemical shift change at step  $i$ ,  $\Delta\nu^0$  is the maximal change in the chemical shift and  $K_A$  is the association constant ( $1/K_D$ ). Fitting was done with OriginPro 9.1 (OriginLab, Northampton, USA). The average CSP were calculated as previously described.<sup>12</sup> The association constant was used to calculate the percentage of Cc bound to CcP in the samples with 1:1 ratio of CcP:Cc. Of Cc, 84% and 83% was bound to CcP\_A and CcP\_B, respectively. The average CSP for the 100% bound form of Cc was extrapolated dividing the average CSP observed by 0.84 or 0.83 respectively. The spectra were also analyzed with TITAN software,<sup>13</sup> after processing the time domain data with nmripe,<sup>14</sup> yielding lower limits for the dissociation rate constant,  $k_a$ , with  $K_D$  fixed at 6  $\mu\text{M}$ .

For PRE analysis, the ratio between the intensity (peak heights) of the peaks of Cc in complex with CcP tagged with MTS or MTSL ( $I_{\text{para}}/I_{\text{dia}}$ ) was used. All the  $I_{\text{para}}/I_{\text{dia}}$  were normalized using the intensity of the residues that were not affected by PRE (20% of the peaks). The uncertainties for the  $I_{\text{para}}/I_{\text{dia}}$  values of each amide were calculated by propagation of two times the standard deviation of the noise level of each spectrum. The PRE was calculated as previously described.<sup>3, 15, 16</sup> The PREs were corrected for the fraction



of Cc bound to CcP (83% to CcP\_B and 84% to CcP\_A) and for the percentage of paramagnetic signal of the tagged CcP as measured by EPR (see above and Table S3.2). The error in the  $R_{2\text{dia}}$  values were obtained by calculating two times the standard deviation of the  $R_{2\text{dia}}$  of several PRE experiments conducted on the complexes Cc:CcP\_A or Cc:CcP\_B respectively. A lower limit for the PRE was set to  $5\text{ s}^{-1}$ , because smaller PREs cannot be measured accurately, while the upper limit was determined by the noise level of the spectrum, i.e. the lowest point from which the peaks in the paramagnetic spectrum are broadened beyond detection. These limits were scaled by dividing with the fraction of protein bound and the fraction of paramagnetic CcP as derived from the EPR signal.

### Monte Carlo simulations of encounter complex ensemble

The structures of CcP and Cc were taken from the PDB 2PCC.<sup>17</sup> On both proteins hydrogen atoms were added with the module HBUILD<sup>18</sup> in the program CHARMM.<sup>19</sup> The positions of the heavy atoms were preserved while only the hydrogens were minimized with the CHARMM force field.<sup>20</sup> For the mutant CcP B four mutations, as stated in the experiment, were introduced: K21E, K29E, K90E, and K97E using Pymol.<sup>21</sup> The heme ligands of CcP and Cc were considered to be in the oxidized state. The electrostatic potential of CcP was calculated with the program APBS.<sup>22</sup> In order to include the solvent, the dielectric constants of the protein and the water were set to 4 and 80, respectively. The calculation was performed at 303 K and in the presence of 120 mM NaCl. The electrostatic potentials were saved on a grid with a diameter of 22.5 nm.

The electrostatic docking procedure was done with the program suite MCMAP.<sup>23</sup> The protein CcP was considered as receptor while Cc as a ligand was moving randomly in the electrostatic field of CcP. The simulation consisted of 250 runs with  $10^6$  steps for each at a temperature of 303 K. For the resulting ensemble only encounters fulfilling the Metropolis MC criterion<sup>24</sup> were saved. To account for the encounter complex, different ensembles were created in which encounters within a distance of 0.3 nm to the surface of CcP or without a distance criterion were considered as valid encounter. For each resulting ensemble, randomly chosen 5000 encounters were used for further analysis. The resulting ensembles were analyzed more in detail for the possibility of an electron transfer reaction from CcP to Cc, from which the one with a surface distance of 0.3 nm was used further. An electron transfer reaction was considered as possible if the minimal edge-to-edge distance of the Trp191 indole of CcP to the heme of Cc was less than 1.6 nm.

### Kinetic measurements

Immediately prior to the measurements, Cc was reduced with sodium ascorbate in 20 mM sodium phosphate solution, 270 mM NaCl, pH 8. Subsequently, using PD10 columns, both Cc and CcP were brought into a buffer containing 20 mM sodium phosphate solution and NaCl, pH 6 with the desired ionic strength, 752 mM, 622 mM, 502 mM, 392 mM, 292 mM, 192 mM or 122 mM NaCl. Resting state CcP was converted into compound I with 1 molar

equivalent  $\text{H}_2\text{O}_2$  yielding a shift of the Soret band from 410 nm to 420 nm. Stopped-flow experiments were performed on a SX20 stopped flow spectrometer (AppliedPhotophysics, Leatherhead, Surrey, UK) with a 1.2 ms deadtime with a 1:1 concentration ratio of Cc and CcP, either 1  $\mu\text{M}$  (concentration after mixing) for buffers with  $I = 752 \text{ mM}$  to  $I = 292 \text{ mM}$  or 0.5  $\mu\text{M}$  for  $I = 192 \text{ mM}$  and  $I = 122 \text{ mM}$ . The kinetic traces were measured following the absorbance at 416 nm (oxidation of Cc, see Text S3.1). The change in absorbance ( $\Delta A_{416}$ ) was fitted to equation (2):

$$\Delta A_{416} = B_0 \cdot \Delta \varepsilon_{416} \cdot \left(1 - \frac{1}{1 + k_2 \cdot B_0 \cdot t}\right) + C \quad (2)$$

where  $B_0$  is the starting concentration of Cc(II) and CpdI,  $\Delta \varepsilon_{416}$  is the difference in extinction coefficient at 416 nm for oxidized and reduced Cc,  $-40 \text{ mM}^{-1} \text{ cm}^{-1}$  (25-27) and  $C$  corrects for the baseline voltage of the spectrometer. Equation 2 is based on the analytical solution of the differential equation for the change in concentrations of Cc(II) and CpdI in the case that the starting concentrations are equal and the stoichiometry of conversion is 1:1. It was used to obtain the bimolecular rate constant  $k_2$ , which depends on the rate constant of association ( $k_a$ ), the dissociation rate constant ( $k_{-a}$ ) and the electron transfer rate ( $k_{et}$ ), equation (3):

$$k_2 = \frac{k_a k_{et}}{k_{-a} + k_{et}} \quad (3)$$

Under the assumption that electron transfer is much faster than dissociation ( $k_{-a} \ll k_{et}$ ), the observed rate approaches the association rate constant,  $k_2 \approx k_a$ .<sup>28, 29</sup> The analysis of the data was done with OriginPro 9.1 (OriginLab, Northampton, USA). Every curve resulted from the average of fourteen single measurements. The reported  $k_a$  is the average of at least three curves each fitted to the equation 2. The curves presented an artifact at the beginning of the measurement, probably due to the mixing phase, which was not considered in the fitting (Figure S3.3). Since the equation used to fit the kinetics assumes a 1:1 ratio in concentration between Cc and CcP and due to the complexity of the Cc:CcP cycle, just the rapid decay caused by the oxidation of Cc( $\text{Fe}^{+2}$ ) was fitted to obtain the  $k_a$ . In the second part the curves, other reactions can have a relevant influence on the absorbance at 416 nm, particularly the conversion of CpdII to CcP. The errors in the rate constants represent the standard deviation between the rates obtained from the single fits at each salt concentration (Table S3.1).

## Supporting Text

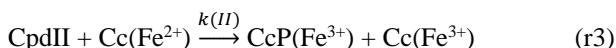
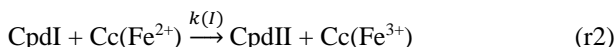
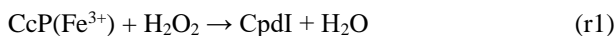
### Text S3.1. Affinity and binding of Cc is similar for CcP\_A and CcP\_B

NMR spectroscopy was used to compare the general characteristics of binding of Cc to CcP\_B with binding to CcP\_A experimentally.  $^{15}\text{N}$  labelled Cc was titrated into a solution of unlabeled CcP and the effects on the  $^{15}\text{N}$ - $^1\text{H}$  HSQC spectrum were analyzed. At a low

ratio of Cc to CcP, most Cc is in the bound state and with increasing ratio more Cc is in the free state. The resonances shifted during the titration, indicating that Cc binding and release are in the fast-exchange regime.<sup>30</sup> The sizes and direction of the chemical shift perturbations (CSP) were similar in both titrations (Figure S3.2), indicating that the mode of binding is similar. The dissociation constant was  $K_D$  of  $6 (\pm 1) \times 10^{-6}$  M in both cases (Figure S3.1), in line with other reports.<sup>3, 30-32</sup> Line shape analysis using TITAN software<sup>13</sup> with the  $K_D$  fixed to 6  $\mu$ M yields a lower limit of the dissociation rate constant of  $\sim 6,400$  s<sup>-1</sup>.

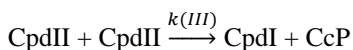
### Text S3.2. Reaction cycle and stopped flow measurements

The reaction catalyzed by CcP consists of the reduction of H<sub>2</sub>O<sub>2</sub> to water using electrons transferred from Cc. The reaction proceeds through a complicated cycle, during which two molecules of Cc interact with CcP, each sequentially contributing one electron.



During this process, CcP reduces hydrogen peroxide forming the intermediate called compound I (CpdI), which, after receiving one electron from Cc, is converted into compound II (CpdII). Finally, a second molecule of reduced Cc donates one electron to CpdII restoring the resting state of CcP.<sup>33</sup>

The kinetics were measured by following the absorbance at 416 nm for both the Cc:CcP\_A and Cc:CcP\_B complexes. The kinetics at 416 nm reflect all reactions involving the oxidation of Cc(Fe<sup>2+</sup>) by CpdI or CpdII (Figure S3.3). The reduction of CpdI to CpdII constitutes the reduction of the Trp radical which does not result in spectral changes in the visible region. Note that the kinetics are measured at a ratio of 1:1 between Cc(II) and CpdI. This allows other reactions between the different species in solution to happen as soon as part of the CpdI molecules have been reduced by Cc, such as reaction (r3) or the dismutation reaction between two CpdII molecules:



For this reason, only the first part of the stopped-flow traces was fitted (Figure S3.3).

## Supporting Figures

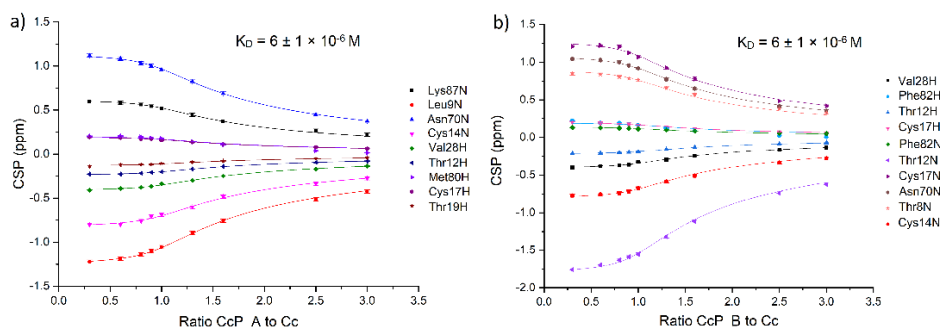


**Figure S3.1.** Affinity between Cc and CcP. Titration curves for  $^{15}\text{N}$  ferric Cc and CcP\_A (a) or CcP\_B (b). The CSP for several  $^1\text{H}$  and  $^{15}\text{N}$  nuclei of Cc are plotted as a function of the ratio CcP and Cc. The lines represent global fits with a shared  $K_D$ , indicated above the plots.

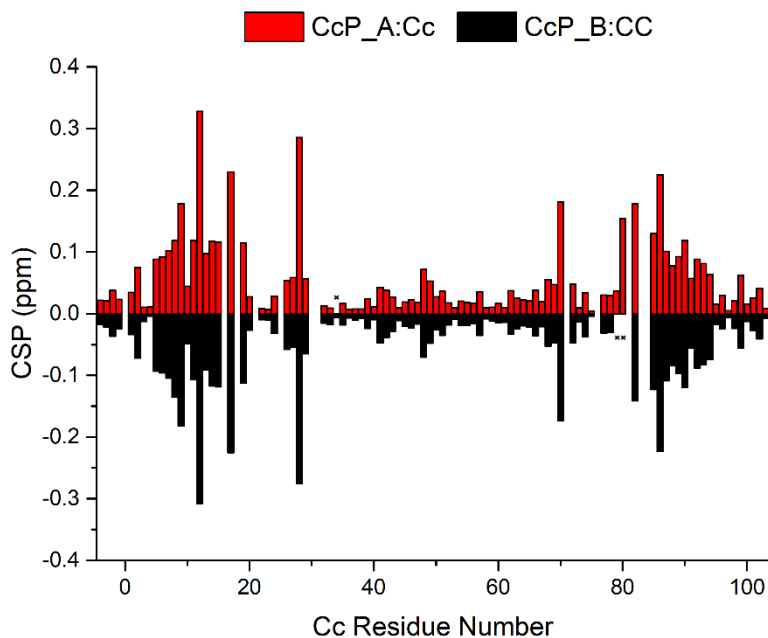


**Figure S3.2.** Chemical shift perturbations upon complex formation. Comparison of the average CSP extrapolated to the 100% bound state for the complexes CcP\_A:Cc (red) and CcP\_B:Cc (black). The small black crosses indicate residues for which no data are available.

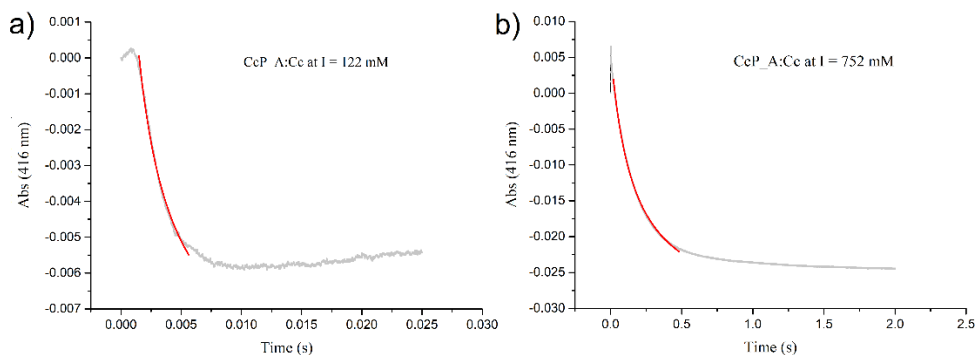


**Figure S3.3.** Representative stopped flow data. Kinetic traces for the reaction between Cc and CcP\_A at low (a) and high (b) ionic strength. Experimental data is in grey, fit to equation 2 is in red.

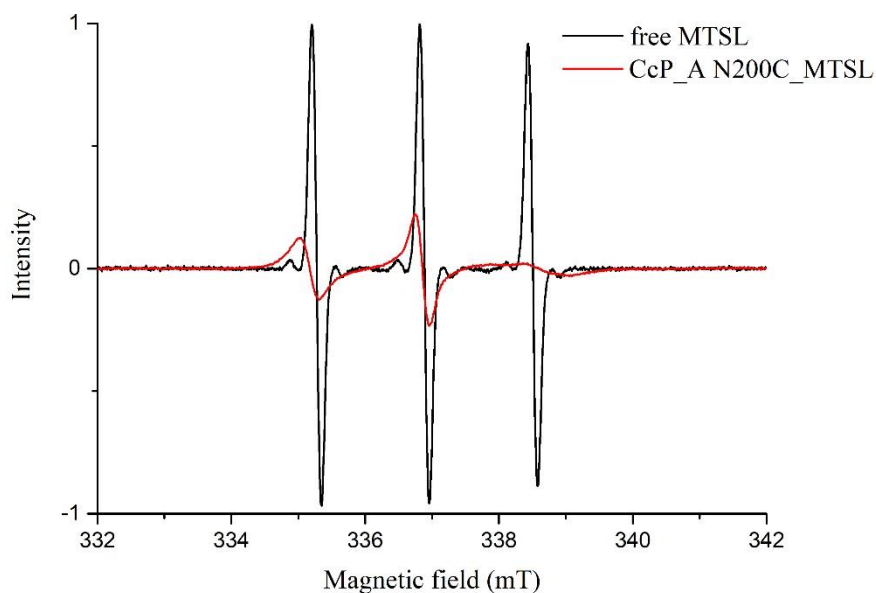


**Figure S3.4.** EPR spectra used to establish the fraction of paramagnetic CcP after labelling with MTSL. The spectra were normalized for concentration and number of scans. The measurements were performed at 9.8 GHz at room temperature, using 0.63 mW microwave power, 2 G modulation amplitude, 100 kHz modulation frequency and a time constant of 10.24 msec.

## Supporting Tables

**Table S3.1.** Rate constants for the reaction of the Cc:CcP\_A and Cc:CcP\_B complexes. The error represents the standard error of the mean between the curves at each salt concentration.

Ionic strength (mM)	CcP_A		CcP_B	
	$k_a$ ( $M^{-1}s^{-1}$ )	standard error (%)	$k_a$ ( $M^{-1}s^{-1}$ )	standard error (%)
752	$6.2 \cdot 10^6$	9.4	$7.1 \cdot 10^6$	5.0
622	$1.2 \cdot 10^7$	4.4	$1.3 \cdot 10^7$	5.2
502	$2.4 \cdot 10^7$	4.4	$3.3 \cdot 10^7$	8.6
392	$4.5 \cdot 10^7$	3.4	$5.8 \cdot 10^7$	3.9
292	$1.5 \cdot 10^8$	1.8	$2.1 \cdot 10^8$	5.9
192	$6.8 \cdot 10^8$	7.3	$8.5 \cdot 10^8$	3.9
122	$1.5 \cdot 10^9$	4.7	$2.1 \cdot 10^9$	17.3

**Table S3.2.** Percentage of paramagnetic signal of CcP tagged with MTSL measured through EPR experiments. The error is estimated to be  $\pm 5$  percent points.

	N24C	N87C	N200C
<b>CcP_A</b>	59%	28%	82%
<b>CcP_B</b>	45%	35%	50%

## References

- (1) Volkov, A. N., Worrall, J. A. R., Holtzmann, E., and Ubbink, M. (2006) Solution structure and dynamics of the complex between cytochrome *c* and cytochrome *c* peroxidase determined by paramagnetic NMR, *Proc. Natl. Acad. Sci. U. S. A.* 103, 18945-18950.

- (2) Goodin, D. B., Davidson, M. G., Roe, J. A., Mauk, A. G., and Smith, M. (1991) Amino-acid substitutions at tryptophan-51 of cytochrome-*c* peroxidase - Effects on coordination, species preference for cytochrome *c*, and electron-transfer, *Biochemistry* 30, 4953-4962.
- (3) Schilder, J., Lohr, F., Schwalbe, H., and Ubbink, M. (2014) The cytochrome *c* peroxidase and cytochrome *c* encounter complex: The other side of the story, *FEBS Lett.* 588, 1873-1878.
- (4) Teske, J. G., Savenkova, M. I., Mauro, J. M., Erman, J. E., and Satterlee, J. D. (2000) Yeast cytochrome *c* peroxidase expression in *Escherichia coli* and rapid isolation of various highly pure holoenzymes, *Protein Expr. Purif.* 19, 139-147.
- (5) Pollock, W. B., Rosell, F. I., Twitchett, M. B., Dumont, M. E., and Mauk, A. G. (1998) Bacterial expression of a mitochondrial cytochrome *c*. Trimethylation of lys72 in yeast iso-1-cytochrome *c* and the alkaline conformational transition, *Biochemistry* 37, 6124-6131.
- (6) Morar, A. S., Kakouras, D., Young, G. B., Boyd, J., and Pielak, G. J. (1999) Expression of N-15-labeled eukaryotic cytochrome *c* in *Escherichia coli*, *J. Biol. Inorg. Chem.* 4, 220-222.
- (7) Lescop, E., Schanda, P., and Brutscher, B. (2007) A set of BEST triple-resonance experiments for time-optimized protein resonance assignment, *J. Magn. Reson.* 187, 163-169.
- (8) Gao, Y., Boyd, J., Williams, R. J. P., and Pielak, G. J. (1990) Assignment of proton resonances, identification of secondary structural elements, and analysis of backbone chemical shifts for the C102T variant of yeast iso-1-cytochrome *c* and horse cytochrome *c*, *Biochemistry* 29, 6994-7003.
- (9) Fetrow, J. S., and Baxter, S. M. (1999) Assignment of <sup>15</sup>N chemical shifts and <sup>15</sup>N relaxation measurements for oxidized and reduced iso-1-cytochrome *c*, *Biochemistry* 38, 4480-4492.
- (10) Volkov, A. N., Vanwetswinkel, S., Van de Water, K., and van Nuland, N. A. J. (2012) Redox-dependent conformational changes in eukaryotic cytochromes revealed by paramagnetic NMR spectroscopy, *J. Biomol. NMR* 52, 245-256.

- (11) Kannt, A., Young, S., and Bendall, D. S. (1996) The role of acidic residues of plastocyanin in its interaction with cytochrome *f*, *BBA - Bioenergetics* 1277, 115-126.
- (12) Grzesiek, S., Bax, A., Clore, G. M., Gronenborn, A. M., Hu, J. S., Kaufman, J., Palmer, I., Stahl, S. J., and Wingfield, P. T. (1996) The solution structure of HIV-1 Nef reveals an unexpected fold and permits delineation of the binding surface for the SH3 domain of Hck tyrosine protein kinase, *Nat. Struct. Biol.* 3, 340-345.
- (13) Waudby, C. A., Ramos, A., Cabrita, L. D., and Christodoulou, J. (2016) Two-dimensional NMR lineshape analysis, *Sci. Rep-UK* 6, 8.
- (14) Delaglio, F., Grzesiek, S., Vuister, G. W., Zhu, G., Pfeifer, J., and Bax, A. (1995) NMRPIPE - A multidimensional spectral processing system based on Unix Pipes, *J. Biomol. NMR* 6, 277-293.
- (15) Bashir, Q., Volkov, A. N., Ullmann, G. M., and Ubbink, M. (2010) Visualization of the encounter ensemble of the transient electron transfer complex of cytochrome *c* and cytochrome *c* peroxidase, *J. Am. Chem. Soc.* 132, 241-247.
- (16) Battiste, J. L., and Wagner, G. (2000) Utilization of site-directed spin labeling and high-resolution heteronuclear nuclear magnetic resonance for global fold determination of large proteins with limited nuclear Overhauser effect data, *Biochemistry* 39, 5355-5365.
- (17) Pelletier, H., and Kraut, J. (1992) Crystal structure of a complex between electron transfer partners, cytochrome *c* peroxidase and cytochrome *c*, *Science* 258, 1748-1755.
- (18) Brunger, A. T., and Karplus, M. (1988) Polar hydrogen positions in proteins: empirical energy placement and neutron diffraction comparison., *Proteins* 4, 148-156.
- (19) Brooks, B. R., Bruccoleri, R. E., Olafson, B. D., States, D. J., Swaminathan, S., and Karplus, M. (1983) CHARMM: A program for macromolecular energy, minimization, and dynamics calculations., *J. Comput. Chem.* 4, 187-217.
- (20) MacKerell, A. D., Bashford, D., Bellott, M., Dunbrack, R. L., Evanseck, J. D., Field, M. J., Fischer, S., Gao, J., Guo, H., Ha, S., Joseph-McCarthy, D., Kuchnir, L., Kuczera, K., Lau, F. T. K., Mattos, C., Michnick, S., Ngo, T., Nguyen, D. T., Prodhom, B., Reiher, W. E., Roux, B., Schlenkrich, M., Smith, J. C., Stote, R., Straub, J., Watanabe, M., Wiorkiewicz-Kuczera, J., Yin, D., and Karplus, M.



- (1998) All-atom empirical potential for molecular modeling and dynamics studies of proteins, *J. Phys. Chem. B* 102, 3586-3616.
- (21) Schrödinger, L. The PyMOL Molecular Graphics System, Version 1.3.
- (22) Jurrus, E., Engel, D., Star, K., Monson, K., Brandi, J., Felberg, L. E., Brookes, D. H., Wilson, L., Chen, J. H., Liles, K., Chun, M. J., Li, P., Gohara, D. W., Dolinsky, T., Konecny, R., Koes, D. R., Nielsen, J. E., Head-Gordon, T., Geng, W. H., Krasny, R., Wei, G. W., Holst, M. J., McCammon, J. A., and Baker, N. A. (2018) Improvements to the APBS biomolecular solvation software suite, *Protein Sci.* 27, 112-128.
- (23) Foerster, J. M., Poehner, I., and Ullmann, G. M. (2018) MCMMap-Computational tool for mapping energy landscapes of transient protein-protein interactions, *ACS Omega* 3, 6465-6475.
- (24) Metropolis, N., Rosenbluth, A. W., Rosenbluth, M. N., Teller, A. H., and Teller, E. (1953) Equation of state calculations by fast computing machines., *J. Chem. Phys.* 21, 1087-1092.
- (25) Hahm, S., Miller, M. A., Geren, L., Kraut, J., Durham, B., and Millett, F. (1994) Reaction of horse cytochrome-*c* with the radical and the oxyferryl heme in cytochrome-*c* peroxidase compound-I, *Biochemistry* 33, 1473-1480.
- (26) Coulson, A. F., Erman, J. E., and Yonetani, T. (1971) Studies on cytochrome *c* peroxidase. XVII. Stoichiometry and mechanism of the reaction of compound ES with donors, *J. Biol. Chem.* 246, 917-924.
- (27) Ho, P. S., Hoffman, B. M., Kang, C. H., and Margoliash, E. (1983) Control of the transfer of oxidizing equivalents between heme iron and free radical site in yeast cytochrome *c* peroxidase, *J. Biol. Chem.* 258, 4356-4363.
- (28) Ho, P. S., Hoffman, B. M., Solomon, N., Kang, C. H., and Margoliash, E. (1984) Kinetics and energetics of intramolecular electron-transfer in yeast cytochrome-*c* peroxidase, *Biochemistry* 23, 4122-4128.
- (29) Schreiber, G., Haran, G., and Zhou, H. X. (2009) Fundamental aspects of protein-protein association kinetics, *Chem. Rev.* 109, 839-860.
- (30) Worrall, J. A. R., Kolczak, U., Canters, G. W., and Ubbink, M. (2001) Interaction of yeast iso-1-cytochrome *c* with cytochrome *c* peroxidase investigated by N-15,H-1 heteronuclear NMR spectroscopy, *Biochemistry* 40, 7069-7076.

- (31) Matthis, A. L., and Erman, J. E. (1995) Cytochrome *c* peroxidase-catalyzed oxidation of yeast iso-1 ferrocycytochrome *c* by hydrogen peroxide. Ionic strength dependence of the steady-state parameters., *Biochemistry* 34, 9985-9990.
- (32) Corin, A. F., Hake, R. A., McLendon, G., Hazzard, J. T., and Tollin, G. (1993) Effects of surface amino acid replacements in cytochrome *c* peroxidase on intracomplex electron transfer from cytochrome *c*, *Biochemistry* 32, 2756-2762.
- (33) Kim, K. L., Kang, D. S., Vitello, L. B., and Erman, J. E. (1990) Cytochrome-*c* peroxidase catalyzed oxidation of ferrocycytochrome-*c* by hydrogen-peroxide - Ionic-strenght dependence of the steady-state rate parameters, *Biochemistry* 29, 9150-9159.

# Chapter 4

**Charge distribution on a protein surface determines whether productive or futile encounter complexes are formed.**

Based on the research article:

Di Savino, A., Foerster, J. M., Ullmann, M., and Ubbink, M. Charge distribution on a protein surface determines whether productive or futile encounter complexes are formed. *Biochemistry*, 60(10), 747–755.

**Abstract**

Protein complex formation depends strongly on electrostatic interactions. The distribution of charges on the surface of redox proteins is often optimized by evolution to guide recognition and binding. To test to what degree the electrostatic interactions between cytochrome *c* peroxidase (CcP) and cytochrome *c* (Cc) are optimized, we produced five CcP variants, each with a different charge distribution on the surface. Monte Carlo simulations show that the addition of negative charges attracts Cc to the new patches, and the neutralization of the charges in the regular, stereospecific binding site for Cc abolishes the electrostatic interactions in that region entirely. For CcP variants with the charges in the regular binding site intact, additional negative patches slightly enhance productive complex formation, despite disrupting the optimized charge distribution. Removal of the charges in the regular binding site result in a dramatic decrease in the complex formation rate, even in the presence of highly negative patches elsewhere on the surface. It is concluded that additional charge patches can result in either productive or futile encounter complexes, depending on whether negative residues are located also in the regular binding site.

## Introduction

Protein complex formation proceeds through several steps. Freely diffusing proteins can collide and either move away again or form an encounter complex, which may or may not result in the formation of the stereospecific and active complex. The encounter complex is an ensemble of configurations in which the proteins sample each other's surface.<sup>1</sup> Formation is initially driven by electrostatic interactions but as the proteins get close, hydrophobic interactions can also come into play.<sup>2-9</sup> If the encounter results in the stereospecific complex, it is called productive, otherwise it is futile.<sup>10,11</sup> The rate of formation of the active complex defines association rate constant ( $k_a$ ). If complex formation is not optimized,  $k_a$  can be four-five orders of magnitude lower than the number of collisions, because in most cases the proteins do not collide with binding sides oriented toward each other. Highly optimized protein complexes have  $k_a$  values close to the diffusion limit, due to strong electrostatic pre-orientation.<sup>12</sup> Harel *et al.*<sup>10</sup> studied complex formation of TEM1- $\beta$ -lactamase (TEM1) and its inhibitor,  $\beta$ -lactamase-inhibitor protein (BLIP). They showed that charge mutations can enhance productive encounter complex formation, thus increasing the association rate without affecting the dissociation rate. However, other mutations modify the encounter complex without affecting the association rate or increase  $k_a$  without altering the encounter complex. The fractions of productive and futile encounter complexes can be altered with charge mutations on the proteins surface, even if they are far from the stereospecific binding site. By enhancing or disrupting a 'pathway' from the encounter site to the binding site in the stereospecific complex, they can either facilitate the formation of the active complex, or promote the early dissociation of the proteins.<sup>13</sup> The relation between productive vs. futile encounters and such electrostatic pathways on the protein surface was also suggested for the complex of cytochrome P450cam and putidaredoxin.<sup>14</sup> Despite their name, futile encounter complexes can have a role in protein functionality. Recently, it was shown that futile encounter complexes can regulate the activity of a protein complex through the formation of competitive encounters with a third protein.<sup>15</sup>

Electron transfer (ET) protein complexes are often highly optimized in complex formation and usually have a high fraction of encounter state. We selected the complex formed by cytochrome *c* (Cc) (CYC1, UniProtKB P00044) and cytochrome *c* peroxidase (CcP) (CCP1, UniProtKB P00431) to study the importance of the charge distribution on the protein surface in relation to rate of formation of the stereospecific complex. The protein complex formed by Cc and CcP has been extensively studied and has become a paradigm for biological ET. CcP catalyzes the reduction of  $H_2O_2$  in yeast mitochondria through a cycle of reactions. The crystallographic structure of the complex with Cc published in 1992 represents the stereospecific complex,<sup>16</sup> and a second low-affinity binding site is present at ionic strength values below  $\sim 100$  mM.<sup>17-20</sup> Electrostatic interactions are very important in the association reaction.<sup>18,20-23</sup> Erman and coworkers<sup>24-26</sup> measured the association rate between Cc and several charge-reversal mutants of CcP, showing that, interestingly, not

only residues close to the stereospecific binding site but also more distant ones have a role in the association. In a study from our groups, the charge distribution on the surface of CcP was changed strongly by addition of a negative patch on one side of CcP.<sup>27</sup> Monte Carlo simulations and paramagnetic relaxation enhancement (PRE) experiments showed that Cc interacts with the added patch, enlarging the surface visited in the encounter complex. The added charges also slightly enhance  $k_a$ . To investigate further to what degree the distribution of charges on the surface of CcP affects the association with Cc, here we analyze an additional four mutants of CcP with radically different charge distributions. Monte Carlo simulations show that the mutations alter the encounter complex, attracting Cc to the added negative patches. The association rates were measured through stopped flow experiments for a wide range of ionic strength values. Surprisingly, the added patches turn out to yield either productive or futile encounters, depending on whether the stereospecific site has its charges intact or not.

## Results

### *Rearranging the CcP charge distribution creates new interactions sites.*

Electrostatic interactions play an important role in the complex of Cc and CcP and appear to guide Cc to the binding site for fast electron transfer.<sup>28–31</sup> To test to what degree the electrostatic interactions are optimized for the association between Cc and CcP, we produced five CcP variants with a different charge distribution on their surface (Figure 4.1a,b). The CcP mutants were designed with three strategies, creation of an additional negative patch, neutralization of the negative charges in the wild type binding site for Cc, or a combination of both. Wild type CcP is named here CcP\_A. In variants CcP\_B and CcP\_D an additional negative patch was introduced (charge change -8) on the side and the back of CcP, respectively. Variants CcP\_C and CcP\_E carry the same additional charges as CcP\_B and CcP\_D and have a +8 charge change around the stereospecific binding site as defined by the structures of the wild type complex determined by crystallography and NMR.<sup>16,32</sup> As a result, CcP\_C and CcP\_E present a net charge change of zero. Finally, CcP\_F only has the mutations in the stereospecific binding site, resulting a charge change of +8 and rendering CcP close to neutral. Some data on CcP\_A and CcP\_B were reported in a previous paper but are included here for completeness.<sup>27</sup>

Monte Carlo simulations in which Cc was docked on CcP a large number of times based solely on electrostatic interactions and steric constraints, showed that the negative charges introduced on the surface of CcP attract Cc to the new sites (Figure 4.1c). The new patches strongly attract Cc, both in CcP\_B and CcP\_D and this effect is further enhanced in CcP\_C and CcP\_E, suggesting that in all four mutants the encounter states would have Cc mostly or entirely at the new patches. Note that in the stereospecific complex next to electrostatic interactions, other favorable interactions are present in the WT type complex that are not modelled in these calculations, so it is expected that the shift in the interactions for the entire complex could be less than as shown in Figure 4.1c. For CcP\_F, the calculations

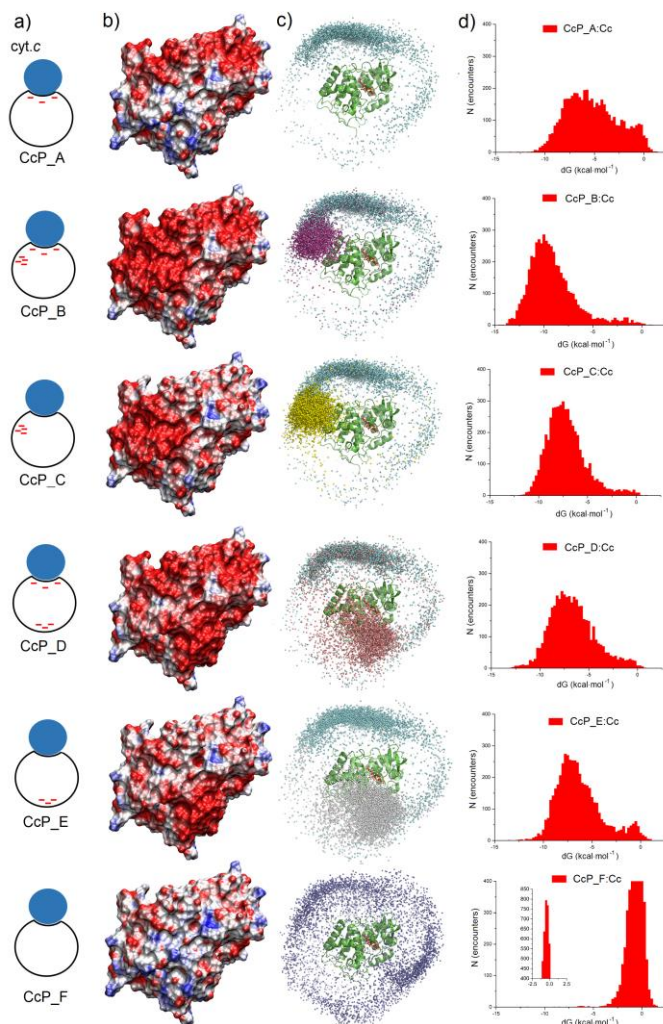


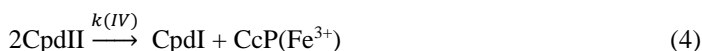
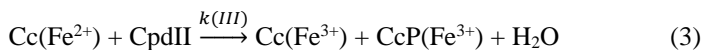
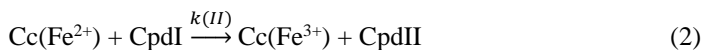
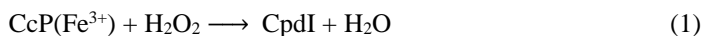
**Figure 4.1.** CcP variants. a) Schematic representation of the complexes formed by Cc and the CcP variants. Cc is represented as a blue circle bound at the stereospecific binding site and the CcP variants are represented as open circles with the negative charges on the surface indicated as red dashes; b) Electrostatic potential plotted on the surface of the CcP variants ranging from -5 (red) to 5 kcal/e<sup>0</sup> (blue) at an ionic strength of 120 mM; c) The structure of CcP (green ribbon, heme in red) is surrounded by the centers of the mass of Cc in the ensemble of encounters of the complexes Cc:CcP\_A (cyan), Cc:CcP\_B (magenta), Cc:CcP\_C (yellow), Cc:CcP\_D (salmon), Cc:CcP\_E (grey) and Cc:CcP\_F (purple) as obtained from rigid body Monte Carlo simulations; d) Energy distribution of the encounter complexes between Cc and the CcP variants as obtained from rigid body Monte Carlo simulations. The inset shows the entire distribution for CcP\_F using a different vertical scale.

show a more even distribution of Cc around CcP, as expected for a nearly neutral partner.

The energy distribution of the encounter complexes formed by the WT complex (Figure 4.1d) ranges from 0 to around -10 kcal/mol. The energy of most populated encounters is between about -4 to -7 kcal/mol; nevertheless a significant fraction of the encounters, around 25%, has an energy between -3 and 1 kcal/mol. The encounter complexes formed by Cc in presence of CcP\_B, CcP\_C, CcP\_D, or CcP\_E show that the encounters are distributed in more narrow peaks shifted to more negative energy compared to the WT encounter complexes, suggesting that they have a more favorable interactions than in Cc:CcP\_A complex. In particular, the most favorable interactions are formed between Cc and CcP\_B, with a peak at -10 kcal/mol. As expected, the least favorable encounters are formed by the Cc:CcP\_F complex, which presents a very narrow peak centered on -0.5 kcal/mol.

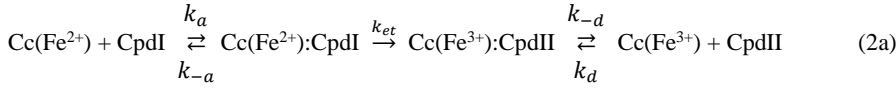
***CcP turnover involves two reduction steps.***

Cc and CcP have high association ( $k_a$ ) and dissociation ( $k_a$ ) rate constants:  $k_a = 10^8 - 10^9 \text{ M}^{-1}\text{s}^{-1}$  at 200 mM ionic strength,<sup>33</sup>  $k_a \geq 6,400 \text{ s}^{-1}$ .<sup>27</sup> The encounter complex represents 30% of the total complex,<sup>30,32</sup> the affinity is in the micromolar range ( $K_D = 5 \text{ }\mu\text{M}$ ),<sup>34</sup> and ET is fast ( $>50,000 \text{ s}^{-1}$ ).<sup>35</sup> To establish the effect of charge redistribution on the formation of the stereospecific, electron transfer active complex, the rate of oxidation of reduced Cc, Cc( $\text{Fe}^{2+}$ ), was measured for the different CcP variants. Stopped flow experiments were performed following the work by Miller *et al.* (1994).<sup>33</sup> Cc( $\text{Fe}^{2+}$ ) oxidation was followed by measuring the absorbance change at 416 nm over time in the cycle of reactions that allows CcP to reduce  $\text{H}_2\text{O}_2$  to water. First, resting state CcP, CcP( $\text{Fe}^{3+}$ ), is reacted with hydrogen peroxide to create compound I (CpdI, reaction 1).<sup>36-39</sup> Then, after mixing with Cc( $\text{Fe}^{2+}$ ), a first molecule of Cc is oxidized to yield compound II (CpdII) and Cc( $\text{Fe}^{3+}$ ), reaction 2. A second Cc( $\text{Fe}^{2+}$ ) molecule can then reduce CpdII to resting state CcP, reaction 3.<sup>40</sup> Reactions 2 and 3 both contribute to the change in absorbance at 416 nm. Furthermore, a slow regain of absorbance was observed, which we attributed to dismutation of CpdII into CpdI and resting state CcP (reaction 4).



Immediately after mixing, reaction 2 dominates because the concentration of CpdI is maximal and that of CpdII still zero. Reaction 2 can be broken up in several steps, reaction 2a:





The observed color change occurs after the electron transfer step ( $k_{et}$ ) and thus the observed rate constant in the stopped-flow trace,  $k_{obs}$ , describes the first two parts of the reaction 2a. It can readily be shown that under pseudosteady state conditions ( $\frac{\partial \text{Cc}(\text{Fe}^{2+})\text{:CpdI}}{\partial t} = \frac{\partial \text{Cc}(\text{Fe}^{3+})\text{:CpdII}}{\partial t} = 0$ ) equation (8) holds, giving the relation between the simulated rate  $k(II)$  and the association rate constant  $k_a$ :

$$k(II) = \frac{k_a k_{et}}{k_{-a} + k_{et}} \quad (8)$$

To test whether the pseudosteady state assumption is applicable, the  $k_{obs}$  was obtained by fitting the initial part of the curve and the complete curve was simulated using differential equations that describe reaction (2) – (4), yielding estimates of the  $k(II)$ ,  $k(III)$  and  $k(IV)$ . The two methods are illustrated in Figures 4.2 and S4.1. Note that the fitting method using the analytical solution given in equation 1 can be applied only at equal concentrations of Cc and CcP and it neglects reactions other than reaction 2, so it only fits the initial part of the decay (Figure 4.2). The remaining part is strongly affected by the other reactions. The simulation method covers the entire curve and has the advantage of not being limited to a specific ratio of concentrations between the proteins, enabling to evaluate the variation in the obtained rate due to concentration errors. This approach results in a more reliable error estimation for the rate constants. Excellent simulations could be obtained, but it should be noted that under some conditions there is some correlation between the obtained rate constants, so the three variables were not completely independent in all data sets (Table

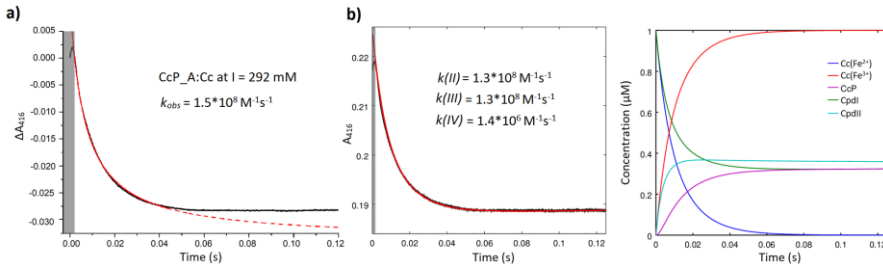


**Figure 4.2.** Comparison between fitting and simulation of the reaction performed by Cc and CcP\_A at ionic strength 292 mM measured at the stopped flow. A grey area covers the first part of the measured data affected by a stopped flow artefact and thus excluded from the analysis. a) Fitting of the fast decay to equation 1 (see Materials and Methods in the Supplementary Information). The data are shown as a solid black line, the fit is represented by the red line. The extrapolation of the fit is shown as a dashed line. b) Left, simulation (red line) of the reactions 2-4 to fit the same data (black) as in panel (a). Right, the concentrations over time of all the species involved in the Cc:CcP cycle as derived from the simulation.

S4.3). Because of this correlation between parameters, we used simulations rather than fittings of the differential equations to avoid ending up in unrealistic local minima or with extreme values. For the analysis of the mutants, the primary interest is in  $k(II)$ . The values for this rate constant obtained by simulation matched the fitted  $k_{obs}$  values (Table S4.4), indicating that equation 8 is well approximated and  $k(II)$  can be used as a lower limit for the association rate constant  $k_a$ . For WT Cc and CcP, the electron transfer rate ( $k_{et}$ ) is much larger than the dissociation rate constant ( $k_d$ ), so the observed rate constant approximates the association rate constant,  $k(II) \approx k_a$ .<sup>12,41</sup> In the remainder of the work, simulations were used for data analysis.

### *Cc association rates vary strongly for CcP variants*

Due to the favorable electrostatic interactions between the Cc and CcP, the association rate constant for the WT proteins is high at low ionic strength and strongly decreases with increasing salt concentration (Figure 4.3).<sup>18,20–23</sup> It is estimated that at high salt concentration, at around 1.25 M ionic strength, all the mutants converge to the same  $k_a$ . At low salt concentration the complexes formed by Cc and the CcP variants A, B and D have a high  $k_a$ , likely to be very close to the diffusion limit (Figure 4.3). At ionic strength values between 292 mM and 622 mM ( $17 \text{ mM}^{1/2}$  -  $25 \text{ mM}^{1/2}$  range on the horizontal scale in Figure

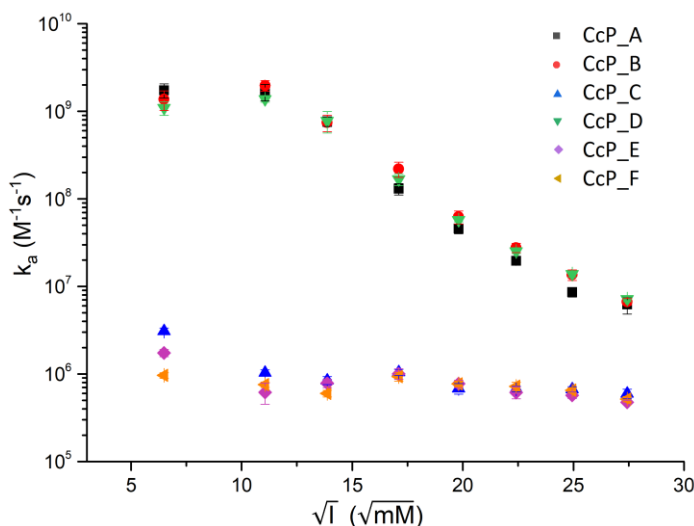


**Figure 4.3.** Rate of association ( $k_a$ ) between Cc and the CcP variants. The  $k_a$  values, plotted as a function of the square root of the ionic strength, were obtained from the simulations of the stopped flow kinetics. Errors were calculated as the standard deviation between replicates and simulations performed at different CcP concentrations (see Materials and Methods in the Supplementary Information for details).

4.3) the association rate constant for Cc binding to CcP variant B is slightly higher than with CcP\_A (Table S4.5). Similarly, CcP\_D is slightly faster than CcP\_A in the range 392 mM – 622 mM range of ionic strength. (Figure 4.3 and Table S4.5). Only at ionic strength values lower than 122 mM, the association with CcP\_B and CcP\_D is slightly slower than with the wild type CcP. The association rate constant for binding of Cc to CcP variants C, E and F is strongly reduced compared to that for the CcP\_A. At ionic strength values higher than 170 mM (14 mM<sup>1/2</sup>) the complexes formed by Cc and the mutants of CcP C and E show the same basal association rate as the complex formed with CcP\_F. Only a significant difference is present at I = 44 mM (7 mM<sup>1/2</sup>)(Table S4.5). In this condition the mutant CcP\_C binds faster to Cc than CcP\_E and CcP\_F.

### Discussion

To test the importance of the charge distribution on the surface of CcP for the interactions with Cc, five CcP mutants were created with different electrostatic potential and charge distribution on their surfaces (Figure 4.1.a, b). Monte Carlo simulations were performed for the wild type and mutated Cc:CcP complexes. The energy distributions for the Cc:CcP complexes (Figure 4.1d) show that the charge interactions between Cc and the CcP mutants, apart from the more neutral CcP\_F, are more favorable than for the WT complex, in line with the increased overall negative charge on the mutants CcP\_B and CcP\_D. Interestingly, also mutants CcP\_C and CcP\_E, which have the same net charge as CcP\_A, yield somewhat more favorable interactions. The reason could be that in the mutants an artificially highly negative patch is constructed. Often, charges on protein surfaces are compensated by nearby residues to ensure better protein stability. The simulations also demonstrate that these new patches strongly attract Cc, an effect that is enhanced further for the mutants in which the charges in the normal binding site are removed (CcP\_C and CcP\_E, Figure 4.1.c). Thus, it can be expected that the encounter complex of Cc and CcP is shifted toward binding at the new patches, which we demonstrated before for CcP\_B using paramagnetic NMR spectroscopy.<sup>27</sup> In the Monte Carlo simulations it is assumed that all residues in the negative patches are charged but it cannot be excluded that mutual repulsion leads to increased pK<sub>a</sub> values, rendering the patches with a lower net charge at the experimental pH value of 6.0. Furthermore, the simulations only consider electrostatic interactions and therefore neglect other favorable interactions that could play an important role at the stereospecific binding site. To determine whether productive complex formation, leading to ET from Cc to Cpd(I), can occur in the mutant complexes, stopped flow experiments were performed and association rate constants determined. The six CcP variants analyzed can be divided in two groups: CcP variants with the wild type charges in the binding site intact (CcP\_A, CcP\_B and CcP\_D), and variants in which these charges were neutralized (CcP\_E, CcP\_C and CcP\_F). The rate constants of association of the first group of CcP variants are similar and strongly dependent on the ionic strength due to the favorable electrostatic interactions between the Cc and CcP (Figure 4.3).<sup>18,20–23</sup> The second group instead presents a much lower association rate constant that is nearly independent of ionic strength. Clearly, the charges around the stereospecific binding site for Cc are

therefore fundamental for the formation of a productive encounter complex and efficient ET, in agreement with previous literature.<sup>24–26</sup> All variants of CcP bind the heme group, yielding similar UV-visible spectra as WT CcP, and they can all form CpdI and be reduced by Cc. Thus, the mutations do not affect the integrity of CcP. We cannot exclude however that the mutations around the stereospecific binding site subtly affect the protein surface, thus contributing to reduced formation of the ET active complex.

It can be expected that at high salt concentration, around 1.25 M ionic strength, all variants converge to the same basal association rate constant of  $\sim 5 \times 10^5 \text{ M}^{-1} \text{ s}^{-1}$ , which is independent of ionic strength. The highest value observed,  $k_a = 2 \times 10^9 \text{ M}^{-1} \text{ s}^{-1}$ , shows that the electrostatic interactions can increase the rate 4000-fold compared to ET by random collision. The obtained rate constant  $k(II)$  is a lower limit estimate of  $k_a$  (equation 8), so the actual  $k_a$  could be even larger, but it seems to approach the diffusion limit, as is suggested by the leveling off of the  $k_a$  at very low ionic strength (Figure 4.3). Another explanation for such levelling off relates to the balance of monopole-dipole effects on the interactions as a function of ionic strength.<sup>42–44</sup>

The results indicate that the charges added on the surface of CcP\_B and CcP\_D do not negatively affect the formation of the stereospecific complex. We previously reported that the enlarged encounter region on CcP\_B in fact slightly increases the association rate constant.<sup>27</sup> Our hypothesis is that the added charges enhance the electrostatic interactions between Cc and CcP, outweighing the negative effect of interacting at a site more distant from the stereospecific binding site. In other words, the additional charges enhance the probability of productive complex formation and binding at the new patch therefore, by definition, represent a productive encounter. Surprisingly, a similar result is observed with CcP\_D. The association rate constants between Cc and CcP\_D at ionic strength values between 392 mM and 622 mM (from  $20 \text{ mM}^{1/2}$  to  $25 \text{ mM}^{1/2}$ ) are significantly higher than the association measured for the wild type complex (Table S4.5). The differences are small for both CcP\_B and CcP\_D but are consistently higher than for CcP\_A in that ionic strength range (Tables S4.5 and S4.6). The rigid-body Monte Carlo simulations shows that Cc is strongly attracted by the new negative patch of CcP\_D, located on the opposite side of the protein with respect to the stereospecific binding site (Figure 4.1) and still it results in a slight increase in the rate of productive complex formation at moderate-high ionic strength values. Thus, analogous to CcP\_B, it is concluded that the positive effect of the extra charges outweighs the remote binding relative to the reaction site, yielding more productive encounters for this variant. At ionic strength values lower than 122 mM ( $11 \text{ mM}^{1/2}$ ) the association rate constants between Cc and CcP\_D is significantly lower than for the WT complex. This suggests that at low salt concentration the interaction between Cc and the new negative patch on CcP\_D reduces the probability of Cc finding the stereospecific binding site. Similar biphasic behavior, with reduced ET rates at low ionic strength was reported before, for example for plastocyanin and plant cytochrome *f*.<sup>45</sup> Perhaps the most surprising result is that the new patches cannot compensate at all for the loss of the charge interactions at the stereospecific binding site. At ionic strength values

higher than 192 mM ( $14 \text{ mM}^{1/2}$ ) the complexes formed by Cc and CcP\_C and CcP\_E, which have a net charge identical to WT CcP, show the same, basal association rate constant as the complex formed with CcP\_F, which has a charge change of +8 relative to WT CcP and is overall close to neutral. So, whereas the added charged patches appear to enhance the productive encounter formation in the presence of the charges in the stereospecific binding site, they have no effect on productive complex formation whatsoever if the binding site charges have been neutralized, at least at moderate and high ionic strength. An effect is only observed at 44 mM ionic strength ( $7 \text{ mM}^{1/2}$ ), at which condition the association rates constants show the order  $\text{CcP}_\text{C} > \text{CcP}_\text{E} > \text{CcP}_\text{F}$ . Apparently, at this salt concentration the electrostatic interactions are strong enough to result in slightly more productive encounters, with the largest effect for the charged patch that is closest to the stereospecific binding site (CcP\_C). Similar results were obtained by Harel *et al.*<sup>10</sup> studying the complex formed by TEM1 and BLIP. Creating different mutants of BLIP and using stopped flow association rate measurements in combination with Brownian Dynamics simulations, they showed that increasing the number of charge interactions that led to successful binding (fruitful trajectories) increases the rate of association between the two proteins.

## Conclusions

Our results indicate that in the presence of favorable charges in the binding site, the efficiency of the active protein complex formation depends more on the overall strength of the electrostatic interactions than on the distribution of charges on the protein surface. Nonetheless, the position of the charges on the protein surface can slightly affect productive complex formation, depending on the ionic strength conditions. At moderate and high ionic strength, additional charges enhance it, whereas at low ionic strength it can be reduced, as seen for CcP\_D. The neutralization of the charges at the stereospecific binding site for Cc strongly affects the association of the two proteins, abolishing the electrostatic interactions entirely, as judged from the ionic strength independence of complex formation with CcP\_F. Addition of highly charged patches distant from the stereospecific binding site only slightly enhances complex formation at low ionic strength and as no effect at moderate or high ionic strength. In this case, although the Monte Carlo simulations clearly show that electrostatic interactions are strong for CcP\_C and CcP\_E, apparently no trajectories are present for Cc to diffuse from the charged patch toward the stereospecific binding site, rather than to dissociate from CcP.<sup>10,14</sup> Therefore, in the absence of the negative charges in the stereospecific binding site, the encounters at the new patches have become futile ones.

## References

- (1) McLendon, G. (1991) Control of biological electron transport via molecular recognition and binding: The “velcro” model, in *Long-Range Electron Transfer in Biology*, p 159. Springer Berlin Heidelberg, Berlin, Heidelberg.
- (2) Kim, Y. C., Tang, C., Clore, G. M., and Hummer, G. (2008) Replica exchange

- simulations of transient encounter complexes in protein-protein association. *Proc. Natl. Acad. Sci. U. S. A.* *105*, 12855–12860.
- (3) Van de Water, K., van Nuland, N. A. J., and Volkov, A. N. (2014) Transient protein encounters characterized by paramagnetic NMR. *Chem. Sci.* *5*, 4227–4236.
- (4) Scanu, S., Foerster, J. M., Ullmann, G. M., and Ubbink, M. (2013) Role of hydrophobic interactions in the encounter complex formation of the plastocyanin and cytochrome *c* complex revealed by paramagnetic NMR spectroscopy. *J. Am. Chem. Soc.* *135*, 7681–7692.
- (5) Sugase, K., Dyson, H. J., and Wright, P. E. (2007) Mechanism of coupled folding and binding of an intrinsically disordered protein. *Nature* *447*, 1021–U11.
- (6) Camacho, C. J., Weng, Z., Vajda, S., and DeLisi, C. (1999) Free energy landscapes of encounter complexes in protein-protein association. *Biophys. J.* *76*, 1166–1178.
- (7) Camacho, C. J., Kimura, S. R., DeLisi, C., and Vajda, S. (2000) Kinetics of desolvation-mediated protein-protein binding. *Biophys. J.* *78*, 1094–1105.
- (8) Camacho, C. J., and Vajda, S. (2002) Protein-protein association kinetics and protein docking. *Curr. Opin. Struct. Biol.* *12*, 36–40.
- (9) Rajamani, D., Thiel, S., Vajda, S., and Camacho, C. J. (2004) Anchor residues in protein-protein interactions. *Proc. Natl. Acad. Sci. U. S. A.* *101*, 11287–11292.
- (10) Harel, M., Spaar, A., and Schreiber, G. (2009) Fruitful and futile encounters along the association reaction between proteins. *Biophys. J.* *96*, 4237–4248.
- (11) Fawzi, N. L., Doucleff, M., Suh, J. Y., and Clore, G. M. (2010) Mechanistic details of a protein-protein association pathway revealed by paramagnetic relaxation enhancement titration measurements. *Proc. Natl. Acad. Sci. U. S. A.* *107*, 1379–1384.
- (12) Schreiber, G., Haran, G., and Zhou, H. X. (2009) Fundamental aspects of protein-protein association kinetics. *Chem. Rev.* *109*, 839–860.
- (13) An, S. Y., Kim, E.-H., and Suh, J.-Y. (2018) Facilitated protein association via engineered target search pathways visualized by paramagnetic NMR spectroscopy. *Structure* *26*, 887–893.e2.
- (14) Andrałojć, W., Hiruma, Y., Liu, W. M., Ravera, E., Nojiri, M., Parigi, G., Luchinat, C., and Ubbink, M. (2017) Identification of productive and futile encounters in an electron transfer protein complex. *Proc. Natl. Acad. Sci. U. S. A.* *114*, E1840–E1847.
- (15) Strickland, M., Kale, S., Strub, M. P., Schwieters, C. D., Liu, J., Peterkofsky, A., and Tjandra, N. (2019) Potential regulatory role of competitive encounter complexes in paralogous phosphotransferase systems. *J. Mol. Biol.* *431*, 2331–2342.
- (16) Pelletier, H., and Kraut, J. (1992) Crystal structure of a complex between electron transfer partners, cytochrome *c* peroxidase and cytochrome *c*. *Science* (80). *258*, 1748–1755.
- (17) Stemp, E. D. A., and Hoffman, B. M. (1993) Cytochrome *c* peroxidase binds two molecules of cytochrome *c*: evidence for a low-affinity, electron-transfer-active site on

cytochrome *c* peroxidase. *Biochemistry* 32, 10848–10865.

(18) Zhou, J. S., and Hoffman, B. M. (1994) Stern-Volmer in reverse - 2/1 stoichiometry of the cytochrome *c* cytochrome *c* peroxidase electron-transfer complex. *Science* (80). 265, 1693–1696.

(19) Mauk, M. R., Ferrer, J. C., and Mauk, A. G. (1994) Proton linkage in formation of the cytochrome *c*-cytochrome *c* peroxidase complex: Electrostatic properties of the high- and low-affinity cytochrome binding sites on the peroxidase. *Biochemistry* 33, 12609–12614.

(20) Van de Water, K., Sterckx, Y. G. J., and Volkov, A. N. (2015) The low-affinity complex of cytochrome *c* and its peroxidase. *Nat. Commun.* 6, 7073.

(21) Matthis, A. L., and Erman, J. E. (1995) Cytochrome *c* peroxidase-catalyzed oxidation of yeast iso-1 ferrocycytochrome *c* by hydrogen peroxide. Ionic strength dependence of the steady-state parameters. *Biochemistry* 34, 9985–9990.

(22) Matthis, A. L., Vitello, L. B., and Erman, J. E. (1995) Oxidation of yeast iso-1 ferrocycytochrome *c* by yeast cytochrome *c* peroxidase compounds I and II. Dependence upon ionic strength. *Biochemistry* 34, 9991–9999.

(23) McLendon, G., Zhang, Q., Billstone, V., Wallin, S. A., Miller, R. M., Spears, K. G., and Hoffman, B. M. (1993) Thermodynamic and kinetic aspects of binding and recognition in the cytochrome *c*/cytochrome *c* peroxidase complex. *J. Am. Chem. Soc.* 115, 3665–3669.

(24) Erman, J. E., Vitello, L. B., Pearl, N. M., Jacobson, T., Francis, M., Alberts, E., Kou, A., and Bujarska, K. (2015) Binding of yeast cytochrome *c* to forty-four charge-reversal mutants of yeast cytochrome *c* peroxidase: isothermal titration calorimetry. *Biochemistry* 54, 4845–4854.

(25) Pearl, N. M., Jacobson, T., Arisa, M., Vitello, L. B., and Erman, J. E. (2007) Effect of single-site charge-reversal mutations on the catalytic properties of yeast cytochrome *c* peroxidase: Mutations near the high-affinity cytochrome *c* binding site. *Biochemistry* 46, 8263–8272.

(26) Pearl, N. M., Jacobson, T., Meyen, C., Clementz, A. G., Ok, E. Y., Choi, E., Wilson, K., Vitello, L. B., and Erman, J. E. (2008) Effect of single-site charge-reversal mutations on the catalytic properties of yeast cytochrome *c* peroxidase: Evidence for a single, catalytically active, cytochrome *c* binding domain. *Biochemistry* 47, 2766–2775.

(27) Di Savino, A., Foerster, J., La Haye, T., Blok, A., Timmer, M., Ullmann, M., and Ubbink, M. (2020) Efficient encounter complex formation and electron transfer to cytochrome *c* peroxidase with an additional, distant electrostatic binding site. *Angew. Chemie Int. Ed.* 132, 23239–23243.

(28) Gabdouliline, R. R., and Wade, R. C. (2001) Protein-protein association: investigation of factors influencing association rates by Brownian dynamics simulations. *J. Mol. Biol.* 306, 1139–1155.

(29) Northrup, S. H., Boles, J. O., and Reynolds, J. C. (1988) Brownian dynamics of cytochrome *c* and cytochrome *c* peroxidase association. *Science* (80-. ). 241, 67–70.

- (30) Bashir, Q., Volkov, A. N., Ullmann, G. M., and Ubbink, M. (2010) Visualization of the encounter ensemble of the transient electron transfer complex of cytochrome *c* and cytochrome *c* peroxidase. *J. Am. Chem. Soc.* 132, 241–247.
- (31) Castro, G., Boswell, C. A., and Northrup, S. H. (1998) Dynamics of protein-protein docking: Cytochrome *c* and cytochrome *c* peroxidase revisited. *J. Biomol. Struct. Dyn.* 16, 413–424.
- (32) Volkov, A. N., Worrall, J. A. R., Holtzmann, E., and Ubbink, M. (2006) Solution structure and dynamics of the complex between cytochrome *c* and cytochrome *c* peroxidase determined by paramagnetic NMR. *Proc. Natl. Acad. Sci. U. S. A.* 103, 18945–18950.
- (33) Miller, M. A., Liu, R. Q., Hahm, S., Geren, L., Hibdon, S., Kraut, J., Durham, B., and Millett, F. (1994) Interaction domain for the reaction of cytochrome *c* with the radical and the oxyferryl heme in cytochrome *c* peroxidase compound I. *Biochemistry* 33, 8686–8693.
- (34) Worrall, J. A. R., Kolczak, U., Canters, G. W., and Ubbink, M. (2001) Interaction of yeast iso-1-cytochrome *c* with cytochrome *c* peroxidase investigated by N-15,H-1 heteronuclear NMR spectroscopy. *Biochemistry* 40, 7069–7076.
- (35) Geren, L., Hahm, S., Durham, B., and Millett, F. (1991) Photoinduced electron-transfer between cytochrome *c* peroxidase and yeast cytochrome *c* labeled at cys-102 with(4-bromomethyl-4'-methylbipyridine) bis(bypyridine) ruthenium<sup>2+</sup>. *Biochemistry* 30, 9450–9457.
- (36) Mauro, J. M., Fishel, L. A., Hazzard, J. T., Meyer, T. E., Tollin, G., Cusanovich, M. A., and Kraut, J. (1988) Tryptophan-191→ Phenylalanine, a proximal-side mutation in yeast cytochrome *c* peroxidase that strongly affects the kinetics of ferrocycytochrome *c* oxidation. *Biochemistry* 27, 6243–6256.
- (37) Sivaraja, M., Goodin, D. B., Smith, M., and Hoffman, B. M. (1989) Identification by ENDOR of Trp191 as the free-radical site in cytochrome *c* peroxidase compound ES. *Science* (80-. ). 245, 738–740.
- (38) Erman, J. E., Vitello, L. B., Mauro, J. M., and Kraut, J. (1989) Detection of an oxyferryl porphyrin  $\pi$ -cation-radical intermediate in the reaction between hydrogen peroxide and a mutant yeast cytochrome *c* peroxidase. Evidence for tryptophan-191 involvement in the radical site of compound. *Biochemistry* 28, 7992–7995.
- (39) Fishel, L. A., Farnum, M. F., Miller, M. A., Kraut, J., Mauro, J. M., Liu, Y., Tan, X. ling, and Scholes, C. P. (1991) Compound I radical in site-directed mutants of cytochrome *c* peroxidase as probed by electron paramagnetic resonance and electron-nuclear double resonance. *Biochemistry* 30, 1986–1996.
- (40) Kim, K. L., Kang, D. S., Vitello, L. B., and Erman, J. E. (1990) Cytochrome *c* peroxidase catalyzed oxidation of ferrocycytochrome *c* by hydrogen-peroxide - Ionic-strenght dependence of the steady-state rate parameters. *Biochemistry* 29, 9150–9159.
- (41) Ho, P. S., Hoffman, B. M., Solomon, N., Kang, C. H., and Margoliash, E. (1984) Kinetics and energetics of intramolecular electron-transfer in yeast cytochrome *c* peroxidase. *Biochemistry* 23, 4122–4128.



## Chapter 4

- (42) Koppenol, W. H., and Margoliash, E. (1982) The asymmetric distribution of charges on the surface of horse cytochrome c - Functional implications. *J. Biol. Chem.* 257, 4426–4437.
- (43) Van Leeuwen, J. W. (1983) The ionic strength dependence of the rate of a reaction between two large proteins with a dipole moment. *Biochim. Biophys. Acta - Protein Struct. Mol. Enzymol.* 743, 408–421.
- (44) Watkins, J. A., Cusanovich, M. A., Meyer, T. E., and Tollin, G. (1994) A “parallel plate” electrostatic model for bimolecular rate constants applied to electron transfer proteins. *Protein Sci.* 3, 2104–2114.
- (45) Meyer, T. E., Zhao, Z. G., Cusanovich, M. A., and Tollin, G. (1993) Transient kinetics of electron transfer from a variety of c-type cytochromes to plastocyanin. *Biochemistry* 32, 4552–4559.

## Supplementary Information:

### Materials and Methods

#### Mutagenesis

The *Saccharomyces cerevisiae* CcP (CCP1, UniProtKB P00431) considered WT in this study (CcP\_A) contains the mutation C128A to avoid dimerization and the additional sequence MKT at the N-terminus for enhanced production levels.<sup>1,2</sup> The gene was subcloned into a pET2a(+) vector.<sup>3</sup> CcP\_B additionally has the mutations K21E, K29E, K90E, and K97E; <sup>4</sup> CcP\_C contains the same mutations as in CcP\_B and D35N, E36Q, E119Q, E202Q, E210Q, E215Q, D225N and E291Q that neutralize the charges of the WT binding site; CcP\_D has mutations K75E, K76Q, N79D, Q87E, K91Q, K98Q, N142D in comparison to CcP\_A; CcP\_E has the same mutations as in mutant CcP\_D and the mutations that neutralize the charges of the WT binding site as in CcP\_C; CcP\_F only has the neutralization charges for the WT binding site (See Table S4.1). The DNA constructs were produced by a commercial company and verified by DNA sequencing.

#### Protein Production

CcP was expressed in *Escherichia coli* BL21 Star (DE3)pLysS (Life Technologies Europe BV, Bleiswijk, the Netherlands). The production and purification were performed as previously described<sup>1,3,5</sup> with some differences according to the CcP variant purified. Buffers with different ionic strength values were used to build the gradient for elution during the anion-exchange chromatography; 50 mM potassium phosphate pH 5 and 500 mM potassium phosphate pH 5 for CcP\_A and CcP\_C and CcP\_E; 500 mM KCl was added to the second buffer to elute CcP\_B and CcP\_D. The purification of CcP\_F comprised a precipitation step with 40% w/w ammonium sulphate at 25°C, followed by dialysis against 20 mM potassium phosphate pH 5 overnight. Finally, the sample was loaded on an SP column, the column was washed with 20 mM potassium phosphate pH 5 and eluted with 20 column volumes of a gradient to 20 mM potassium phosphate and 1 M NaCl, pH 5. *S. cerevisiae* Cc (CYC1, UniProtKB P00044) was expressed using the iso-1-cytochrome *c* gene in a pUC19 based plasmid and purified following the protocols previously described.<sup>3,6</sup>

#### Monte Carlo simulations

The structures were prepared and the Monte Carlo docking simulations were done as described in Di Savino *et al.* (2020)<sup>4</sup>. The structures of CcP and Cc from the PDB 2PCC<sup>7</sup> were used as basis for the simulations. The hydrogens of the proteins were added with HBUILD<sup>8</sup> in CHARMM<sup>9</sup> and minimized with the CHARMM force field<sup>10</sup>, while the heavy atoms were fixed. The HEME ligands within the protein were considered to be in the oxidized state. For each version of CcP (CcP\_A – CcP\_F) the mutations, described in the Mutagenesis section, were introduced using Pymol<sup>11</sup>. The electrostatic potential was

## Chapter 4

calculated with APBS<sup>12</sup> for each CcP mutant separately. The potential was calculated in the presence of 120 mM NaCl and at a temperature of 303 K. The Monte Carlo docking simulations were done with the program suite MCMMap<sup>13</sup>. Separate simulations were done for each CcP mutant considering its respective electrostatic potential. In the simulation, Cc (ligand) moves randomly in the electrostatic potential of CcP (receptor). From each simulation, 5000 randomly chosen encounters were used for further analysis. A protein pair Cc:CcP was considered as encounter complex if the distance between at least two atoms of each protein respectively was less than 3 Å.

### Kinetic measurements

The results of the kinetics measured for the Cc:CcP\_A and Cc:CcP\_B complexes at ionic strengths from 752 mM to 122 mM were presented in our previous work.<sup>4</sup> The same protocols were followed to measure the reactions between Cc and the other mutants of CcP. The kinetic measurements were performed at the ionic strengths 752 mM, 622 mM, 502 mM, 392 mM, 292 mM, 192 mM, 122 mM and 44 mM on a SX20 stopped flow spectrometer (AppliedPhotophysics, Leatherhead, Surrey, UK) with a 1.2 ms deadtime at room temperature following the absorbance at 416 nm, which indicates oxidation of Cc.<sup>14</sup> Equimolar solutions of Cc and CcP were mixed to a final concentration of 0.5 µM of both Cc and CcP.

### Kinetic data analysis

The stopped flow data were fitted to the equation 1 as previously described:<sup>4</sup>

$$\Delta A_{416} = B_0 \cdot \Delta \varepsilon_{416} \cdot \left(1 - \frac{1}{1 + k_{\text{obs}} \cdot B_0 \cdot t}\right) + C \quad (1)$$

where  $B_0$  is the starting concentration of Cc( $\text{Fe}^{2+}$ ) and CpdI after mixing,  $\Delta \varepsilon_{416}$  is the difference in extinction coefficient at 416 nm for oxidized and reduced Cc,  $-40 \text{ mM}^{-1} \text{ cm}^{-1}$  (<sup>15–17</sup>),  $k_{\text{obs}}$  ( $\text{s}^{-1}$ ) is the observed rate constant of reduction,  $t$  is time (s) and  $C$  corrects for the baseline voltage of the spectrometer.

An independent analysis of the stopped flow data was performed through simulations. Kinetic simulations using GNU Octave<sup>18</sup> were performed to simulate the experimental measurement of the kinetics obtained from a stopped flow measurement. The script is included in Script S4.1. To do so, the reactions 2, 3 and 4 (see Results section) that influence the absorbance at 416 nm during the catalytic cycle were considered. The following differential equations were used to describe the change in concentration of each species in solution during the cycle:

$$\frac{d[\text{Cc}(\text{Fe}^{2+})]}{dt} = -k(II) * [\text{Cc}(\text{Fe}^{2+})] * [\text{CpdI}] - k(III) * [\text{Cc}(\text{Fe}^{2+})] * [\text{CpdII}]; \quad (2)$$

$$\frac{d[\text{CpdI}]}{dt} = -k(II) * [\text{Cc}(\text{Fe}^{2+})] * [\text{CpdI}] + k(IV) * [\text{CpdII}]^2; \quad (3)$$

$$\frac{d[\text{Cc(Fe}^{3+})]}{dt} = k(II) * [\text{Cc(Fe}^{2+})] * [\text{CpdI}] + k(III) * [\text{Cc(Fe}^{2+})] * [\text{CpdII}]; \quad (4)$$

$$\frac{d[\text{CpdIII}]}{dt} = k(II) * [\text{Cc(Fe}^{2+})] * [\text{CpdI}] - k(III) * [\text{Cc(Fe}^{2+})] * [\text{CpdII}] - k(IV) * [\text{CpdII}]^2; \quad (5)$$

$$\frac{d[\text{CcP}]}{dt} = k(IV) * [\text{CpdII}]^2 + k(III) * [\text{Cc(Fe}^{2+})] * [\text{CpdII}]; \quad (6)$$

From the simulated concentrations the stopped flow trace is recreated by summing the contributions of each component to the absorbance at 416 nm following the Beer-Lambert law:

$$A_{416} = \epsilon_{\text{Cc(Fe}^{2+})} * [\text{Cc(Fe}^{2+})] + \epsilon_{\text{CpdI}} * [\text{CpdI}] + \epsilon_{\text{Cc(Fe}^{3+})} * [\text{Cc(Fe}^{3+})] + \epsilon_{\text{CpdII}} * [\text{CpdII}] + \epsilon_{\text{CcP}} * [\text{CcP}] + C \quad (7)$$

The extinction coefficients at 416 nm are 129.1 mM<sup>-1</sup>cm<sup>-1</sup> for Cc(Fe<sup>2+</sup>),<sup>19</sup> 88.8 mM<sup>-1</sup>cm<sup>-1</sup> for Cc(Fe<sup>3+</sup>),<sup>19</sup> and for CcP and CpdI according to Table S4.2. The extinction coefficient for CpdII was considered to be the same as for the corresponding CpdI. The baseline correction term C was optimized manually (variable prod in the script S4.1 in the supporting information). The values of  $k(II)$ ,  $k(III)$  and  $k(IV)$  were independently changed until the simulation was a good fit as judged by visual inspection. The main error for the stopped flow measurement is caused by the error in the concentration of Cc and CpdI. Repeated measurement of the concentration of the samples resulted in a maximum deviation of 20% from the theoretical one. To take this into account in the simulations, every kinetic measurement, consisting of at least three replicates per salt concentration, was simulated at the expected experimental concentration, and at a concentration of CcP 20% lower. The rates of the reactions at a particular salt concentration were calculated as the average of the values obtained from the single simulations. The error of the rates at each salt concentration were calculated as the standard deviation between the rates at different protein concentrations. A t-test was performed to verify whether differences between the association rates of the Cc:CcP complexes are statistically significant. The Bonferroni correction with  $n = 5$  was applied when comparing the data of a CcP variant with the other five variants (Tables S4.5 and S4.6). The analysis of the data suggests that dismutation of CpdII (reaction 4) is much slower than the other reactions. Nonetheless, the occurrence of this reaction explains the increase of the absorbance at 416 nm visible in kinetic traces obtained at low ionic strength.

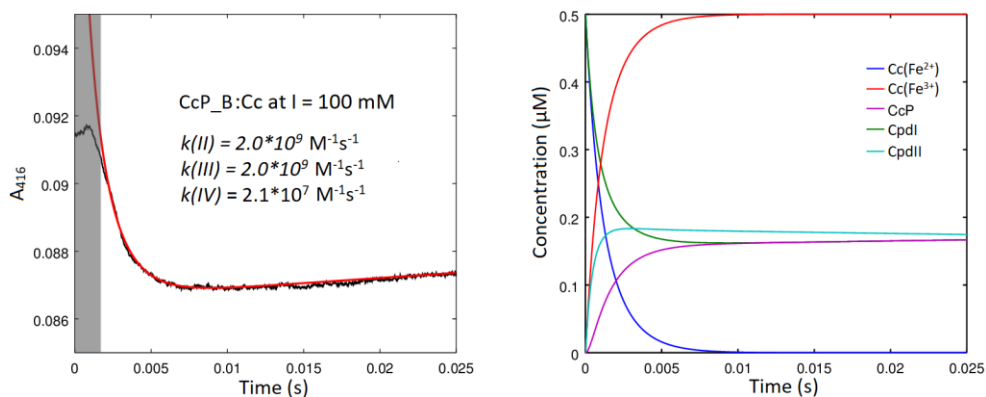


**Figure S4.1.** Example of kinetics measured at low ionic strength. In the panel on the left the experimental data is shown in black, the simulation in red. The first part of the data is affected by an artefact of the stopped flow and thus excluded from the analysis and is shown in a grey area. In the panel on the right the concentrations of all the species involved in the Cc:CcP cycle are shown as a function of time based on the simulated data.

**Table S4.1.** List of mutations performed for each CcP variant.

CcP_A	C128A
CcP_B	C128A, K21E, K29E, K90E, K97E
CcP_C	C128A, K21E, K29E, K90E, K97E, D35N, E36Q, E119Q, E202Q, E210Q, E215Q, D225N, E291Q
CcP_D	C128A, K75E, K76Q, N79D, Q87E, K91Q, K98Q, N142D
CcP_E	C128A, K75E, K76Q, N79D, Q87E, K91Q, K98Q, N142D, D35N, E36Q, E119Q, E202Q, E210Q, E215Q, D225N, E291Q
CcP_F	C128A, D35N, E36Q, E119Q, E202Q, E210Q, E215Q, D225N, E291Q

**Table S4.2.** Extinction coefficients for the CcP variants and their CpdIs at ionic strengths from 44 mM to 752 mM. The extinction coefficients are in  $\text{mM}^{-1} \text{cm}^{-1}$ . The error is estimated to be  $\pm 5 \%$ .

		CcP_A	CcP_B	CcP_C	CcP_D	CcP_E	CcP_F
<b>44 mM</b>	<b>CcP</b>	92	87	88	75	73	80
	<b>CpdI</b>	101	96	99	95	95	92
<b>122 mM</b>	<b>CcP</b>	106	94	103	103	103	99
	<b>CpdI</b>	113	80	117	119	122	87
<b>192 mM</b>	<b>CcP</b>	104	94	100	82	75	88
	<b>CpdI</b>	97	91	99	96	96	88
<b>292 mM</b>	<b>CcP</b>	108	94	98	78	75	93
	<b>CpdI</b>	95	91	98	94	94	92
<b>392 mM</b>	<b>CcP</b>	117	94	103	78	77	99
	<b>CpdI</b>	94	80	85	95	93	97
<b>502 mM</b>	<b>CcP</b>	117	94	114	86	84	99
	<b>CpdI</b>	97	80	105	105	100	87
<b>622 mM</b>	<b>CcP</b>	114	94	109	81	78	85
	<b>CpdI</b>	99	80	95	96	94	89
<b>752 mM</b>	<b>CcP</b>	112	94	102	82	80	99
	<b>CpdI</b>	94	80	102	96	93	87

**Table S4.3.** Rate constants  $k(\text{II})$ ,  $k(\text{III})$  and  $k(\text{IV})$  ( $\text{M}^{-1}\text{s}^{-1}$ ) obtained by simulation of the entire cycle of reactions for the six CcP variants to match the experimental data curves. The error is calculated as standard deviation between the rates obtained by simulations of at least three single measurements at each ionic strength value. The highlighted values are outliers that are not compatible with our model.

CcP_A						
I (mM)	k(II)	st.dev.	k(III)	st.dev.	k(IV)	st.dev.
44	1.7E+09	3.2E+08	1.7E+09	3.2E+08	1.3E+07	4.7E+06
122	1.7E+09	3.6E+08	1.7E+09	3.6E+08	1.5E+07	6.5E+06
192	7.7E+08	9.7E+07	7.7E+08	9.7E+07	4.3E+07	1.8E+07
292	1.3E+08	1.9E+07	1.3E+08	1.9E+07	1.4E+06	9.6E+05
392	4.6E+07	5.8E+06	4.5E+07	6.5E+06	4.0E+05	1.9E+05
502	2.0E+07	2.0E+06	1.6E+07	7.8E+06	2.2E+05	1.1E+05
622	8.6E+06	1.1E+06	1.2E+06	2.6E+06	3.1E+05	1.6E+05
752	6.2E+06	1.4E+06	6.1E+06	1.5E+06	2.1E+05	3.1E+05

CcP_B						
I (mM)	k(II)	st.dev.	k(III)	st.dev.	k(IV)	st.dev.
44	1.4E+09	3.5E+08	1.4E+09	3.5E+08	1.8E+06	2.1E+06
122	2.0E+09	2.8E+08	2.0E+09	2.8E+08	2.1E+07	9.5E+06
192	7.5E+08	1.6E+08	7.5E+08	1.6E+08	1.1E+07	4.5E+06
292	2.2E+08	4.3E+07	2.2E+08	4.3E+07	1.9E+06	1.1E+06
392	6.2E+07	1.1E+07	5.7E+07	1.1E+07	1.6E+05	1.5E+05
502	2.8E+07	3.3E+06	2.8E+07	3.3E+06	1.9E+05	1.9E+05
622	1.4E+07	1.9E+06	1.1E+07	3.2E+06	3.1E+05	2.1E+05
752	6.7E+06	6.0E+05	7.5E+06	2.0E+06	3.0E+04	7.3E+04

CcP_C						
I (mM)	k(II)	st.dev.	k(III)	st.dev.	k(IV)	st.dev.
44	3.1E+06	2.6E+05	1.2E+06	2.1E+05	7.6E+03	8.6E+03
122	1.0E+06	7.5E+04	-2.6E+04	5.8E+04	5.0E+04	2.2E+04
192	8.5E+05	8.9E+04	1.5E+05	6.9E+04	7.5E+04	1.9E+04
292	1.0E+06	8.6E+04	5.2E+05	1.6E+05	3.2E+04	1.3E+04
392	6.8E+05	9.3E+04	4.1E+05	1.8E+05	8.0E+03	1.1E+04
502	6.7E+05	4.9E+04	4.7E+05	6.9E+04	1.3E+04	7.4E+03
622	6.7E+05	4.9E+04	5.5E+05	1.3E+05	4.5E+03	6.4E+03
752	6.0E+05	7.6E+04	1.8E+05	5.7E+04	3.1E+04	1.4E+04

CcP_D						
I (mM)	k(II)	st.dev.	k(III)	st.dev.	k(IV)	st.dev.
44	1.1E+09	1.9E+08	6.6E+08	3.3E+08	5.2E+06	2.1E+06
122	1.4E+09	1.1E+08	1.4E+09	1.1E+08	8.0E+06	2.2E+06
192	7.8E+08	2.1E+08	3.8E+08	6.0E+07	6.8E+06	3.7E+06
292	1.7E+08	2.6E+07	1.0E+08	1.8E+07	4.3E+06	2.0E+06
392	5.8E+07	2.9E+06	5.4E+07	4.8E+06	6.8E+05	5.4E+05
502	2.5E+07	1.5E+06	2.0E+07	8.2E+05	6.8E+05	1.5E+05
622	1.4E+07	1.1E+06	1.2E+07	2.6E+06	9.4E+04	1.6E+05
752	7.2E+06	4.8E+05	4.2E+06	7.2E+05	6.4E+05	2.4E+05

CcP_E						
I (mM)	k(II)	st.dev.	k(III)	st.dev.	k(IV)	st.dev.
44	1.74E+06	1.60E+05	8.46E+05	1.60E+05	2.25E+04	2.2E+04
122	6.18E+05	1.67E+05	1.40E+04	8.64E+04	5.13E+04	2.2E+04
192	7.83E+05	8.81E+04	1.18E+05	5.12E+04	6.63E+04	1.9E+04
292	1.01E+06	1.37E+05	4.88E+05	3.00E+05	3.48E+04	1.4E+04
392	7.73E+05	7.64E+04	6.03E+05	1.24E+05	-2.29E+04	1.6E+04
502	6.15E+05	9.52E+04	2.60E+05	5.68E+04	3.08E+04	9.5E+03
622	5.69E+05	4.59E+04	2.46E+05	6.21E+04	4.11E+04	1.7E+04
752	4.74E+05	2.27E+04	1.95E+05	3.81E+04	4.38E+04	1.0E+04

CcP_F						
I (mM)	k(II)	st.dev.	k(III)	st.dev.	k(IV)	st.dev.
44	9.6E+05	7.3E+04	3.1E+05	8.0E+04	2.5E+04	9.4E+03
122	7.6E+05	5.3E+04	4.8E+04	6.2E+04	3.2E+04	1.1E+04
192	6.0E+05	5.2E+04	-4.1E+04	6.2E+04	3.5E+04	2.0E+04
292	9.3E+05	1.1E+05	3.6E+05	1.6E+05	3.4E+04	7.5E+03
392	7.7E+05	6.2E+04	3.7E+05	1.4E+05	2.6E+04	1.2E+04
502	7.2E+05	8.2E+04	1.7E+05	9.3E+04	2.8E+04	7.3E+03
622	6.5E+05	4.5E+04	2.9E+04	3.6E+04	1.9E+04	4.2E+03
752	5.2E+05	3.6E+04	2.0E+04	2.2E+04	2.9E+04	2.7E+03



**Table S4.4.** Association rate constants ( $\text{M}^{-1}\text{s}^{-1}$ ) for the Cc:CcP\_A complexes obtained by simulation and by fitting at ionic strength values from 44 mM to 752 mM. The error is calculated as standard deviation between the rates obtained by fitting or simulations of at least three single measurements at each ionic strength value.

		<b>CcP_A</b>	
		<b>k<sub>a</sub></b>	<b>st.dev.</b>
<b>44 mM</b>	<b>fitting</b>	1.5E+09	2.1E+08
	<b>simulations</b>	1.7E+09	3.2E+08
<b>122 mM</b>	<b>fitting</b>	1.5E+09	1.2E+08
	<b>simulations</b>	1.7E+09	3.6E+08
<b>192 mM</b>	<b>fitting</b>	6.8E+08	1.3E+08
	<b>simulations</b>	7.7E+08	9.7E+07
<b>292 mM</b>	<b>fitting</b>	1.5E+08	4.4E+06
	<b>simulations</b>	1.3E+08	1.9E+07
<b>392 mM</b>	<b>fitting</b>	4.5E+07	3.3E+06
	<b>simulations</b>	4.4E+07	5.8E+06
<b>502 mM</b>	<b>fitting</b>	2.4E+07	3.3E+06
	<b>simulations</b>	2.0E+07	2.0E+06
<b>622 mM</b>	<b>fitting</b>	1.2E+07	6.6E+05
	<b>simulations</b>	8.2E+06	1.1E+06
<b>752 mM</b>	<b>fitting</b>	6.2E+06	1.1E+06
	<b>simulations</b>	6.2E+06	1.4E+06

**Table S4.5.** p-values obtained from the t-test performed by comparing the rate of association ( $k(\text{II})$ ) of the Cc:CcP complexes at ionic strength values from 44 mM to 752 mM. The grey boxes indicate p-values  $> 0.01$ , meaning that the difference in the rates of association is considered not to be significant. Bonferroni correction was applied using  $p < 0.05$  for individual comparisons and  $n = 5$  for the number of comparisons for each variant.

I (mM)	CcP_A/CcP_B	CcP_A/CcP_C	CcP_A/CcP_D	CcP_A/CcP_E	CcP_A/CcP_F
752	3.3E-01	2.4E-08	4.6E-02	2.1E-08	2.2E-08
622	5.2E-05	1.1E-06	1.5E-07	1.0E-06	1.1E-06
502	2.3E-08	3.0E-12	5.4E-04	2.7E-12	3.0E-12
392	8.4E-05	9.6E-08	8.4E-04	9.7E-08	9.7E-08
292	1.3E-06	2.3E-12	5.9E-02	2.3E-12	2.3E-12
192	6.9E-01	1.8E-11	8.8E-01	1.8E-11	1.8E-11
122	7.6E-02	3.3E-06	5.8E-02	3.3E-06	3.3E-06
44	4.5E-02	1.3E-06	4.1E-04	1.2E-06	1.2E-06

I (mM)	CcP_B/CcP_C	CcP_B/CcP_D	CcP_B/CcP_E	CcP_B/CcP_F	CcP_C/CcP_D
752	1.1E-08	8.9E-02	1.4E-08	1.4E-08	1.0E-09
622	2.6E-07	7.2E-01	2.5E-07	2.6E-07	1.1E-17
502	2.6E-15	4.9E-02	2.4E-15	2.6E-15	6.2E-05
392	2.2E-12	1.4E-01	2.2E-12	2.2E-12	3.6E-05
292	6.9E-11	1.7E-02	6.9E-11	6.9E-11	1.1E-03
192	5.4E-09	6.9E-01	5.4E-09	5.4E-09	1.1E-06
122	1.9E-07	2.8E-04	1.9E-07	1.9E-07	6.5E-07
44	1.0E-05	6.7E-02	1.0E-05	1.0E-05	4.3E-09

I (mM)	CcP_C/CcP_E	CcP_C/CcP_F	CcP_D/CcP_E	CcP_D/CcP_F	CcP_E/CcP_F
752	2.3E-03	2.3E-02	1.7E-09	1.6E-09	1.4E-02
622	3.5E-04	5.5E-01	1.0E-17	1.0E-17	3.7E-03
502	1.6E-01	1.7E-01	6.0E-05	6.2E-05	3.1E-02
392	6.7E-02	5.3E-02	3.6E-05	3.6E-05	9.6E-01
292	6.3E-01	6.6E-02	1.1E-03	1.1E-03	4.1E-01
192	2.9E-01	3.2E-05	1.1E-06	1.1E-06	2.0E-02
122	9.1E-05	3.2E-04	6.5E-07	6.5E-07	6.2E-02
44	4.8E-08	2.1E-08	4.3E-09	4.2E-09	3.4E-07

## Chapter 4

**Table S4.6.** Number of independent simulations performed to calculate the rate constants  $k(\text{II})$ ,  $k(\text{III})$  and  $k(\text{IV})$ , and used in t-test.

I (mM)	CcP_A	CcP_B	CcP_C	CcP_D	CcP_E	CcP_E
752	12	8	8	8	10	8
622	7	8	8	16	14	6
502	12	16	8	4	8	8
392	8	15	7	4	8	12
292	14	14	8	4	4	6
192	12	12	8	10	4	13
122	8	8	5	6	8	4
44	8	8	8	11	8	10

**Script S4.1.** Script used to perform the simulations on GNU Octave<sup>18</sup> of the entire cycle of reactions for the six CcP variants to match the experimental data curves.

```
# Model:
# S(1) + E(2) k2<Kd>k1 ES(3) k4<Ke>k3 P(4) + E(2)
# Cc(Fe2+) (1) + CcPI (2) k1-> Cc(Fe3+) (3) + CcPII (4)
# Cc(Fe2+) (1) + CcPII (4) k2 -> Cc(Fe3+) (3) + CcP(Fe3+) (5)
# CcPII (4) + CcPII (4) k3-> CcPI (2) + CcP(Fe3+) (5)
# k1>=k2>k3
# Load data and adjust
data = csvread("kinetic_data.csv");
time = data(:,1);

# Set variables
num3 = columns(data);
prod = data(:,2: num3);
prod = prod+0.0929; # adjust to match data and simulations on the y axes

# Define rates and differential equations (1000 = 109)
function xdot = f (x,t)
k1 = 1230;
k2 = k1;
k3 = 13;
xdot = zeros (5,1);
xdot(1) = -k1*x(1)*x(2)-k2*x(1)*x(4);
xdot(2) = -k1*x(1)*x(2)+k3*x(4)*x(4);
xdot(3) = k1*x(1)*x(2)+k2*x(1)*x(4);
xdot(4) = k1*x(1)*x(2)-k2*x(1)*x(4)-k3*x(4)*x(4);
```

```

    xdot(5) = k3*x(4)*x(4)+k2*x(1)*x(4);
endfunction;

x0 = [0.5; 0.5; 0; 0; 0];
t = logspace(-5,-1,1000);
y1 = lsode("f", x0, time);
y2 = lsode("f", x0, time);
res = (y2(:,1)/1000)* εCc(Fe2+) +(y2(:,3)/1000)* εCc(Fe3+) + (y2(:,5)/1000)* εCcP(Fe3+)
+(y2(:,2)/1000)* εCpdl +(y2(:,4)/1000)* εCpdlI; #fill in the right ε for each species according
to the salt concentration

plc = y1;
time1 = time + 0.001;

# Plot the results
# Normal plot of data and simulated product curves
h = figure('Position',[300,250,1300,500], 'Paperorientation', 'landscape', 'Paperposition',
[0.0 1.0 11.0 6.0]);
subplot (1, 2, 1);
plot (time, prod, "-r", "linewidth", 2, time-0.0002, res, "-k", "linewidth", 1);
axis([0, 0.025, 0.085, 0.095]);

set(gca, "linewidth", 2, "fontsize", 12)
xlabel ("Time (s)", "fontsize", 12);
ylabel ("A_{416}", "fontsize", 12);

# Log plot of all elements for last concentration
subplot (1, 2, 2);
plot (time,plc,"linewidth", 1);
axis([0, 0.025, 0, 0.5]);

set(gca, "linewidth", 2, "fontsize", 12);
xlabel ("Time (s)");
ylabel ("Concentration (uM)");
legend ("Cc(Fe2+) ", "CcPI", " Cc(Fe3+) ", "CcPII", "CcP", "location", "east");

save result.txt plc
save time.txt time

```

## References

- (1) Goodin, D. B., Davidson, M. G., Roe, J. A., Mauk, A. G., and Smith, M. (1991) Amino-acid substitutions at tryptophan-51 of cytochrome *c* peroxidase - Effects on coordination, species preference for cytochrome *c*, and electron-transfer. *Biochemistry* 30, 4953–4962.
- (2) Volkov, A. N., Worrall, J. A. R., Holtzmann, E., and Ubbink, M. (2006) Solution structure and dynamics of the complex between cytochrome *c* and cytochrome *c* peroxidase determined by paramagnetic NMR. *Proc. Natl. Acad. Sci. U. S. A.* 103, 18945–18950.
- (3) Schilder, J., Lohr, F., Schwalbe, H., and Ubbink, M. (2014) The cytochrome *c* peroxidase and cytochrome *c* encounter complex: The other side of the story. *Febs Lett.* 588, 1873–1878.
- (4) Di Savino, A., Foerster, J., La Haye, T., Blok, A., Timmer, M., Ullmann, M., and Ubbink, M. (2020) Efficient encounter complex formation and electron transfer to cytochrome *c* peroxidase with an additional, distant electrostatic binding site. *Angew. Chemie Int. Ed.* 132, 23239–23243.
- (5) Teske, J. G., Savenkova, M. I., Mauro, J. M., Erman, J. E., and Satterlee, J. D. (2000) Yeast cytochrome *c* peroxidase expression in *Escherichia coli* and rapid isolation of various highly pure holoenzymes. *Protein Expr. Purif.* 19, 139–147.
- (6) Pollock, W. B., Rosell, F. I., Twitchett, M. B., Dumont, M. E., and Mauk, A. G. (1998) Bacterial expression of a mitochondrial cytochrome *c*. Trimethylation of lys72 in yeast iso-1-cytochrome *c* and the alkaline conformational transition. *Biochemistry* 37, 6124–6131.
- (7) Pelletier, H., and Kraut, J. (1992) Crystal structure of a complex between electron transfer partners, cytochrome *c* peroxidase and cytochrome *c*. *Science* (80-. ). 258, 1748–1755.
- (8) Brünger, A. T., and Karplus, M. (1988) Polar hydrogen positions in proteins: Empirical energy placement and neutron diffraction comparison. *Proteins Struct. Funct. Bioinforma.* 4, 148–156.
- (9) Brooks, B. R., Bruccoleri, R. E., Olafson, B. D., States, D. J., Swaminathan, S., and Karplus, M. (1983) CHARMM: A program for macromolecular energy, minimization, and dynamics calculations. *J. Comput. Chem.* 4, 187–217.
- (10) MacKerell, A. D., Bashford, D., Bellott, M., Dunbrack, R. L., Evanseck, J. D., Field, M. J., Fischer, S., Gao, J., Guo, H., Ha, S., Joseph-McCarthy, D., Kuchnir, L., Kuczera, K., Lau, F. T. K., Mattos, C., Michnick, S., Ngo, T., Nguyen, D. T., Prodhom, B., Reiher, W. E., Roux, B., Schlenkrich, M., Smith, J. C., Stote, R., Straub, J., Watanabe, M., Wiórkiewicz-Kuczera, J., Yin, D., and Karplus, M. (1998) All-atom empirical potential for molecular modeling and dynamics studies of proteins. *J. Phys. Chem. B* 102, 3586–3616.
- (11) Schrödinger, L. The PyMOL molecular graphics system, Version 1.3.
- (12) Jurrus, E., Engel, D., Star, K., Monson, K., Brandi, J., Felberg, L. E., Brookes, D. H., Wilson, L., Chen, J., Liles, K., Chun, M., Li, P., Gohara, D. W., Dolinsky, T., Konecny, R.,

Koes, D. R., Nielsen, J. E., Head-Gordon, T., Geng, W., Krasny, R., Wei, G. W., Holst, M. J., McCammon, J. A., and Baker, N. A. (2018) Improvements to the APBS biomolecular solvation software suite. *Protein Sci.* 27, 112–128.

(13) Foerster, J. M., Poehner, I., and Ullmann, G. M. (2018) MCMap - A computational tool for mapping energy landscapes of transient protein-protein interactions. *ACS Omega* 3, 6465–6475.

(14) Miller, M. A., Liu, R. Q., Hahm, S., Geren, L., Hibdon, S., Kraut, J., Durham, B., and Millett, F. (1994) Interaction domain for the reaction of cytochrome *c* with the radical and the oxyferryl heme in cytochrome *c* peroxidase compound I. *Biochemistry* 33, 8686–8693.

(15) Hahm, S., Miller, M. A., Geren, L., Kraut, J., Durham, B., and Millett, F. (1994) Reaction of horse cytochrome *c* with the radical and the oxyferryl heme in cytochrome *c* peroxidase compound-I. *Biochemistry* 33, 1473–1480.

(16) Coulson, A. F., Erman, J. E., and Yonetani, T. (1971) Studies on cytochrome *c* peroxidase. XVII. Stoichiometry and mechanism of the reaction of compound ES with donors. *J. Biol. Chem.* 246, 917–924.

(17) Ho, P. S., Hoffman, B. M., Kang, C. H., and Margoliash, E. (1983) Control of the transfer of oxidizing equivalents between heme iron and free radical site in yeast cytochrome *c* peroxidase. *J. Biol. Chem.* 258, 4356–4363.

(18) John W. Eaton, David Bateman, Søren Hauberg, and R. W. (2014) GNU Octave version 3.8.1 manual: a high-level interactive language for numerical computations. *Creat. Indep. Publ. Platf.* URL <https://www.gnu.org/software/octave/doc/v5.2.0/>

(19) Margoliash, E., and Frohwirt, N. (1959) Spectrum of horse-heart cytochrome *c*. *Biochem. J.* 71, 570–578.

# Chapter 5

**Enhancing the population of encounter complex affects protein complex formation efficiency.**

Based on the research article:

Di Savino, A. and Ubbink, M. Enhancing the population of encounter complex affects protein complex formation efficiency, *Under revision*.

**Abstract**

Optimal charge distribution is considered to be important for efficient formation of protein complexes. Electrostatic interactions guide encounter complex formation that precedes the formation of an active protein complex. However, disturbing the optimized distribution by introduction of extra charged patches on cytochrome *c* peroxidase does not lead to a reduction in productive encounters with its partner cytochrome *c*. To test whether a complex with a high population of encounter complex is more easily affected by suboptimal charge distribution, the interactions of cytochrome *c* mutant R13A with wild type cytochrome *c* peroxidase and a variant with an additional negative patch were studied. The complex of the peroxidase and cytochrome *c* R13A was reported to have an encounter state population of 80%, compared to 30% for the wild type cytochrome *c*. NMR analysis confirms the dynamic nature of the interaction and demonstrates that the mutant cytochrome *c* samples the introduced negative patch. Kinetic experiments show that productive complex formation is 5-7 fold slower at moderate and high ionic strength values for cytochrome *c* R13A but the association rate is not affected by the additional negative patch on cytochrome *c* peroxidase, showing that the total charge on the protein surface can compensate for less optimal charge distribution. At low ionic strength (44 mM), the association with the mutant cytochrome *c* reaches the same high rates as found for wild type cytochrome *c*, approaching the diffusion limit.



## Introduction

Electrostatic interactions play a major role in protein complex formation. The collision of free proteins in solution can result in early dissociation or lead to the formation of the stereospecific and active complex. Electrostatic interactions can promote the interactions between proteins, guiding the formation of an encounter complex.<sup>1–5</sup> The encounter complex is a very dynamic ensemble of configurations in which proteins sample each other's surface.<sup>6</sup> It can lead to the formation of the stereospecific and active complex, in which case the encounter is productive.<sup>7</sup> In case of an early dissociation, the encounter is futile.<sup>8</sup> The charge distribution on the surface is considered to be critical to enhance the number of productive encounters, by guiding the incoming partner to the binding site and reducing the surface area to be searched.<sup>9</sup> Previous studies showed how charge mutations can affect the interactions between proteins. For example, on the complex formed by TEM1- $\beta$ -lactamase (TEM1) and its inhibitor,  $\beta$ -lactamase-inhibitor protein (BLIP), charge mutations can enhance the formation of the productive encounter complex resulting in a higher association rate ( $k_a$ ) but without lowering the dissociation rate. Alternatively, they can alter the encounter complex without any effect on the  $k_a$ , or improve the  $k_a$  without affecting the encounter complex.<sup>7</sup> Charge mutations can modify the balance of productive and futile encounter complexes, even if located far from the stereospecific binding site. The outcome of the mutation depends on

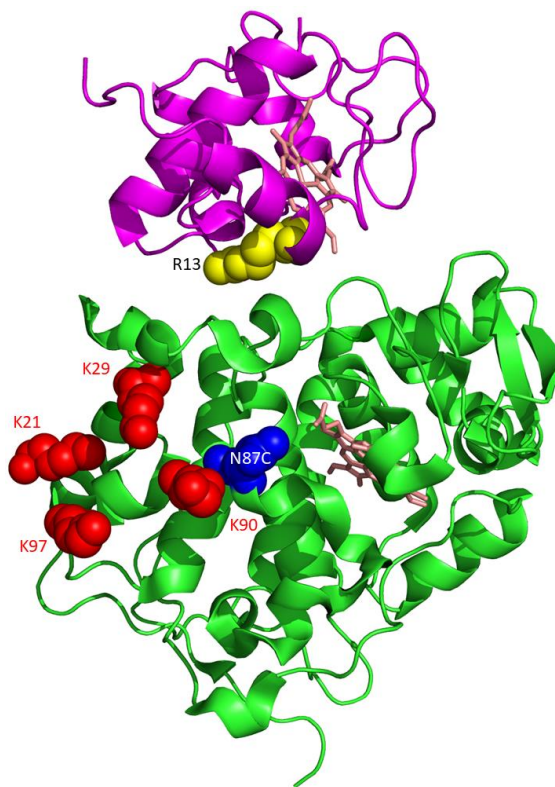


**Figure 5.1.** Mutations in the Cc:CcP complex. The crystal structure of the stereospecific complex formed by Cc (magenta ribbons) and CcP (green ribbons) is shown (PDB 2PCC<sup>13</sup>). The heme groups are shown in salmon sticks, residue R13 is indicated in yellow spacefill representation, the Lys residues that were mutated to Glu to introduce additional negative charges in CcP\_B are indicated in red, and residue N87 of CcP mutated to cysteine for spin labelling in blue spacefill. The figure was made with Pymol<sup>12</sup>.

For example, on the complex formed by TEM1- $\beta$ -lactamase (TEM1) and its inhibitor,  $\beta$ -lactamase-inhibitor protein (BLIP), charge mutations can enhance the formation of the productive encounter complex resulting in a higher association rate ( $k_a$ ) but without lowering the dissociation rate. Alternatively, they can alter the encounter complex without any effect on the  $k_a$ , or improve the  $k_a$  without affecting the encounter complex.<sup>7</sup> Charge mutations can modify the balance of productive and futile encounter complexes, even if located far from the stereospecific binding site. The outcome of the mutation depends on

the optimization or interruption of favorable electrostatic ‘pathways’.<sup>10</sup> The effect of the charged pathways was observed for the complex of cytochrome P450cam and putidaredoxin.<sup>11</sup>

Because of their biological functions, electron transfer (ET) proteins often form transient complexes and the charge distribution on their surface is highly optimized to have favorable electrostatic interactions, leading to efficient protein complex formation. These complexes usually have low affinity ( $K_D$  in the  $\mu\text{M}$ -mM range), a consequence of the association and dissociation rate constants both being high. Protein complexes with highly optimized electrostatic interactions have  $k_a$  values that approach the limit set by translational diffusion.<sup>1</sup> The ET complex formed by cytochrome *c* (Cc) and cytochrome *c* peroxidase (CcP) from baker’s yeast (*Saccharomyces cerevisiae*) is one of the most studied and best characterized ET complexes. The formation of the complex is guided by electrostatic interactions between the positively charged binding site on Cc and the negatively charges on CcP.<sup>13–17</sup> The encounter state represents 30% of the complex, while 70% is in the stereospecific complex and Cc samples merely 15% of the surface of CcP.<sup>18,19</sup> Several studies have shown that mutations in the interface between Cc and CcP strongly affect association,<sup>20–22</sup> so we wondered how important the optimized charge distribution is for the efficiency of the ET reaction. To test this, negative patches were added distant from the stereospecific binding site on CcP, enlarging the surface sampled by Cc in the encounter state. Interestingly, the new negative charges create productive encounters, slightly enhancing the  $k_a$ , even if located far from the stereospecific binding site (<sup>23</sup> and <sup>24</sup>). This suggests that the overall charge on CcP surface is more important than the charge distribution. We considered that this could be a consequence of the stability of the stereospecific state as compared to the encounter state. To test this idea, for the current work, we turned to a mutant of Cc, R13A, reported to form a complex with Cc with 80% population of the encounter state.<sup>25</sup> Arg13 has been shown to be a hot-spot in the interactions of the stereospecific complex and its mutation to Ala shifts the balance toward the encounter state and reduces the affinity by 30 fold.<sup>25,26</sup> This mutant was used to study the interaction with native CcP (CcP\_A) and a variant with eight additional negative charges on the side of CcP relative to the stereospecific binding site (CcP\_B, Figure 5.1)(<sup>23</sup> and <sup>24</sup>). Chemical shift perturbation (CSP) analysis and paramagnetic relaxation enhancement (PRE) experiments show that the complex is highly dynamic and that Cc visits the new negative patch in CcP\_B. Kinetic experiments yield reduced association rates for the mutant Cc at moderate and high ionic strength values, but surprisingly, the addition of the negative patch does not reduce the number of productive encounters. At low ionic strength, the mutant Cc associates as fast as wild type (wt) Cc with CcP. The results are discussed in the context of the importance of charge optimization for complex formation.

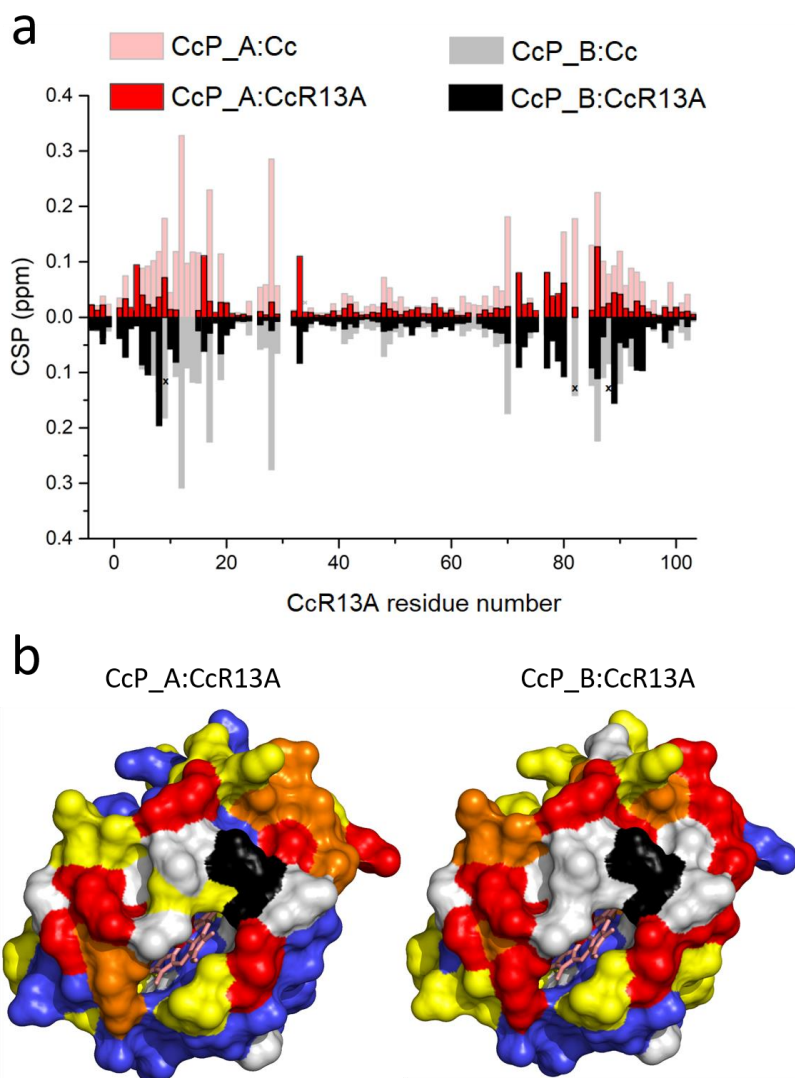


**Figure 5.2.** CSP upon complex formation. a) Comparison between the average CSP for the complexes CcP\_A:Cc R13A (in red), CcP\_B:Cc R13A (in black), CcP\_A:wt Cc (in red shading) and CcP\_B:wt Cc (in grey).<sup>23</sup> The black crosses indicate residues for which data are not available; b) CSP map for <sup>15</sup>N Cc R13A in complex with CcP\_A (left) and CcP\_B (right). The surface model of Cc (PDB 2PCC<sup>13</sup>, haem in salmon sticks) is colored according to the code: residues with  $\Delta\delta_{\text{avg}} \geq 0.06$  ppm are red, 0.04-0.06 ppm are orange, 0.02-0.04 ppm are yellow,  $<0.02$  ppm are blue, the residues for which no data are available are light gray and residue R13 is black (See Table S5.1 for the list of red, orange and yellow residues).

## Results

***The Cc R13A – CcP interaction is predominantly in the encounter state.*** Binding to CcP causes considerable changes in the amide chemical shifts of Cc.<sup>27</sup> These changes are thought to be caused predominantly by the stereospecific complex. In this state, Cc is partly desolvated and engages in specific interactions, whereas in the encounter complex Cc is thought to remain solvated and assume multiple orientations.<sup>28</sup> Cc R13A was shown to shift the equilibrium between encounter and stereospecific states toward the former.<sup>25</sup> In line with those findings, the chemical shift perturbations (CSP) observed for the <sup>15</sup>N Cc R13A binding to CcP\_A are much smaller than those for wt Cc (Figure 5.2a, red bars). Also upon binding to CcP\_B the CSP remain overall smaller for Cc R13A than for wt Cc, indicating that the complex is mainly in the encounter state. Cc R13A interacts with the same surface to CcP\_A and CcP\_B (Figure 5.2b) but some differences can be observed. The CSP pattern shows several larger perturbations when binding to CcP\_B (in the region of residues 5-10 and around residue 90), suggesting the formation of several more specific interactions.

***Cc R13A binds the new patch on CcP\_B.*** To establish whether the introduction of the added negative charges in CcP\_B influence the encounter complex with Cc R13A, PRE experiments were performed. CcP\_A and CcP\_B were tagged with the spin label MTSL after mutating residue N87, which is located close to the added negative patch (Figure 5.1), to cysteine. The tag causes enhanced relaxation for nuclear spins in <sup>15</sup>N labelled Cc R13A

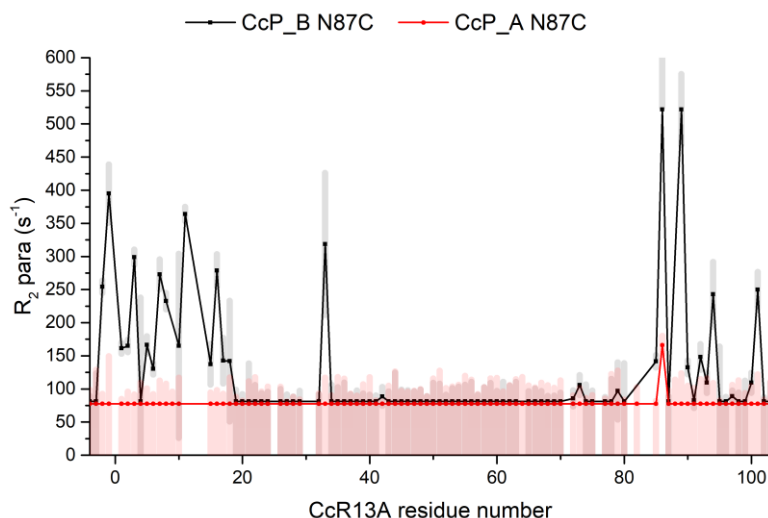


**Figure 5.3.** Probing new interactions with PRE NMR. The PREs are shown for amide nuclear spins of Cc R13A in presence of CcP\_A (in red) or CcP\_B (in black), tagged with MTSL at Cys87, which is located close to the negative patch added on CcP\_B. The error bars are indicated as shaded regions and represent the propagated 2× SD errors of the raw data. The observed PREs were divided by 0.15 to correct for the fraction of CcP that was paramagnetic (see text).

that come within  $\sim 2.5$  nm of the tag during the interactions with CcP. EPR experiments show that only 15% of the MTSL remained paramagnetic during the tagging reaction (and remains stable afterward). We have observed before that MTSL gets partly reduced during the reaction with CcP so routinely the paramagnetic fraction is established by EPR. The interaction of Cc with CcP is very fast on the NMR timescale so all Cc molecules sample many CcP molecules rapidly, averaging the effect of interactions with diamagnetic and paramagnetic CcP molecules. Figure 5.3 presents the observed PRE for the amides of Cc R13A upon interacting with CcP\_A and CcP\_B labelled at Cys87 with MTSL. The PREs have been corrected for the 15% paramagnetic labelling by dividing the observed PREs by 0.15. In CcP\_A significant PRE signal was observed for only one aminoacidic residue, indicating that Cc R13A does not interact with the surface close to N87. Upon complex formation with CcP\_B, large PREs are observed, indicating that Cc R13A visits the region with the extra charges in proximity of the paramagnetic tag on CcP\_B. Clearly, the encounter complex includes the new patch on CcP\_B, in line with the findings for wt Cc.<sup>23</sup>

**Cc R13A reacts more slowly with CcP.** To determine whether the R13A mutation in Cc influences the association rate constant with CcP, it was measured as a function of the ionic strength using stopped-flow measurements. Following the work of Miller et al. (1994),<sup>29</sup> the association rate constant can be measured by observing ET from Cc( $\text{Fe}^{2+}$ ) to CcP compound I (CpdI). The ET rate constant is high, so the observed second order rate constant is a lower-limit estimate of the association rate constant, as explained in detail in a

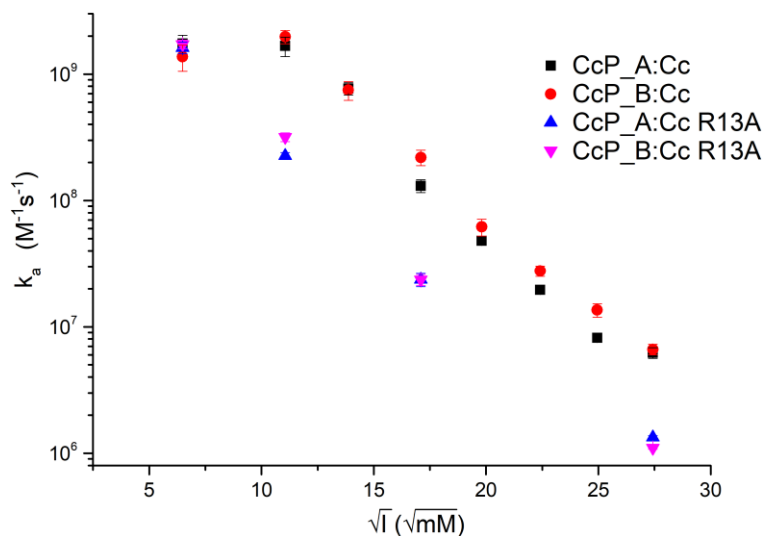


**Figure 5.4.** Rate of association ( $k_a$ ) between the Cc and CcP variants. The  $k_a$  values, plotted as a function of the square root of the ionic strength, were obtained from the simulations of the stopped flow kinetics. Errors were calculated as the standard deviation between replicates and simulations performed at different CcP concentrations (see Materials and Methods of <sup>24</sup> for details).

previous paper.<sup>24</sup> The association rate constant for wt Cc to CcP\_A and CcP\_B is strongly dependent on the ionic strength (Figure 5.4, data reproduced from ref <sup>23</sup> and <sup>24</sup>), due to the favorable electrostatic interactions between the Cc and CcP surfaces.<sup>30–34</sup> Following the same approach, the association rate constant ( $k_a$ ) was measured for Cc R13A and CcP\_A or CcP\_B. In a wide range of ionic strength values, from 122 mM (11 mM<sup>1/2</sup> on the axis of Figure 5.4) to 730 mM (27 mM<sup>1/2</sup>), the  $k_a$  of the complexes formed by Cc R13A are 5-7 fold lower than for the complexes formed by wt Cc (Tables S5.2, S5.3 and S5.4). However, curiously, at the lowest ionic strength tested, 44 mM (7 mM<sup>1/2</sup>) the  $k_a$  of the Cc R13A complexes reaches the same level as those for the complexes formed by wt Cc. Before, the surprising observation was made that the introduction of a strong negative patch on CcP distant from the stereospecific binding site did not lower the  $k_a$  for wt Cc, but rather increased it somewhat.<sup>24</sup> Similarly, for Cc R13A, we observe that the formation of the ET active complex is not slowed down by the additional charges on CcP\_B, as compared to CcP\_A.

## Discussion

Volkov *et al.*<sup>25</sup> showed that the Cc mutation Arg13 to Ala drastically increases the population of the encounter complex with CcP, from 30% to 80%. Also, the binding constant ( $K_B$ ) decreases from  $1.9 \times 10^5 \text{ M}^{-1}$  of the wt complex to  $0.06 \times 10^5 \text{ M}^{-1}$  for Cc R13A bound to CcP. We previously reported that the addition of a negative patch on a side of the binding site of CcP (CcP\_B) enlarges the area sampled by Cc in the encounter complex. Since the  $k_a$  for Cc and CcP\_B is slightly higher than that for the wt complex, it was concluded that the added charges result in more productive encounters.<sup>23</sup> The aim of the present study was to investigate to what degree the delicate balance between stereospecific complex and encounter complex influences the association between Cc and CcP by comparing the interactions between CcP with wt Cc and Cc R13A.

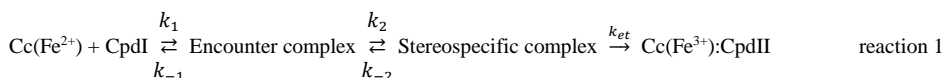
The CSP analysis shows that Cc R13A forms a much more dynamic complex with both CcP\_A and CcP\_B, than does wt Cc, in line with a more populated encounter state. The Cc R13A CSP patterns obtained with the two variants of CcP are not the same, contrary to the finding for wt Cc.<sup>23</sup> In the latter, the stereospecific complex is more populated and the main contributor to the CSP. The CSP differences observed for Cc R13A indicate differences in the interactions with CcP\_A and CcP\_B. This observation is further supported by the PRE results that show clearly that the region with the new negative patch in CcP\_B is visited by Cc R13A. It does not do so in CcP\_A, in accord with the Monte Carlo simulations reported in ref. <sup>25</sup>, which showed that the encounter complexes of wt Cc and Cc R13A with CcP\_A are very similar and comprise the surface area of CcP around the stereospecific binding site.

To test to what degree the increased dynamics in the complexes formed by Cc R13A influence the formation of the active complex, the  $k_a$  for binding to CcP\_A or CcP\_B was determined. The favorable electrostatic interactions between Cc R13A and the CcP variants cause a strong ionic strength dependence of  $k_a$ . At an ionic strength of 122 mM and higher,

## Chapter 5

the  $k_a$  values for the complexes formed by Cc R13A are 5-7 fold lower than for wt Cc at the same ionic strength. Surprisingly, at the lowest ionic strength tested, 44 mM, the  $k_a$  of the complexes formed by Cc R13A and either CcP variants reaches the  $k_a$  of the complexes formed by wt Cc. So, whereas the rate constant plateaus at low ionic strength for wt Cc, the one for Cc R13A monotonically increases.

The plateau reached for wt Cc can have various reasons. It could be that monopole-dipole interactions may come into play<sup>35,36</sup> at low ionic strength that work against each other and causing the leveling off of the  $k_a$ . However, this effect is observed for CcP\_A and CcP\_B and even for CcP\_D, which has a strong new negative patch at the far end from the stereospecific binding site.<sup>24</sup> These three variants have widely different dipoles, yet all show the same behavior. Alternatively, the diffusion limit may be reached, so increasing charge interactions further does not result in faster association. A third explanation is that the encounter complex, which is dominated by electrostatic interactions is most favorable at low ionic strength and thus, the balance between encounter and stereospecific complex shifts to the former at low ionic strength, reducing the rate of formation of the active complex. Such ‘inhibition’ by strong charge interactions outside the stereospecific binding site has been proposed before.<sup>37–40</sup> It is not trivial to determine which of the latter two explanations is applicable here. We used simulation of complex formation to evaluate ranges that the  $k_a$  values can assume.



The association reaction can be described by reactions 1, in which CpdII refers to compound II, the second intermediate in the reduction of hydrogen peroxide by CcP. Cc and CcP associate to form the encounter complex, which can evolve to the stereospecific complex in which ET can occur. At  $I = 122$  mM, the  $K_B$  value, the population of the encounter complex and the  $k_a$  values have been reported for both wt Cc and Cc R13A in complex with CcP\_A,<sup>(24,25, this work)</sup> restraining the microscopic rate constants in reaction 1. Details are given in the supporting information (Text S5.1) and Table S5.5 gives estimated values. Simulation shows that the 7-fold lower  $k_a$  value observed for Cc R13A is attributable to a combination of a lower  $k_1$  and the lower population of the stereospecific complex (implying that the second equilibrium is more to the left). Cc R13A lacks the positive side chain of Arg13 in the binding interface, so a lowered  $k_1$  is to be expected, because of weaker electrostatic interactions. The  $k_a$  observed for Cc R13A at 44 mM can be found by increasing  $k_1$  and lowering  $k_{-1}$  without changing the population of the encounter state. For wt Cc, it could be that the  $k_1$  obtained at  $I = 122$  mM ( $2 \times 10^9 \text{ M}^{-1}\text{s}^{-1}$  for CcP\_A) represents the diffusion limit and cannot increase further at  $I = 44$  mM. If it does increase, it must be accompanied by a substantially increased population (from 30% to >90%) of the encounter state to obtain the experimental  $k_a$  value, which is nearly the same as the one at  $I = 122$  mM (Table S5.5). In summary, these simulation data do not allow to favor one of these explanations. This analysis shows that the lower association rate constant of Cc R13A

is due to reduced electrostatic interactions and less favorable binding at the stereospecific complex. At low ionic strength this difference with wt Cc is eliminated, because of the plateau reached by  $k_a$  of wt Cc.

## Conclusions

Our CSP data confirm that the mutation of the Arg 13 of Cc to Ala enhances the dynamic component in the binding with the CcP variants. While it was shown that the binding mode of wt Cc with CcP\_A and CcP\_B is the same,<sup>23</sup> the interactions of Cc R13A with CcP\_B differ more from those with CcP\_A and are somewhat more specific. Paramagnetic relaxation enhancement (PRE) experiments showed that, similarly to what shown for the Cc:CcP\_B complex,<sup>23</sup> the added charges enlarge the surface of CcP visited by Cc R13A. The new patch disturbs the optimized charge distribution on the surface of CcP, yet it does not result in less productive encounters because the association rate constant is not reduced. Stopped flow experiments were used to evaluate the influence of the higher population of encounter state on the association rate between Cc R13A and the CcP variants. At ionic strength values above 122 mM (11 mM<sup>1/2</sup>), the  $k_a$  exhibits a 5-7 fold reduction compared to wt Cc, indicating that the population of the encounter state has a role in balancing dynamics and specificity in the protein complex formation, and thus can be critical for the efficiency of ET.

## References

- (1) Schreiber, G., Haran, G., and Zhou, H. X. (2009) Fundamental aspects of protein-protein association kinetics. *Chem. Rev.* 109, 839–860.
- (2) Ubbink, M. (2012) Dynamics in transient complexes of redox proteins. *Biochem. Soc. Trans.* 40, 415–418.
- (3) Yang, J., Zeng, Y., Liu, Y., Gao, M., Liu, S., Su, Z., and Huang, Y. (2020) Electrostatic interactions in molecular recognition of intrinsically disordered proteins. *J. Biomol. Struct. Dyn.* Taylor and Francis Ltd.
- (4) Zhou, H. X., and Pang, X. (2018) Electrostatic interactions in protein structure, folding, binding, and condensation. *Chem. Rev.* American Chemical Society.
- (5) Clore, G. M. (2014) Interplay between conformational selection and induced fit in multidomain protein-ligand binding probed by paramagnetic relaxation enhancement. *Biophys. Chem.* Elsevier B.V.
- (6) Schilder, J., and Ubbink, M. (2013) Formation of transient protein complexes. *Curr. Opin. Struct. Biol.* 23, 911–918.
- (7) Harel, M., Spaar, A., and Schreiber, G. (2009) Fruitful and futile encounters along the association reaction between proteins. *Biophys. J.* 96, 4237–4248.
- (8) Fawzi, N. L., Doucleff, M., Suh, J. Y., and Clore, G. M. (2010) Mechanistic details of a



## Chapter 5

protein-protein association pathway revealed by paramagnetic relaxation enhancement titration measurements. *Proc. Natl. Acad. Sci. U. S. A.* 107, 1379–1384.

(9) Adam, G., and Delbrück, M. (1968) Reduction of dimensionality in biological diffusion processes, in *Structural Chemistry and Molecular Biology* (A. Rich, N. D., Ed.), p 198. W. H. Freeman and Co., San Francisco.

(10) An, S. Y., Kim, E.-H., and Suh, J.-Y. (2018) Facilitated protein association via engineered target search pathways visualized by paramagnetic NMR spectroscopy. *Structure* 26, 887-893.e2.

(11) Andrałojć, W., Hiruma, Y., Liu, W. M., Ravera, E., Nojiri, M., Parigi, G., Luchinat, C., and Ubbink, M. (2017) Identification of productive and futile encounters in an electron transfer protein complex. *Proc. Natl. Acad. Sci. U. S. A.* 114, E1840–E1847.

(12) Schrödinger, L. The PyMOL molecular graphics system, Version 1.3.

(13) Pelletier, H., and Kraut, J. (1992) Crystal structure of a complex between electron transfer partners, cytochrome *c* peroxidase and cytochrome *c*. *Science* (80-. ). 258, 1748–1755.

(14) Gabdoulline, R. R., and Wade, R. C. (2001) Protein-protein association: investigation of factors influencing association rates by Brownian dynamics simulations. *J. Mol. Biol.* 306, 1139–1155.

(15) Poulos, T. L., Freer, S. T., Alden, R. A., Edwards, S. L., Skogland, U., Takio, K., Eriksson, B., Xuong, N. H., Yonetani, T., and Kraut, J. (1980) Crystal-structure of cytochrome-c peroxidase. *J. Biol. Chem.* 255, 575–580.

(16) Louie, G. V., Hutcheon, W. L. B., and Brayer, G. D. (1988) Yeast iso-1-cytochrome *c*: A 2.8 Å resolution three-dimensional structure determination. *J. Mol. Biol.* 199, 295–314.

(17) Northrup, S. H., Boles, J. O., and Reynolds, J. C. (1988) Brownian dynamics of cytochrome *c* and cytochrome *c* peroxidase association. *Science* (80-. ). 241, 67–70.

(18) Volkov, A. N., Worrall, J. A. R., Holtzmann, E., and Ubbink, M. (2006) Solution structure and dynamics of the complex between cytochrome *c* and cytochrome *c* peroxidase determined by paramagnetic NMR. *Proc. Natl. Acad. Sci. U. S. A.* 103, 18945–18950.

(19) Bashir, Q., Volkov, A. N., Ullmann, G. M., and Ubbink, M. (2010) Visualization of the encounter ensemble of the transient electron transfer complex of cytochrome *c* and cytochrome *c* peroxidase. *J. Am. Chem. Soc.* 132, 241–247.

(20) Erman, J. E., Vitello, L. B., Pearl, N. M., Jacobson, T., Francis, M., Alberts, E., Kou, A., and Bujarska, K. (2015) Binding of yeast cytochrome *c* to forty-four charge-reversal mutants of yeast cytochrome *c* peroxidase: isothermal titration calorimetry. *Biochemistry* 54, 4845–4854.

(21) Pearl, N. M., Jacobson, T., Arisa, M., Vitello, L. B., and Erman, J. E. (2007) Effect of single-site charge-reversal mutations on the catalytic properties of yeast cytochrome *c*

peroxidase: Mutations near the high-affinity cytochrome *c* binding site. *Biochemistry* 46, 8263–8272.

(22) Pearl, N. M., Jacobson, T., Meyen, C., Clementz, A. G., Ok, E. Y., Choi, E., Wilson, K., Vitello, L. B., and Erman, J. E. (2008) Effect of single-site charge-reversal mutations on the catalytic properties of yeast cytochrome *c* peroxidase: Evidence for a single, catalytically active, cytochrome *c* binding domain. *Biochemistry* 47, 2766–2775.

(23) Di Savino, A., Foerster, J., La Haye, T., Blok, A., Timmer, M., Ullmann, M., and Ubbink, M. (2020) Efficient encounter complex formation and electron transfer to cytochrome *c* peroxidase with an additional, distant electrostatic binding site. *Angew. Chemie Int. Ed.* 132, 23239–23243.

(24) Di Savino, A., Foerster, J. M., Ullmann, G. M., and Ubbink, M. (2021) The charge distribution on a protein surface determines whether productive or futile encounter complexes are formed. *Biochemistry* 17, 60(10), 747–755.

(25) Volkov, A. N., Bashir, Q., Worrall, J. A. R., Ullmann, G. M., and Ubbink, M. (2010) Shifting the equilibrium between the encounter state and the specific form of a protein complex by interfacial point mutations. *J. Am. Chem. Soc.* 132, 11487–11495.

(26) Volkov, A. N., Bashir, O., Worrall, J. A. R., and Ubbink, M. (2009) Binding hot spot in the weak protein complex of physiological redox partners yeast cytochrome *c* and cytochrome *c* peroxidase. *J. Mol. Biol.* 385, 1003–1013.

(27) Worrall, J. A. R., Kolczak, U., Canters, G. W., and Ubbink, M. (2001) Interaction of yeast iso-1-cytochrome *c* with cytochrome *c* peroxidase investigated by N-15,H-1 heteronuclear NMR spectroscopy. *Biochemistry* 40, 7069–7076.

(28) Worrall, J. A. R., Reinle, W., Bernhardt, R., and Ubbink, M. (2003) Transient protein interactions studied by NMR spectroscopy: The case of cytochrome *c* and adrenodoxin. *Biochemistry* 42, 7068–7076.

(29) Miller, M. A., Liu, R. Q., Hahm, S., Geren, L., Hibdon, S., Kraut, J., Durham, B., and Millett, F. (1994) Interaction domain for the reaction of cytochrome *c* with the radical and the oxyferryl heme in cytochrome *c* peroxidase compound I. *Biochemistry* 33, 8686–8693.

(30) Zhou, J. S., and Hoffman, B. M. (1994) Stern-Volmer in reverse - 2/1 stoichiometry of the cytochrome *c* cytochrome *c* peroxidase electron-transfer complex. *Science* (80-. ). 265, 1693–1696.

(31) Van de Water, K., Sterckx, Y. G. J., and Volkov, A. N. (2015) The low-affinity complex of cytochrome *c* and its peroxidase. *Nat. Commun.* 6, 7073.

(32) Matthis, A. L., and Erman, J. E. (1995) Cytochrome *c* peroxidase-catalyzed oxidation of yeast iso-1 ferrocycytochrome *c* by hydrogen peroxide. Ionic strength dependence of the steady-state parameters. *Biochemistry* 34, 9985–9990.

(33) Matthis, A. L., Vitello, L. B., and Erman, J. E. (1995) Oxidation of yeast iso-1 ferrocycytochrome *c* by yeast cytochrome *c* peroxidase compounds I and II. Dependence

## Chapter 5

upon ionic strength. *Biochemistry* 34, 9991–9999.

(34) McLendon, G., Zhang, Q., Billstone, V., Wallin, S. A., Miller, R. M., Spears, K. G., and Hoffman, B. M. (1993) Thermodynamic and kinetic aspects of binding and recognition in the cytochrome *c*/cytochrome *c* peroxidase complex. *J. Am. Chem. Soc.* 115, 3665–3669.

(35) Van Leeuwen, J. W. (1983) The ionic strength dependence of the rate of a reaction between two large proteins with a dipole moment. *Biochim. Biophys. Acta - Protein Struct. Mol. Enzymol.* 743, 408–421.

(36) Watkins, J. A., Cusanovich, M. A., Meyer, T. E., and Tollin, G. (1994) A “parallel plate” electrostatic model for bimolecular rate constants applied to electron transfer proteins. *Protein Sci.* 3, 2104–2114.

(37) Meyer, T. E., Zhao, Z. G., Cusanovich, M. A., and Tollin, G. (1993) Transient kinetics of electron transfer from a variety of *c*-type cytochromes to plastocyanin. *Biochemistry* 32, 4552–4559.

(38) Suh, J. Y., Tang, C., and Clore, G. M. (2007) Role of electrostatic interactions in transient encounter complexes in protein-protein association investigated by paramagnetic relaxation enhancement. *J. Am. Chem. Soc.* 129, 12954–12955.

(39) Hazzard, J. T., McLendon, G., Cusanovich, M. A., and Tollin, G. (1988) Formation of electrostatically-stabilized complex at low ionic strength inhibits interprotein electron transfer between yeast cytochrome *c* and cytochrome *c* peroxidase. *Biochem. Biophys. Res. Commun.* 151, 429–434.

(40) Bernal-Bayard, P., Molina-Heredia, F. P., Hervás, M., and Navarro, J. A. (2013) Photosystem i reduction in diatoms: As complex as the green lineage systems but less efficient. *Biochemistry* 52, 8687–8695.

## Supporting Information

### Materials and Methods

#### Sample Preparation

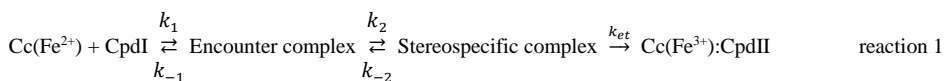
*S. cerevisiae* Cc and CcP and their variants Cc R13A and CcP\_B, were expressed and purified as previously described.<sup>1-5</sup> The EPR and the PRE experiments were performed as previously reported.<sup>3,4,6</sup> For PRE analysis, two sets of  $R_2$ dia values were obtained: one was obtained using CCPN analysis version 2.4.0 and the second one fitting the resonances to a lore line shape using FuDA (kindly previously provided by Dr. D. Fleming Hansen, University College London). The two sets of  $R_2$ dia values were averaged to obtain the final  $R_2$ dia, and their standard deviation was reported as error. The PREs were corrected for the percentage of paramagnetic signal of the MTSL tagged CcP (15% for both CcP\_A and CcP\_B, see Results) and for the fraction of Cc bound to CcP. The percentage of Cc R13A bound to CcP was calculated using the previously reported binding constant.<sup>7</sup> The assignment of the  $^{15}\text{N}$  Cc R13A HSQC was obtained comparing the spectrum with the assignment of the wt Cc spectrum<sup>8-10</sup> (BMRB 17845). Several residues, mostly around the mutation site, could not be assigned. The chemical shift perturbations (CSP) were measured by overlaying the HSQC spectra of Cc R13A bound to CcP tagged with the diamagnetic tag MTS to the spectrum of free Cc R13A. The average CSP were calculated as previously reported.<sup>11</sup>

#### Kinetic experiments

The stopped flow experiments, the simulations of the kinetics and the analysis of the data was performed as previously described.<sup>12</sup> The t-test analysis for significance in difference of  $k_a$  values is given in Tables S5.3 and S5.4.

#### Text S5.1. Simulation of the rates for the Cc:CcP\_A and CcR13A:CcP\_A complexes

The model for the association reaction is given by reaction 1. The observable is the absorbance change associated with the oxidation of ferrous Cc within the complex with Cc.<sup>12</sup>



The rates constants in reaction 1 for CcP\_A in complex with wt Cc or Cc R13A were simulated using equation S1:

$$k_a = \frac{k_1 k_2 k_{et}}{k_{-2} k_{-1} + k_{-1} k_{et} + k_2 k_{et}} \quad \text{equation S1}$$

## Chapter 5

Equation S1 is derived by assuming pseudosteady conditions for the two intermediate states, the encounter complex and the stereospecific complex.

The macroscopic  $K_D$  is given by:

$$K_D = \frac{k_{-1}k_{-2}}{k_1k_2} \quad \text{equation S2}$$

The fraction of the encounter  $f_{enc}$  complex is given by:

$$f_{enc} = \frac{k_{-2}}{k_2 + k_{-2}} \quad \text{equation S3}$$

At  $I = 120$  mM,  $k_a$ ,  $K_D$ , and  $f_{enc}$  have been determined for wt Cc and Cc R13A in complex with wt CcP (CcP\_A).<sup>(5,7,12; this work)</sup> These values were defined as targets to simulate by varying  $k_1$ ,  $k_{-1}$ ,  $k_2$  and  $k_{-2}$ .  $k_{et}$  was set to  $50,000 \text{ s}^{-1}$  (<sup>12</sup>) and assumed to be independent of ionic strength. The  $K_D$  defines the ratio of  $k_2$  and  $k_{-2}$  but not their absolute values. It was assumed that Cc reorients fast within the encounter complex, on a timescale of the rotational diffusion constant (low ns range), but this choice has little effect on the results.

**Table S5.1.** CSP classes used in the maps. The resonances of  $^{15}\text{N}$  CcR13A in complex with CcP\_A and CcP\_B are listed in descending order (from left to right) according to the shift intensity in ppm. The residues with CSP <0.02 ppm are omitted as their shift intensity is considered not significant.

**CcP\_A:CcR13A:**

<b><math>\geq 0.06</math> ppm</b>	Lys 86	Gln 16	His 33	Lys 4	Gly 77	Lys 72	Leu 9	Met 80
<b>0.04-0.06 ppm</b>	Lys 89	Lys 79	Asp 90	Lys 5	Thr 78	Thr 8		
<b>0.02-0.04 ppm</b>	Ser 2 Glu 88 Asn 70 Leu 58	Asp 93 Val 57 Lys 87 Gly 1	Cys 17 Gln 42 Lys 100 Leu 68	Val 28 Lys 73 Ala 7 Arg 91	Thr 19 Gly 6 Ala 3 Gly 41	Tyr 48 Glu -3 Phe 82	Val 20 Lys -1 Leu 98	Tyr 74 Leu 94 Lys 54
<b>no data</b>	Thr 12 Pro 76	Arg 13 Ala 81	Cys 14 Gly 83	Pro 25 Gly 84	Pro 30	Asn 31	Met 64	Pro 71

**CcP\_B:CcR13A:**

<b><math>\geq 0.06</math> ppm</b>	Thr 8 Leu 85 Gln 16	Lys 89 Lys 72 Phe 10	Lys 86 Lys 5	Met 80 His 33	Gly 6 Lys 11	Leu 94 Lys 79	Asp 93 Ser 2	Gly 77 Thr 19
<b>0.04-0.06 ppm</b>	Arg 91 Asn 92	Lys 73	Lys -1	Asn 70	Asp 90	Leu 98	Thr 78	Gly 1
<b>0.02-0.04 ppm</b>	Lys 87 Gly 34 Asp 60 Glu 21 Ile 95	Ile 53 Tyr 48 Glu -3 Asp 50 Asn 52	Val 20 Val 57 Lys 99 Glu 66	Thr 69 Ala 7 Tyr 67 Ala 43	Cys 17 Leu 15 Gly 41 Ala 0	Leu 68 Val 28 Ala 3 Trp 59	Tyr 74 Phe -2 Thr 96 Lys 54	Ile 75 Thr 49 Leu 58 Thr 102
<b>no data</b>	Leu 9 Pro 71	Thr 12 Pro 76	Arg 13 Ala 81	Cys 14 Phe 82	Pro 25 Gly 83	Pro 30 Gly 84	Asn 31 Glu 88	Met 64

## Chapter 5

**Table S5.2** Association rate constants ( $\text{M}^{-1}\text{s}^{-1}$ ) for CcP\_A and CcP\_B in complex with Cc and Cc R13A. The rate constants and error are calculated as described in <sup>12</sup>.

<b>I (mM)</b>	<b>CcP_A:Cc</b>		<b>CcP_B:Cc</b>		<b>CcP_A:CcR13A</b>		<b>CcP_B:CcR13A</b>	
	<b>k<sub>a</sub></b>	<b>st.dev.</b>	<b>k<sub>a</sub></b>	<b>st.dev.</b>	<b>k<sub>a</sub></b>	<b>st.dev.</b>	<b>k<sub>a</sub></b>	<b>st.dev.</b>
752	6.2E+06	6.0E+05	6.7E+06	8.3E+04	1.3E+06	3.8E+04	1.1E+06	2.5E+04
622	8.2E+06	3.3E+05	1.4E+07	1.7E+06				
502	2.0E+07	1.2E+06	2.8E+07	2.6E+06				
392	4.4E+07	4.5E+06	6.2E+07	9.4E+06				
292	1.3E+08	1.5E+07	2.2E+08	3.1E+07	2.4E+07	2.9E+06	2.4E+07	2.4E+06
192	7.7E+08	8.6E+07	7.5E+08	1.3E+08				
122	1.7E+09	3.0E+08	2.0E+09	2.4E+08	2.3E+08	1.3E+07	3.2E+08	2.5E+07
44	1.7E+09	2.9E+08	1.4E+09	3.2E+08	1.6E+09	1.7E+08	1.7E+09	1.4E+08

**Table S5.3.** p-values obtained from the t-test performed by comparing the rate of association ( $k(\text{II})$ ) of the Cc:CcP complexes at ionic strength values from 44 mM to 752 mM. The grey boxes indicate p-values  $> 0.016$ , meaning that the difference in the rates of association is considered not to be significant. Bonferroni correction was applied using  $p < 0.05$  for individual comparisons and  $n = 3$  for the number of comparisons for each variant.

I (mM)	CcP_A:Cc/CcP_B:Cc	CcP_A:Cc /CcP_A:CcR13A	CcP_A:Cc/CcP_B:CcR13A
752	3.3E-01	1.0E-07	6.7E-08
292	1.3E-06	6.7E-12	1.4E-11
122	7.6E-02	8.7E-06	1.3E-05
44	4.5E-02	3.8E-01	8.8E-01

I (mM)	CcP_B:Cc/CcP_A:CcR13A	CcP_B:Cc /CcP_B:CcR13A	CcP_A:CcR13A/CcP_B:CcR13A
752	2.5E-08	2.5E-08	2.4E-04
292	2.1E-10	2.4E-10	1.0E+00
122	4.2E-07	5.4E-07	7.2E-06
44	1.0E-01	2.8E-02	5.6E-01



## Chapter 5

**Table S5.4.** Number of independent simulations performed to calculate the rate constants  $k(\text{II})$  and used in t-test.

<b>I (mM)</b>	<b>CcP_A:Cc</b>	<b>CcP_B:Cc</b>	<b>CcP_A:CcR13A</b>	<b>CcP_B:CcR13A</b>
752	12	8	8	8
622	7	8		
502	12	16		
392	8	15		
292	14	14	10	10
192	12	12		
122	8	8	12	8
44	8	8	8	10

**Table S5.5.** Estimated rate constants for the Cc:CcP\_A and CoR13A:CcP\_A complexes at 122 mM (11 mM<sup>1/2</sup>) and 44 mM (7 mM<sup>1/2</sup>) ionic strength.

	wtCc:CcPA 11 mM <sup>1/2</sup>	Target	CcR13A:CcPA 11 mM <sup>1/2</sup>	Target	wtCc:CcPA 7 mM <sup>1/2</sup>	Target	CcR13A:CcPA 7 mM <sup>1/2</sup>	Target
$k_1$ (M <sup>-1</sup> s <sup>-1</sup> )	2.00E+09		8.00E+08		3.00E+09		1.95E+09	
$k_{-1}$ (s <sup>-1</sup> )	2.30E+04		3.10E+04		2.50E+03		2.50E+03	
$k_2$ (s <sup>-1</sup> )	6.00E+07		1.70E+07		5.00E+06		1.70E+07	
$k_{-2}$ (s <sup>-1</sup> )	2.60E+07		7.00E+07		7.00E+07		7.00E+07	
$k_{ex}$ (s <sup>-1</sup> )	5.00E+04		5.00E+04		5.00E+04		5.00E+04	
$K_D$ (M)	4.98E-06	5.00E-06	1.60E-04	1.66E-04	1.17E-05		5.28E-06	
$k_4$ (M <sup>-1</sup> s <sup>-1</sup> )	1.67E+09	1.66E+09	2.25E+08	2.26E+08	1.76E+09	1.74E+09	1.62E+09	1.62E+09
fraction encounter	0.30	0.30	0.80	0.80	0.93		0.80	
time E>S, $k_2^{-1}$ (ns)	16.67		58.82		200.00		58.82	
$k_4(R13A)/k_4(wt)$			0.14	0.14			0.93	0.93

## References

- (1) Volkov, A. N., Worrall, J. A. R., Holtzmann, E., and Ubbink, M. (2006) Solution structure and dynamics of the complex between cytochrome *c* and cytochrome *c* peroxidase determined by paramagnetic NMR. *Proc. Natl. Acad. Sci. U. S. A.* *103*, 18945–18950.
- (2) Goodin, D. B., Davidson, M. G., Roe, J. A., Mauk, A. G., and Smith, M. (1991) Amino-acid substitutions at tryptophan-51 of cytochrome *c* peroxidase - Effects on coordination, species preference for cytochrome *c*, and electron-transfer. *Biochemistry* *30*, 4953–4962.
- (3) Schilder, J., Lohr, F., Schwalbe, H., and Ubbink, M. (2014) The cytochrome *c* peroxidase and cytochrome *c* encounter complex: The other side of the story. *Febs Lett.* *588*, 1873–1878.
- (4) Di Savino, A., Foerster, J., La Haye, T., Blok, A., Timmer, M., Ullmann, M., and Ubbink, M. (2020) Efficient encounter complex formation and electron transfer to cytochrome *c* peroxidase with an additional, distant electrostatic binding site. *Angew. Chemie Int. Ed.* *132*, 23239–23243.
- (5) Volkov, A. N., Bashir, O., Worrall, J. A. R., and Ubbink, M. (2009) Binding hot spot in the weak protein complex of physiological redox partners yeast cytochrome *c* and cytochrome *c* peroxidase. *J. Mol. Biol.* *385*, 1003–1013.
- (6) Bashir, Q., Volkov, A. N., Ullmann, G. M., and Ubbink, M. (2010) Visualization of the encounter ensemble of the transient electron transfer complex of cytochrome *c* and cytochrome *c* peroxidase. *J. Am. Chem. Soc.* *132*, 241–247.
- (7) Volkov, A. N., Bashir, Q., Worrall, J. A. R., Ullmann, G. M., and Ubbink, M. (2010) Shifting the equilibrium between the encounter state and the specific form of a protein complex by interfacial point mutations. *J. Am. Chem. Soc.* *132*, 11487–11495.
- (8) Gao, Y., Boyd, J., Williams, R. J. P., and Pielak, G. J. (1990) Assignment of proton resonances, identification of secondary structural elements, and analysis of backbone chemical shifts for the C102T variant of yeast iso-1-cytochrome *c* and horse cytochrome *c*. *Biochemistry* *29*, 6994–7003.
- (9) Fetrow, J. S., and Baxter, S. M. (1999) Assignment of <sup>15</sup>N chemical shifts and <sup>15</sup>N relaxation measurements for oxidized and reduced iso-1-cytochrome *c*. *Biochemistry* *38*, 4480–4492.
- (10) Volkov, A. N., Vanwetswinkel, S., Van de Water, K., and van Nuland, N. A. J. (2012) Redox-dependent conformational changes in eukaryotic cytochromes revealed by paramagnetic NMR spectroscopy. *J. Biomol. Nmr* *52*, 245–256.
- (11) Grzesiek, S., Bax, A., Clore, G. M., Gronenborn, A. M., Hu, J. S., Kaufman, J., Palmer, I., Stahl, S. J., and Wingfield, P. T. (1996) The solution structure of HIV-1 Nef reveals an unexpected fold and permits delineation of the binding surface for the SH3 domain of Hck tyrosine protein kinase. *Nat. Struct. Biol.* *3*, 340–345.
- (12) Di Savino, A., Foerster, J. M., Ullmann, G. M., and Ubbink, M. (2021) The charge

distribution on a protein surface determines whether productive or futile encounter complexes are formed. *Biochemistry* 17, 60(10), 747–755.

(13) Geren, L., Hahm, S., Durham, B., and Millett, F. (1991) Photoinduced electron-transfer between cytochrome *c* peroxidase and yeast cytochrome *c* labeled at cys-102 with(4-bromomethyl-4'-methylbipyridine) bis(bypyridine) ruthenium<sup>2+</sup>. *Biochemistry* 30, 9450–9457.

# Chapter 6

## General discussion and concluding remarks

## General discussion and concluding remarks

***Electrostatic interactions in protein complex formation.*** Understanding the process of the protein complex formation provides important insights into how protein complexes can be regulated. Electrostatic interactions can promote the recognition between proteins or between a protein and its ligand.<sup>1-5</sup> Electrostatics allow two proteins with opposite charges on their surface to be attracted and find each other in a very crowded environment, such as the inside of a cell. Electrostatic interactions drive the formation of the encounter complex, pre-orient the two proteins for binding<sup>6</sup> and minimize the area searched on the protein surface,<sup>7</sup> guiding the two proteins to the binding site. As a result, favorable electrostatic interactions accelerate the association rate of protein complexes.<sup>8-11</sup> Nevertheless, strong electrostatic interactions in the encounter complex can also disturb the binding to the stereospecific binding site slowing down the association.<sup>12-16</sup> This apparent contradiction is explained by the “Velcro model” introduced by McLendon in 1991.<sup>17</sup> He suggested that electron transfer proteins interact in a dynamic ensemble of orientations with similar energy, comparable to complementary sticky “Velcro” patches, rather than in a single static configuration. As a consequence, if the interactions between the proteins allow them to easily change orientation and sample different areas of the protein surface, a favorable electrostatic pathway can guide the proteins to bind to the stereospecific binding site. At the same time, many orientations with similar energy reduce specificity, i.e. there is competition between forming the stereospecific, active complex and the dynamic encounter complex. Second, if the electrostatic interactions between two “Velcro” patches are strong enough to fix the proteins in a sub-set of configurations, for example at low ionic strength, the formation of the stereospecific complex can also be hindered. These mechanisms allow the encounter complex to regulate the delicate equilibrium between high association rate and specificity, crucial for the biological function of transient complexes such as electron transfer protein complexes. In fact, the ET in the respiration or photosynthetic redox chains can be limited by the efficiency of protein interactions. Thus, electron transfer proteins achieve their efficiency through high association and high dissociation rates and a large population of encounter complex. The distance between the area sampled by the encounter complex and stereospecific binding site, and the presence of favorable electrostatic interactions leading to the latter determine the function of the encounter complex. If the encounter complex is close to the stereospecific binding site or a favorable electrostatic path leads to it, the encounter complex usually promotes the formation of the final and active complex and thus it is called productive.<sup>10</sup> If the encounter complex is far away from the stereospecific binding site and in absence of electrostatic pathways leading to it, the proteins will most probably dissociate without forming the active complex and the encounter complex is called futile.<sup>18,19</sup>

### ***Characterization of the encounter complex by paramagnetic NMR spectroscopy.***

Although the importance of the encounter complex has been recognized by different studies,<sup>1,20,21</sup> it is still challenging to characterize it, due to its very elusive nature. Paramagnetic NMR, relaxation enhancement experiments (PRE) in particular, proved to be

an exquisite tool for investigating lowly populated states.<sup>22</sup> A paramagnetic tag attached to the protein surface causes relaxation of the nearby nuclear spins. The effect is measurable as a reduction in intensity of the resonances of the partner protein, enabling the observation of the surface sampled during the interactions (Chapter 1). We used the paramagnetic tag MTSL, which causes relaxation in a  $\sim 2.5$  nm radius from the tag (Chapter 3 and 5). While the tagging protocol is apparently straightforward, the application of the technique to haem proteins turns out to be challenging due to the instability of the paramagnetic signal of the attached tag. The presence of the tag on the protein surface was routinely tested by mass spectrometry, indicating a 100 % efficiency of tagging, confirmation by EPR however gave much more variable results. The EPR measured a paramagnetic signal corresponding to a tagging ranging from 15 % to almost 90 % without any apparent differences in the conditions. It is unclear what causes the reduction of the MTSL, although it may be a consequence of chemistry catalyzed by the haem group in CcP. Mass spectrometry of CcP shows that older samples have undergone oxidations and Cc can become reduced after several hours in the presence of CcP, despite the apparent lack of electron donors. Since only a fraction of the paramagnetic signal remains stable after tagging, we recommend always testing the tagging efficiency with EPR measurements. The PREs are then corrected for the tagging efficiency of paramagnetic tag, which can be done only if the proteins interact in the fast exchange regime relative to the maximal PRE. Furthermore, a single tethered tag as MTSL can affect the PRE measurements due to its mobility. The linker of the tag can have different conformations causing a degree of averaging over the space of the spin label.<sup>23</sup> The tag may have a preferred orientation different from expected due to interactions with residues on the surface. This could result in a ‘false’ negative in which the absence of PREs is due the tag conformation on the protein surface and not lack of protein-protein interactions. For these reasons it is important to perform the experiment by tagging the protein on more sites close to the region of interest, to ensure the collection of consistent data. A solution could be to use a double armed paramagnetic tag as the CLaNP spin labels, but avoiding strongly charged probes that could interfere with the binding.<sup>24</sup>

**Overall charge vs. charge distribution.** This thesis represents a follow-up of the previous research done on the Cc:CcP complex. The encounter complex formed by Cc and CcP was characterized with PRE and successfully simulated using Monte Carlo simulations based exclusively on electrostatic interactions.<sup>25</sup> Other studies have described the importance of the electrostatic interactions in the Cc:CcP complex,<sup>26,27</sup> supporting the idea that the distribution of the charges on the protein surface is optimized by evolution to perform the most efficient reaction. This work challenged that assumption, testing the effect of modifying the charge distribution on the surface of CcP, the subsequent effects on the encounter complex with Cc, and consequently on the association rate and activity of the protein complex. Five CcP variants were designed, which combine the addition of new negative patches with the neutralization of the charges in the stereospecific binding site (Chapter 4). Monte Carlo simulations showed that Cc is strongly attracted to the added negative patches, particularly in absence of the native (wt) charges in the binding site,

almost completely shifting the encounter complex to the added patches (Chapters 3 and 4). PRE experiments on the complexes formed by wt CcP and the CcP variant with added negative charges on a side of the binding site (CcP\_B) confirmed that Cc samples the new negative patch (Chapters 3 and 5). Although PRE experiments were not performed on the other CcP variants because of their low yields, it is reasonable to assume that they would have provided similar results. Stopped flow experiments enabled us to test how the new encounter complexes affect the association rate with Cc, showing that the addition of a new negative patch slightly enhances the  $k_a$  of the complex, no matter how far the new charges are from the stereospecific binding site (Chapters 3 and 4). Hence the new encounter complexes consist, at least in part, of productive encounters. The increase in the  $k_a$  is not very large and it is not known how many additional encounters form at the new negative patch, thus it cannot be determined what fraction is productive. The neutralization of the charges in the stereospecific binding site strongly reduces the association rate also in presence of the added negative patches (Chapter 4). Whereas the added charges contribute to productive encounters in the presence of the charges in the stereospecific binding site, they are futile in the absence of these charges. Therefore, presence of the wt charges in the binding site is the most important condition to determine if the new encounter complexes are productive or futile (Chapter 4). A second element to consider is the ionic strength at which the association rate is measured. Although the effect measured in this work is small, at low ionic strengths the electrostatic attraction to the new patch can be strong enough to hold Cc away from the binding site for longer, slowing down the association rate of the complex and its activity (Chapter 4).<sup>12–16</sup> In summary, this work proves that, in presence of the wt charges in the binding site of CcP, the overall charge of the protein surface is more important than the specific distribution of the charges (Chapter 3 and 4). Unfortunately, we were not able to obtain crystal structures of the CcP mutants to ascertain that the mutations did not disturb the structure of the protein. Nonetheless, all the CcP variants conserved the UV-vis spectrum of the wt CcP, correctly formed the CpdI intermediate and were able to perform the reaction with Cc. This reassures us that, although it is not possible to exclude small changes in the three-dimensional structure, these did not affect the integrity of CcP. However, it is possible that small modifications of the protein surface in proximity of the stereospecific binding site could slow down the formation of the active complex with Cc.

***Changing the balance between stereospecific and encounter states.*** The next step in our research was to investigate how the charge distribution on the protein surface affects the association rate of the complex when the balance between stereospecific and encounter complex is heavily shifted to the latter (Chapter 5). The wt Cc:CcP complex exists as 70% stereospecific complex and 30% encounter complex.<sup>25</sup> It was previously suggested that the CSP provide a good indication of the dynamics in a protein complex.<sup>28–30</sup> In fact, the CSP are mainly caused by the stereospecific complex, in which the protein complex is mostly in a stable orientation. On the contrary, in the encounter complex the two proteins sample many different orientations, which are averaged in the CSP, resulting in small chemical shifts. The CSPs measured for the complexes Cc:CcP\_A and Cc:CcP\_B are almost



identical, suggesting that the added charges on CcP\_B do not affect the equilibrium between stereospecific and encounter complex (Chapter 3). The mutation of the Arg13 to Ala in the binding site of Cc was shown to increase the encounter complex population from 30 % to 80 %, causing a clear reduction of the CSP.<sup>31</sup> Similarly, the CSP measured for the Cc R13A:CcP\_B complex are significantly smaller compared to the wt complex but slightly larger than for the Cc R13A:CcP\_A complex, suggesting the presence of somewhat more specific interaction (Chapter 5). PRE experiments confirmed that similar to wt Cc (Chapter 3), also Cc R13A visits the negative patch added on CcP\_B and not on CcP\_A, meaning that the added charges enlarged the surface sampled in the encounter state. However, in this case the effect on the association rate is dominated by the R13A mutation on Cc rather than the added patch on CcP\_B. In fact, both the CcP variants tested in complex with Cc R13A present a 5-7 fold decrease in the association rate compared to wt Cc at the same ionic strength. Simulations show that the lower  $k_a$  derives from a combination of factors, a lower rate of encounter complex formation between Cc and CpdI caused by the loss of the positively charged side chain on residue 13, and the lower population of stereospecific complex (Chapter 5). The increase in the association rate in presence of CcP\_B compared to CcP\_A is small and only observed at ionic strengths lower than 120 mM. This study correlates the occupancy of the encounter complex population with the efficiency in the protein complex formation, showing that the delicate balance between encounter and stereospecific complex can be critical for the activity of ET complexes (Chapter 5).

**Experimental considerations.** Both experimental and computational data were used in this work to study the encounter complex. Although the results of the two approaches were qualitatively consistent, it was not possible to gain more precise, quantitative information. Studying the wt Cc:CcP complex, Bashir *et al.* correctly predicted the encounter complex based on only electrostatic interactions. Furthermore, combining Monte Carlo simulations and PRE data, they were able to calculate the relative populations of the stereospecific and encounter complex.<sup>25</sup> Unfortunately, the approach failed when applied to the Cc:CcP\_B complexes (Chapter 3) since it was not possible to correctly fit the experimental data. Furthermore, despite the fact that PRE experiments confirmed the Monte Carlo simulations, showing that Cc visits the regions with the added negative charges, it is surprising to measure faster association rates than in the wt complex, regardless of where these charges are positioned (Chapter 4). In fact, the Monte Carlo simulations show such strong interactions between Cc and the new patches on CcP that a reduction in the association rate of the complex would be expected. However, the Monte Carlo simulations do not take into account the hydrophobic interactions that often have the role of stabilizing protein complexes, including the Cc:CcP complex.<sup>21,32-39</sup> Furthermore, the simulations assume that all the residues introduced by the mutations in the CcP are negatively charged. It should be considered that the clusters of charged residues can have considerably higher  $pK_a$  values compared to the theoretical values of amino acids, making the patch less charged than expected at pH 6. This implies that the Monte Carlo simulations could overestimate the

negative charge of the introduced patches. Despite the quantitative discrepancies in the data acquired by experimental and computational methods, the simulations remain a precious tool for the interpretation of experimental data or to build a hypothesis which can be tested by experiments.

**Conclusions.** This thesis shows that the encounter complex has a critical role not only for the first steps of protein complex formation but for the final activity of the complex. Furthermore, this work gives additional evidence that it is possible to improve the efficiency of the protein complex through charge mutations also far away from the stereospecific binding site (Chapters 3 and 4).<sup>11</sup>

All data reported here and in many other studies are acquired through *in vitro* experiments, performed in ideal, diluted solutions, under specific conditions, which can be far from the *in vivo* environment. As electrostatic interactions and the encounter complex are involved in the formation of protein complexes in living cells, experiments in crowded conditions and new approaches to perform *in vivo* studies could give an important contribution in understanding the mechanisms regulating the protein complex formation in the cell.<sup>40</sup> Our understanding of the encounter complex is still limited. For example, the different biological roles of the encounter complex still need to be explored. Recently, it was suggested that futile encounter complexes could have an important role in the regulation of enzyme activity by forming competitive encounter complexes.<sup>41</sup> Furthermore, we still cannot define the timescale of proteins dynamics within the encounter complex. At the lower end is the rotational correlation time of the free proteins (low ns), if assumed that they are not slowed down much in the encounter complex. At the high end is the lifetime of the complex ( $> 100 \mu\text{s}$ ). It is likely that the proteins in the encounter complex have much freedom and rotate rapidly but strong electrostatic patches may keep them on certain parts of the surface of the partner for prolonged times. Also the height of the energy barrier between encounter state and stereospecific complex is generally unknown. Experimental techniques that can cover this time window to study motions in the encounter complex are few. Although its extreme dynamic nature makes it challenging to investigate, a deep understanding of how the encounter complex affects the protein complex would give an important contribution in the field of the protein-protein interactions.

## References

- (1) Schreiber, G., Haran, G., and Zhou, H. X. (2009) Fundamental aspects of protein-protein association kinetics. *Chem. Rev.* **109**, 839–860.
- (2) Ubink, M. (2012) Dynamics in transient complexes of redox proteins. *Biochem. Soc. Trans.* **40**, 415–418.
- (3) Yang, J., Zeng, Y., Liu, Y., Gao, M., Liu, S., Su, Z., and Huang, Y. (2020) Electrostatic interactions in molecular recognition of intrinsically disordered proteins. *J. Biomol. Struct. Dyn.* Taylor and Francis Ltd.

## Chapter 6

- (4) Zhou, H. X., and Pang, X. (2018) Electrostatic interactions in protein structure, folding, binding, and condensation. *Chem. Rev.* American Chemical Society.
- (5) Clore, G. M. (2014) Interplay between conformational selection and induced fit in multidomain protein-ligand binding probed by paramagnetic relaxation enhancement. *Biophys. Chem.* Elsevier B.V.
- (6) Matthew, J. B., Weber, P. C., Salemm, F. R., and Richards, F. M. (1983) Electrostatic orientation during electron transfer between flavodoxin and cytochrome *c*. *Nature* 301, 169–171.
- (7) Adam, G., and Delbrück, M. (1968) Reduction of dimensionality in biological diffusion processes, in *Structural Chemistry and Molecular Biology* (A. Rich, N. D., Ed.), p 198. W. H. Freeman and Co., San Francisco.
- (8) Harel, M., Cohen, M., and Schreiber, G. (2007) On the dynamic nature of the transition state for protein-protein association as determined by double-mutant cycle analysis and simulation. *J. Mol. Biol.* 371, 180–196.
- (9) Worrall, J. A. R., Reinle, W., Bernhardt, R., and Ubbink, M. (2003) Transient protein interactions studied by NMR spectroscopy: The case of cytochrome *c* and adrenodoxin. *Biochemistry* 42, 7068–7076.
- (10) Andrałójć, W., Hiruma, Y., Liu, W. M., Ravera, E., Nojiri, M., Parigi, G., Luchinat, C., and Ubbink, M. (2017) Identification of productive and futile encounters in an electron transfer protein complex. *Proc. Natl. Acad. Sci. U. S. A.* 114, E1840–E1847.
- (11) An, S. Y., Kim, E.-H., and Suh, J.-Y. (2018) Facilitated protein association via engineered target search pathways visualized by paramagnetic NMR spectroscopy. *Structure* 26, 887–893.e2.
- (12) Meyer, T. E., Zhao, Z. G., Cusanovich, M. A., and Tollin, G. (1993) Transient kinetics of electron transfer from a variety of *c*-type cytochromes to plastocyanin. *Biochemistry* 32, 4552–4559.
- (13) Watkins, J. A., Cusanovich, M. A., Meyer, T. E., and Tollin, G. (1994) A “parallel plate” electrostatic model for bimolecular rate constants applied to electron transfer proteins. *Protein Sci.* 3, 2104–2114.
- (14) Suh, J. Y., Tang, C., and Clore, G. M. (2007) Role of electrostatic interactions in transient encounter complexes in protein-protein association investigated by paramagnetic relaxation enhancement. *J. Am. Chem. Soc.* 129, 12954–12955.
- (15) Hazzard, J. T., McLendon, G., Cusanovich, M. A., and Tollin, G. (1988) Formation of electrostatically-stabilized complex at low ionic strength inhibits interprotein electron transfer between yeast cytochrome *c* and cytochrome *c* peroxidase. *Biochem. Biophys. Res. Commun.* 151, 429–434.
- (16) Bernal-Bayard, P., Molina-Heredia, F. P., Hervás, M., and Navarro, J. A. (2013) Photosystem i reduction in diatoms: As complex as the green lineage systems but less

efficient. *Biochemistry* 52, 8687–8695.

(17) McLendon, G. (1991) Control of biological electron transport via molecular recognition and binding: The “velcro” model, in *Long-Range Electron Transfer in Biology*, p 159. Springer Berlin Heidelberg, Berlin, Heidelberg.

(18) Harel, M., Spaar, A., and Schreiber, G. (2009) Fruitful and futile encounters along the association reaction between proteins. *Biophys. J.* 96, 4237–4248.

(19) Fawzi, N. L., Doucleff, M., Suh, J. Y., and Clore, G. M. (2010) Mechanistic details of a protein-protein association pathway revealed by paramagnetic relaxation enhancement titration measurements. *Proc. Natl. Acad. Sci. U. S. A.* 107, 1379–1384.

(20) Ubbink, M. (2009) The courtship of proteins: Understanding the encounter complex. *Febs Lett.* 583, 1060–1066.

(21) Gerlach, G. J., Carrock, R., Stix, R., Stollar, E. J., and Aurelia Ball, K. (2020) A disordered encounter complex is central to the yeast Abp1p SH3 domain binding pathway. *PLoS Comput. Biol.* 16.

(22) Clore, G. M., and Iwahara, J. (2009) Theory, practice, and applications of paramagnetic relaxation enhancement for the characterization of transient low-population states of biological macromolecules and their complexes. *Chem. Rev.* 109, 4108–4139.

(23) Jeschke, G. (2013) Conformational dynamics and distribution of nitroxide spin labels. *Prog. Nucl. Magn. Reson. Spectrosc.*

(24) Keizers, P. H. J., Desreux, J. F., Overhand, M., and Ubbink, M. (2007) Increased paramagnetic effect of a lanthanide protein probe by two-point attachment. *J. Am. Chem. Soc.* 129, 9292–9293.

(25) Bashir, Q., Volkov, A. N., Ullmann, G. M., and Ubbink, M. (2010) Visualization of the encounter ensemble of the transient electron transfer complex of cytochrome *c* and cytochrome *c* peroxidase. *J. Am. Chem. Soc.* 132, 241–247.

(26) Gabdouliline, R. R., and Wade, R. C. (2001) Protein-protein association: investigation of factors influencing association rates by Brownian dynamics simulations. *J. Mol. Biol.* 306, 1139–1155.

(27) Northrup, S. H., Boles, J. O., and Reynolds, J. C. (1988) Brownian dynamics of cytochrome *c* and cytochrome *c* peroxidase association. *Science* (80-. ). 241, 67–70.

(28) Prudêncio, M., and Ubbink, M. (2004) Transient complexes of redox proteins: structural and dynamic details from NMR studies. *J. Mol. Recognit.* 17, 524–539.

(29) Hom, K., Ma, Q. F., Wolfe, G., Zhang, H., Storch, E. M., Daggett, V., Basus, V. J., and Waskell, L. (2000) NMR studies of the association of cytochrome b5 with cytochrome *c*. *Biochemistry* 39, 14025–14039.

(30) Shao, W., Im, S. C., Zuiderweg, E. R. P., and Waskell, L. (2003) Mapping the binding

interface of the cytochrome *b5*-cytochrome *c* complex by nuclear magnetic resonance. *Biochemistry* 42, 14774–14784.

(31) Volkov, A. N., Bashir, O., Worrall, J. A. R., and Ubbink, M. (2009) Binding hot spot in the weak protein complex of physiological redox partners yeast cytochrome *c* and cytochrome *c* peroxidase. *J. Mol. Biol.* 385, 1003–1013.

(32) Kim, Y. C., Tang, C., Clore, G. M., and Hummer, G. (2008) Replica exchange simulations of transient encounter complexes in protein-protein association. *Proc. Natl. Acad. Sci. U. S. A.* 105, 12855–12860.

(33) Van de Water, K., van Nuland, N. A. J., and Volkov, A. N. (2014) Transient protein encounters characterized by paramagnetic NMR. *Chem. Sci.* 5, 4227–4236.

(34) Scanu, S., Foerster, J. M., Ullmann, G. M., and Ubbink, M. (2013) Role of hydrophobic interactions in the encounter complex formation of the plastocyanin and cytochrome *f* complex revealed by paramagnetic NMR spectroscopy. *J. Am. Chem. Soc.* 135, 7681–7692.

(35) Sugase, K., Dyson, H. J., and Wright, P. E. (2007) Mechanism of coupled folding and binding of an intrinsically disordered protein. *Nature* 447, 1021–U11.

(36) Camacho, C. J., Weng, Z., Vajda, S., and DeLisi, C. (1999) Free energy landscapes of encounter complexes in protein-protein association. *Biophys. J.* 76, 1166–1178.

(37) Camacho, C. J., Kimura, S. R., DeLisi, C., and Vajda, S. (2000) Kinetics of desolvation-mediated protein-protein binding. *Biophys. J.* 78, 1094–1105.

(38) Camacho, C. J., and Vajda, S. (2002) Protein-protein association kinetics and protein docking. *Curr. Opin. Struct. Biol.* 12, 36–40.

(39) Rajamani, D., Thiel, S., Vajda, S., and Camacho, C. J. (2004) Anchor residues in protein-protein interactions. *Proc. Natl. Acad. Sci. U. S. A.* 101, 11287–11292.

(40) Phillip, Y., and Schreiber, G. (2013) Formation of protein complexes in crowded environments-From in vitro to in vivo. *FEBS Lett.* 587, 1046–1052.

(41) Kale, S., Strickland, M., Peterkofsky, A., Liu, J., and Tjandra, N. (2019) Model of a kinetically driven crosstalk between paralogous protein encounter complexes. *Biophys. J.* 117, 1655–1665.

## English summary

The traditional description of the protein complex formation as direct binding of two proteins at their binding sites, in a “lock and key” process, has nowadays been replaced with a much more dynamic model. Often, two proteins free in solution are initially attracted to one another by electrostatic interactions. In the large majority of cases proteins do not interact directly with their stereospecific binding sites, but collide with different regions of their surface. In the presence of favorable electrostatic interactions, one protein interacts with the surface of the second one in an ensemble of very dynamic configurations, referred to as the encounter complex. The encounter complex can be productive when the electrostatic interaction guides the proteins to the stereospecific complex, or the encounter complex can be futile when the two proteins dissociate before forming the final complex. Electrostatic interactions are particularly important for the encounter complex as they are the main forces guiding the process, pre-orientating the proteins and minimizing the area to sample before reaching the stereospecific binding site. Short range hydrophobic interactions can also have a role in the formation and stabilization of the protein complex. Because the encounter complex occupies only a fraction of the protein complex lifetime and it is extremely dynamic, it is invisible to conventional structural biology techniques. The development of paramagnetic relaxation enhancement (PRE) NMR, a technique with a very high sensitivity to lowly populated states, enabled the observation of these dynamic encounters. The technique measures the relaxation induced by a paramagnetic tag attached on the surface of a protein, on nuclei of a second protein that approaches the tag.

Transient complexes, such as redox complexes, are evolutionary optimized to perform very efficient reactions and exhibit a high population of encounter complex. Thus, they represent an excellent subject for study of the encounter complex. In this thesis we chose to work on a well characterized electron transfer (ET) complex formed by cytochrome *c* (Cc) and cytochrome *c* peroxidase (CcP) from *Saccharomyces cerevisiae*. The biological function of the Cc:CcP complex is to protect the cell from oxidative stress, reducing hydrogen peroxide to water. The complex formation is guided by electrostatic interactions between the positively charged binding site of Cc and the negatively charged one of CcP. The encounter complex was successfully predicted by Monte Carlo simulations based on electrostatic interactions. PRE experiments showed that the encounter complex is concentrated on the CcP binding site, sampling only 15 % of the protein surface. The fraction of encounter complex state is the 30 % on the complex lifetime, while the 70 % is in the stereospecific complex.

The aim of the work described in this thesis is to question the importance of the charge distribution on the protein surface for the formation of the active complex. To test the hypothesis that the charge distribution on these proteins is evolutionary optimized for the most efficient protein complex formation, we modified the charge distribution of the CcP surface, producing five CcP variants. The CcP mutants were designed by combining the addition of a new negative patch on a lateral side or on the opposing side of the

## English summary

stereospecific site for Cc, and the neutralization of the native negative charges in the stereospecific binding site.

In **Chapter 3** the CcP variant with an additional negative patch on a side of CcP relative to the stereospecific binding site (CcP\_B) is analyzed through Monte Carlo simulation, PRE and stopped flow experiments to characterize the encounter complex formed with Cc and test the effect of the new charges on the formation of the active complex. Monte Carlo simulations, based solely on electrostatic interactions, show that Cc is strongly attracted to the added negative patch. PRE experiments confirm the Monte Carlo simulations results, showing that the new patch enlarges the area sampled by Cc in the encounter complex with CcP. Interestingly, the measurement of the association rate of the complex through stopped flow experiments shows that the added charges on CcP\_B do not affect the association with Cc negatively. On the contrary, the formation of the Cc:CcP\_B complex is more efficient than the wild type complex. This suggests that the encounter complex between Cc and CcP\_B is a productive encounter complex and that the specific charge distribution on the surface of CcP is not critical for the formation of the active complex. In **Chapter 4** we characterized the complexes formed by Cc and the other CcP variants. Monte Carlo simulations show that Cc is strongly attracted to the added negative charges of the CcP variants, especially in absence of the native charges in the stereospecific binding site. Stopped flow experiments show that the association rate of the Cc:CcP complex is strongly slowed down when the native negative charges in the CcP binding site are neutralized. Surprisingly, the addition of a negative patch on the CcP surface enhances the association rate with Cc regardless of its localization. The finding that adding negative charges even on the opposite side of the binding site improves the affinity with Cc suggests that the overall charge of the CcP surface is more important for the active complex formation than a particular charge distribution. In **Chapter 5** we wondered if this could be caused by the prevalence of the stereospecific complex (70 %) over the encounter state population (30 %). The equilibrium between these two states is sensitive to point mutations in the binding sites. In particular the mutation of the Arg13 in Ala in the Cc binding site enhances the encounter complex from 30 % to 80 %, and causing a 100 fold decrease in the binding constant of the protein complex. To test how a prevalence of encounter complex population would affect the association rate of the complex, we studied the complexes formed by Cc R13A and the two variants of CcP, wt (CcP\_A) and CcP\_B. The chemical shift perturbations (CSP) of the complexes formed by Cc R13A are significantly smaller than in presence of wild type Cc due to the increased dynamics. Similar to the results reported in chapter 3, the PRE experiments show that Cc R13A visits the added charges on the surface of CcP\_B, enlarging the surface sampled in the encounter complex. Finally, kinetics experiments revealed that the addition of the negative charges on CcP\_B does not affect the association with Cc R13A, which is slightly higher than in presence of CcP\_A at low ionic strength. Nevertheless, the Cc R13A complexes displayed a 5-7 fold reduction of the association rate in a wide ionic strength range. This indicates that the balance of the

dynamics in a protein complex, between stereospecific and encounter complex populations, is critical for the efficiency of electron transfer complexes.

**Chapter 6** discusses the results and the techniques presented in this thesis.



## Nederlandse samenvatting

De traditionele beschrijving van twee eiwitten die direct met elkaar een complex vormen, zoals een sleutel en slot, wordt langzamerhand vervangen door een meer dynamisch model. Door middel van willekeurige botsingen komen eiwitten zelden direct met hun specifieke bindingsplaatsen tegen elkaar. Om de efficiëntie van complexvorming te verhogen worden eiwitten in oplossing vaak tot elkaar aangetrokken door elektrostatistische interacties. Gunstige elektrostatistische interacties verkleinen het eiwitoppervlak dat bezocht wordt om de juiste bindingsconformatie te vinden. Bovendien verlengen ze de levensduur van het ontmoetingscomplex (*encounter complex*). Het encounter complex kan productief zijn, indien het leidt tot een actief eiwitcomplex, of zinloos, indien de twee eiwitten elkaar loslaten zonder een actief complex gevormd te hebben. Naast elektrostatistische interacties kunnen op korte afstanden ook hydrofobe interacties een rol spelen. Omdat het encounter complex zeer dynamisch is, is het niet mogelijk het met traditionele biochemische technieken te karakteriseren. Door de ontwikkeling van paramagnetische relaxatieversterking (*paramagnetic relaxation enhancement*, PRE) kernspinresonantie (*nuclear magnetic resonance*, NMR), is het mogelijk om het encounter complex te bestuderen. Deze techniek meet de relaxatie van kernspins van een naderend eiwit, veroorzaakt door een paramagnetische groep gebonden aan het oppervlak van het andere eiwit. PRE is zeer sterk wanneer de kern dicht in de buurt van het paramagnetische centrum komt, waardoor PRE zeer gevoelig voor zulke conformaties, zelfs als ze maar een fractie uitmaken van de gehele populatie conformaties.

Kortstondige eiwitcomplexen, zoals die van redoxeiwitten, zijn evolutionair geoptimaliseerd om zeer snelle en efficiënte reacties uit te voeren. Hierdoor heeft het encounter complex een grotere populatie dan bij complexen met hoge affiniteit en langere levensduur. Daarom zijn deze complexen een uitstekend systeem om het encounter complex te onderzoeken. In dit proefschrift bestuderen wij een al goed begrepen elektronoverdracht complex, bestaand uit cytochroom *c* (Cc) en cytochroom *c* peroxidase (CcP) van *Saccharomyces cerevisiae* (bakkergist). Het Cc:CcP complex is verantwoordelijk voor bescherming van de cel tegen waterstofperoxide, door het te reduceren tot water. Bij de vorming van het complex spelen de positieve ladingen rondom de bindingsplaats van Cc en de negatieve op CcP een grote rol. Het encounter complex kan goed voorspeld worden met Monte Carlo simulaties, die alleen gebaseerd zijn op elektrostatistische interacties. PRE experimenten hebben laten zien dat het encounter complex slechts een beperkt deel (~15%) van het oppervlak van CcP uitmaakt. Het complex bestaat voor 30% uit encounter complex, en de resterende 70% uit het actieve complex.

Het doel van het onderzoek beschreven in dit proefschrift is om de noodzaak van een geoptimaliseerde ladingverdeling op het eiwitoppervlak voor het vormen van het actieve complex aan de orde te stellen. De hypothese dat de juiste verdeling van ladingen cruciaal is voor snelle vorming van het complex, wordt getoetst door het introduceren van nieuwe negatieve ladingen op de oppervlakte van CcP en het neutraliseren van bestaande. Vijf

varianten van CcP zijn ontworpen door nieuwe ladingen op de ‘zijkant’ of aan de ‘achterkant’ van CcP te introduceren, ten opzichte van de bindingsplaats voor het actieve complex. Ook worden de natuurlijke negatieve ladingen rond de bindingsplaats van actieve complex in sommige varianten verwijderd.

In **Hoofdstuk 3** wordt een variant van CcP met nieuwe negatieve ladingen aan de zijkant van het eiwit (CcP\_B) geanalyseerd door middel van Monte Carlo simulaties, PRE, en *stopped flow* experimenten, om te onderzoeken wat voor effect deze nieuwe ladingen hebben op het encounter complex en het vormen van het actieve complex. Monte Carlo simulaties tonen aan dat Cc sterk wordt aangetrokken door de nieuwe negatieve bindingsplek. De resultaten van de PRE-experimenten bevestigen experimenteel die van de Monte Carlo simulaties, en tonen dat de nieuwe plek door Cc in het encounter complex wordt bemonsterd. Alhoewel er dus een groter oppervlak bemonsterd wordt, tonen metingen met *stopped flow* aan dat de vorming van het actieve complex niet negatief beïnvloed wordt door de nieuwe ladingen. Het Cc:CcP\_B complex wordt zelfs sneller gevormd dan het natuurlijke complex. Dit suggereert dat het nieuwe encounter complex tussen Cc en CcP\_B productief is en dat de specifieke verdeling van ladingen over CcP niet cruciaal is voor het snel vormen van het actieve complex. In **Hoofdstuk 4** worden de complexen gevormd door Cc en andere varianten van CcP gekarakteriseerd. Monte Carlo simulaties tonen aan dat Cc aangetrokken wordt door de nieuwe negatieve bindingsplekken op deze varianten, vooral als de oorspronkelijke negatieve ladingen rondom de bindingsplek van het actieve complex verwijderd zijn. *Stopped flow* experimenten tonen aan dat de bindingssnelheid van de Cc:CcP complex sterk verminderd wordt wanneer de oorspronkelijke negatieve ladingen verwijderd zijn. Verbazingwekkend genoeg blijkt dat een nieuwe negatieve bindingsplek vrijwel altijd een positief effect heeft op de bindingsnelheid van Cc, zelfs als de bindingsplek op de achterkant van CcP ligt. Dit toont aan dat de totale lading een grotere rol speelt dan de specifieke verdeling van deze lading over het oppervlak. In **Hoofdstuk 5** wordt getoetst of dit zou kunnen komen door de verdeling tussen het encounter complex en het specifieke complex (30% tegen 70%). Deze verdeling is zeer gevoelig voor specifieke mutaties in de bindingsplek van Cc in het actieve complex. Als Arg13 van Cc veranderd wordt in Ala (R13A), bestaat het complex met CcP voor 80% uit encounter complex. Ook wordt bindingsconstante van het complex honderd keer lager. Om te onderzoeken hoe deze herverdeling van encounter complex en actief complex de bindingssnelheid beïnvloedt, zijn de complexen van Cc R13A en het wildtype CcP (CcP\_A) en CcP\_B bestudeerd. De verstoringen in de chemische verschuivingen in het NMR-spectrum van het complex gevormd door Cc R13A zijn significant kleiner dan die met het wildtype Cc, doordat het complex dynamischer is geworden. Overeenkomstig de metingen van Hoofdstuk 3, tonen de PRE-experimenten dat ook Cc R13A de nieuwe negatieve ladingen op CcP\_B bezoekt, en een groter gedeelte van het eiwitoppervlak bemonstert in het encounter complex. Ten slotte tonen kinetische experimenten aan dat de toegevoegde negatieve ladingen op CcP\_B de bindingssnelheid met Cc R13A niet beïnvloeden, behalve bij lage zoutconcentratie. Desalniettemin laat de Cc R13A een 5- tot

## Nederlandse samenvatting

7-voudige lagere bindingssnelheid zien over een brede reeks zoutconcentraties. Dit geeft aan dat de balans tussen encounter en specifiek complex een belangrijke rol speelt voor de efficiëntie van elektronoverdracht.

In **Hoofdstuk 6** worden de resultaten en technieken van dit proefschrift besproken in een brede context.

## Curriculum Vitae

Antonella Di Savino was born on May 27<sup>th</sup> 1986 in Turin, Italy. After studying engineering at the Polytechnic of Turin for two years, she decided to follow her interest for the biological sciences. She achieved a bachelor degree in Biology followed by a master degree in Cellular and Molecular Biology at the University of Turin. During her internship in the group of Prof. Gianfranco Gilardi, supervised by Dr. Francesca Valetti and Dr. Simone Morra, she developed an interest for biochemistry, particularly for the study of proteins. She moved to the Netherlands to join the research group of Prof. Marcellus Ubbink at Leiden Institute of Chemistry in 2016 to work on protein-protein interactions. Her research project was aimed at understanding the importance of charge distributions on the protein surface for the encounter complex and for protein complex formation.

## List of publications

Ubbink, M., and Di Savino, A. (2018) Chapter 5: Protein-protein interactions, in *New Developments in NMR - Paramagnetism in Experimental Biomolecular NMR* (Luchinat, C., Parigi, G., and Ravera, E., Eds.), pp 134–162. The Royal Society of Chemistry, Cambridge, UK. ISBN: 9781788014960

Di Savino, A., Foerster, J., La Haye, T., Blok, A., Timmer, M., Ullmann, M., and Ubbink, M. (2020) Efficient encounter complex formation and electron transfer to cytochrome *c* peroxidase with an additional, distant electrostatic binding site. *Angew. Chemie Int. Ed.* 132, 23239–23243.

van Son, M., Schilder, J. T., Di Savino, A., Blok, A., Ubbink, M., and Huber, M. (2020) The transient complex of cytochrome *c* and cytochrome *c* peroxidase: Insights into the encounter complex from multifrequency EPR and NMR spectroscopy. *ChemPhysChem* 21, 1060–1069.

Di Savino, A., Foerster, J. M., Ullmann, M., and Ubbink, M. Charge distribution on a protein surface determines whether productive or futile encounter complexes are formed. *Biochemistry*, 60(10), 747–755.

Di Savino, A. and Ubbink, M. Enhancing the population of encounter complex affects protein complex formation efficiency, *Under revision*